FUNGAL DECOMPOSITION DYNAMICS USING FOURIER TRANSFORM INFRARED SPECTROSCOPY AND ATOMIC FORCE MICROSCOPY

by

Jennifer A. Kilic

A Dissertation submitted to the

Graduate School-New Brunswick

Rutgers, The State University of New Jersey

in partial fulfillment of the requirements

for the degree of

Doctor of Philosophy

Graduate Program in Ecology and Evolution

written under the direction of

John Dighton

and approved by

_____

_____

_____

_____

New Brunswick, New Jersey

October 2013

ABSTRACT OF THE DISSERTATION

Fungal Decomposition Dynamics Using Fourier Transform Infrared Spectroscopy and Atomic Force Microscopy

By Jennifer A. Kilic

Dissertation Director:

John Dighton

I studied the decomposition of leaf material at the hyphal scale of resolution and the chemical and physical changes occurring at the fungal/substrate interface using Fourier transform infrared (FTIR) spectroscopy and atomic force microscopy (AFM). The chemical composition of 20 fungal isolates was determined using FTIR and FTIR-attenuated total reflectance (FTIR-ATR) microscopy, with the intention of subtracting fungal FTIR spectra from decomposing leaf spectra in a separate experiment. I found fungi are difficult to differentiate using FTIR spectra.

I performed a twelve month decomposition study placing leaves of white oak, black huckleberry, and pitch pine in leaf litter of the New Jersey pinelands. FTIR-ATR spectra of the leaves at 10x10 micron areas were taken at 0, 6, and 12 months. I found leaf chemistry of oak and huckleberry was similar, but different from pine, prior to decomposition. As decomposition progressed, the chemistry of the leaves appeared to become more similar. Subtracting fungal spectra from the leaf spectra was not possible and complicated analysis of leaf spectra.

AFM was combined with FTIR-ATR to study the fungal hypha/leaf interface at the level of an individual hypha. It was not possible to scan a leaf on the AFM, so a flatter substrate was required. I attempted to cast starch:lignin biofilms as a simple leaf model using published

methods, however it was found that during the film making process the lignin may have been degraded. Instead, manufactured cellophane was used as a model for cellulose. Three fungal species were grown on cellophane squares, and AFM and FTIR-ATR imaging utilized to determine the chemical and physical properties of the cellophane adjacent to the hyphae. Fungal species capable of producing cellulase caused a change in the physical characteristics and chemistry of cellophane adjacent to fungal hyphae.

These experiments demonstrate the chemistry of fungal hyphae and decomposing leaves using FTIR-ATR and chemical and physical changes occurring in a substrate during fungal decomposition using FTIR-ATR and AFM. The novel use of FTIR-ATR and AFM to investigate the fungus/substrate interface at the scale of an individual fungal hypha introduces new methods for studying fungi at this scale of resolution.

DEDICATION

I dedicate this dissertation to my father, Richard Edward Oberle Sr. (1946-2012). His encouragement, love, and support will always be remembered and cherished.

ACKNOWLEDGEMENTS

Without the support and friendship of my advisor, John Dighton, this project may never have reached its full potential. John has taught me that there is more than one way to interpret data and study ecological processes. His breadth of knowledge, humor, and dedication inspire me to continue to grow as a scientist, mentor, and human being. Georgia Arbuckle-Keil was more a co-advisor than dissertation committee member. She guided me through some of the most difficult parts of the preparation of this dissertation – the chemistry. I am grateful to Georgia for dedicating her time and energy to this dissertation and meeting with me frequently to discuss the chemistry behind my project. My other committee members, Peter Morin and Doug Eveleigh have supported me through this process extensively, and both have always had open doors. Peter taught me the valuable lesson that I need to understand the history of my field to truly understand the current issues. As any field progresses and the body of knowledge increases, this becomes a more and more daunting task. It was through Peter, and his passion for ecology, that made this task pleasurable for me. Doug has always encouraged me to read more, learn more, and seek more. I've never visited Doug's office and left empty handed, whether it was a citation for a paper or a stack of books. Through the writing process Doug offered much-needed encouragement along the way in his emails and comments on my chapters.

I am grateful to the many people who have provided me with guidance in my education, my research, and my growth as a scientist over the years. I would especially like to thank Dennis Gray and Kenneth Clark for reviewing our manuscripts and taking the time to offer advice on the direction of my education, and Dr. Ellen Miseo for processing our FTIR-ATR FPA images and her advice on interpretation of those images. I am especially grateful to Marsha Morin, who has the answer to everything! Special thanks to my study partners who helped me prepare for my

qualifying exam, Brian Clough and Orion Weldon. Thank you to the members or associates (past and present) of the Dighton lab and Pinelands Field Station, each of whom has had an impact on my education and has helped me stay sane at different times over the last 6 years: Sharron Hicks Crane, Jennifer Adams Krumins, Melanie Mahgring, Rebecca Bachelor, Katie Malcolm, Sarah Smith, and Natalie Howe.

Working at an off-campus location was sometimes difficult and lonely, but the graduate students in biology and chemistry at Rutgers Camden were always willing to include me in their activities. I thank all of the graduate students in those programs for their support over the years, particularly my good friends Kristin Lammers and Lisa Sibley.

The support of my friends and family was immeasurable during the past 6 years. Thank you to my father, Richard Oberle Sr., my mother, Anna Schina, and my brothers, Richard Oberle Jr. and Michael Schina for their unwavering support. I thank my aunt, Nancy Oberle, for all of the mornings she helped out with my son the last few months, so I could write a little longer. My dearest friends Loretta Lee, Jill Carroll, Colin Boyd, Lynne Roseberry, Laura Christopher, and Debbie Sweeney were always willing to help me relax. Most importantly, I'd like to thank my son, Matthew Kilic. His innocence, curiosity, and wonder are a constant reminder of why I chose the path that I did. He is my ultimate inspiration.

TABLE OF CONTENTS

LIST OF TABLES

LIST OF FIGURES

CHAPTER 1

Introduction

Located on the Atlantic coastal plain in New Jersey, The Pinelands National Reserve is one of the largest continuous tracts of preserved land on the east coast of the United States, comprised of 1.1 million acres of unique habitats. The NJ Pinelands are characterized by porous, sandy acidic soils with high rates of nutrient turnover and very little humus. Upland forest canopies are dominated by pitch pine, oak, or both with understories dominated by blueberry, huckleberry and mountain laurel (Boyd, 1991). Due to the acidic nature of Pinelands soils, fungi dominate the saprotrophic community, and leaf litter decomposition by fungi is a major means to replenish depleted nutrients in the soil. This dissertation aims to investigate fungal decomposition of pinelands leaf litter at the microscale by utilizing unique techniques not often thought of as options for ecologists. Observations of fungal decomposition at this scale may provide a better understanding of fungal foraging strategies and community assembly.

Leaf Litter Decomposition and Fungal Succession

Decomposer communities include a variety of soil and litter organisms including bacteria, fungi, protozoa, and representatives of nearly all terrestrial invertebrate classes including nematodes, mites, and collembola (Swift, Heal and Anderson, 1979). Decomposition is a process achieved by the entire community; no one organism can completely degrade the mixture of complex molecules found in a single leaf (Osono and Takeda, 2002). However, fungi are known to be the primary decomposers of the chemical constituents of detrital plant material, primarily due to their wide variety of degradative enzymes (SInsabaugh, 2005). Plants produce a number of large biopolymers such as pectin, hemicelluloses, cellulose, and lignin. Cellulose is the most abundant biological polymer on Earth, with estimated total annual biomass

production of 1.5 x 10^{12} tons, followed by lignin, the second most abundant biopolymer and most abundant aromatic polymer on Earth (Klemm *et al.*, 2005; Leisola, Pastinen, and Axe, 2012). Although both are highly recalcitrant (lignin more so), there is a relatively wide assortment of fungi, particularly in the Ascomycotina and Basidiomycotina, that produce the enzymes necessary to decompose cellulose (e.g. hydrolytic cellulases and lytic polysaccharase monooxygenases). Much fewer in numbers and diversity are the species of fungi that produce lignin-degrading enzymes (lignin peroxidases and manganese peroxidases). Lignin decomposers are primarily Basidiomycotina, but do include a small number of Ascomycotina genera, particularly *Xylaria* spp. (Dix and Simpson, 1984; Osono and Takeda, 2002; Sinsabaugh, 2005). The dominance of fungi in the decomposition process of leaf material makes them a key participant in the carbon cycle, the importance of which cannot be understated (Sinsabaugh, 2005).

Fungal decomposition of plant material is intimately connected to succession of the fungal community on the leaf. Until now, the decomposition of leaves has been observed in bulk studies of litter bags or individual leaves (Jensen, 1974; Ponge, 1991; Frankland, 1998; Osono and Takeda, 2002; Osono, Hirose, and Fujimaki, 2006). Compositional changes within the leaf and the successive changes in the decomposer community within and on the leaf are well documented in such studies. Ponge (1991) broke down the decomposition process into four successive stages of macroscale community and resource changes, in which fungi play a pivotal role in each. In many cases, fungi act to condition a substrate long before other organisms, including bacteria and soil fauna, are able to utilize the resource (Romani *et al*., 2006).

A freshly fallen leaf is composed of numerous organic compounds, which act as substrates for decomposition. Nucleic acids, proteins, and lipids will all be present, but carbohydrates will dominate the leaf constituents. There will be small mono-, di-, and

oligosaccharides, as well as the larger polymers: pectin, hemicelluloses, cellulose, and lignin. Most fungal taxa, as well as a good number of other organisms, are capable of breaking down the non-carbohydrate and small carbohydrate compounds. These easily degraded components of the leaf allow early colonization by a large number of organisms resulting in relatively rapid depletion, leaving behind the more recalcitrant substrates for the fungi producing cellulolytic and lignolytic enzymes. These serial changes in the resource result in a predictable pattern of succession in the fungal community.

In general, fungal succession on a newly fallen oak leaf in a temperate forest should follow the phases listed below (Frankland, 1998; Kendrick, 2001):

i. First, phylloplane fungi and early saprobes attack. Some phylloplane fungi may have been weak parasites or epiphytic fungi that can now capitalize on the fallen leaf. The early saprobes are leaf litter fungi, usually r-strategists, and can utilize the simple sugars and oligosaccharides of the leaf material. This stage is dominated by the Zygomycotina, few of which are capable of producing cellulose or lignin degrading enzymes.

ii. Next, common leaf litter saprotrophs invade. Ascomycotina dominate, although other fungi may be present as well. They will attack more recalcitrant substances such as pectin, hemicellulose, and cellulose.

iii. By 6 months, Basidiomycotina are present. These tend to be slower-growing K-strategists producing a much more complex suite of enzymes, including enzymes that degrade relatively simple organic compounds and those that degrade more recalcitrant compounds including cellulose and lignin. They can degrade the most recalcitrant plant substances, cellulose and lignin.

iv. After 2 years, the leaf material is well incorporated into the soil and soil fungi compose the fungal community.

There are multiple factors that affect fungal succession patterns including location and environment (Frankland, 1998). In addition to the substrate on which it's growing (location) and the microclimate and the presence/absence of other fungi (environment), fungal succession on a leaf should be determined by the enzymes a fungus possesses and the effects of those enzymes on the leaf material. By tracking the physical and chemical changes in the leaf and relating that to information about which fungi possess which enzymes will shed light on the successional trends in the fungal community and how interactions between fungi occur at the hyphal scale in relation to resource quality.

Fungal Growth Patterns and Foraging

Oak, pine, and huckleberry are all found within the NJ Pinelands, and each species should possess a distinct complement of plant polymers (Ribeiro da Luz, 2006), making them perfectly suited to act as varied substrate choices for the assembly of a fungal community. In addition to differences between species, there is also considerable heterogeneity within a species (Estell *et al.,* 1994) and presumably within individual leaves. The presence of a variety of cell types with varying levels of secondary cell wall development implies that the entire leaf is itself a mosaic of chemical resource patches that are observable only at the microscale. There appear to be no known studies that investigate how a fungus degrades a highly complex substrate such as a leaf at the hyphal level; however, research at the gross scale of individual leaves or mass of leaves or through assays of entire microbial community enzyme suites does exist (Smart and Jackson, 2009). Hyphal branching patterns and rates of growth have been shown to vary depending on resource quality in contrived heterogeneous environments using defined media (Ritz, 1995). Ritz demonstrated that in high-nutrient media, hyphal growth is slow and dense, yet in low-nutrient media, hyphal growth is fast and effuse. By differing foraging

strategies as the mycelium explores a heterogeneous substrate, the fungus allows for conservation of energy. Whereas the fungus will grow many hyphae to increase surface area on high quality resources, but grow few hyphae on low quality resources.

Optimal foraging theory (OFT) is largely an ecological theory applied to an animal's selection of food in relation to the balance between energy expended on the search and energy gained by consumption of the food item (Van Nest and Moore, 2012). Although OFT was first developed in animal behavioral ecology (MacArthur and Pianka, 1966; Emlen, 1966) and based on the hypothesis that animals will maximize their energy intake per unit of foraging time, a large body of research, including proposed mathematical models, has appeared since the introduction of optimal foraging theory addressing the foraging behaviors and energetic trade-offs in animals (Charnov, 1976; Pyke, Pulliam, and Charnov, 1977; Pyke, 1984), plants (Cahill and McNickle, 2011; Gleason and Fry, 1997; Kelly, 1990), and more recently, mycorrhizal fungi (Gavito and Olsson, 2008a & 2008b; Johnson, 2009) at a large scale of resolution. Of the models of mycelium growth of saprotrophic fungi, none appear to address optimal foraging theory.

The *modus operandi* of fungi is to present the largest possible surface area to the environment through which it can secrete enzymes and recover end products of enzyme activity for growth. This activity not only changes the chemical structure of the substrate, but also alters the physical structure by solubilization along with the deposition of proteinaceous material (enzymes). The "zone of influence" of an individual hypha would be the area over which the secreted enzymes exert an effect on the substrate and from which the hypha can garner resources. An optimal foraging strategy for fungi would be to maximize fungal hyphal length and to organize branching patterns to optimize the surface area covered but to minimize overlap of zones of influence between adjacent hyphae. The fact that fungal mycelia can alter their foraging strategy between rich and poor resource bases has been shown (Rayner, 1991;

Ritz 1995), however the interaction between the hypha, its underlying substrate, and the immediate effect of the hypha on substrate physical and chemical changes has only recently started to be investigated (Oberle-Kilic, Dighton, and Arbuckle-Keil, 2013).

With advances in microscopy, imaging, and methods to determine chemical composition, we now have the ability to monitor changes in leaf chemistry as a fungal hypha forages across its surface. Combining tools commonly used in analytical chemistry (Fourier transform infrared spectroscopy (FTIR) and FTIR-ATR (attenuated total reflectance)) and physics (atomic force microscopy (AFM)) may enable measurement of the precise effects that a fungal hypha induces in the carbohydrate chemistry and surface structure of a substrate. Determining the physical and chemical changes to the substrate at this scale will identify the unique contribution of individual fungal species to the decomposition process. These changes in the resource will then influence changes in the fungal community over time, allowing a greater understanding of the resource control (bottom up regulation) of assembly rules for saprotrophic fungal communities during resource succession (Jumpponen and Egerton-Warburton, 2005).

Fourier Transform Infrared (FTIR) Spectroscopy

Fourier transform infrared spectroscopy (FTIR) is a tool traditionally used in the field of analytical chemistry, but is increasingly being applied in the biological sciences in analyzing complex biological systems (Movasaghi, Rehman, Rehman, 2008; Duygu *et al.*, 2009). FTIR spectroscopy involves the absorption of infrared radiation by the sample resulting in molecular vibrations (i.e. bending or stretching of covalent bonds and/or groups of atoms in a molecule). The molecular vibration can be observed if there is an overall change in the dipole moment of the chemical bond and/or groups of atoms as a result of the vibration. Each observable chemical group in a molecule will vibrate at a specific frequency characteristic of its structure.

The resulting IR spectrum is a plot of the intensity of IR radiation absorbed (y axis) at specific wavelengths (x-axis) in units of wavenumber (cm^{-1}), which is commonly used for this region of electromagnetic radiation. The complex pattern of peaks produced by a sample, its IR spectrum, can then be analyzed to obtain compositional information.

In polyatomic covalent molecules, there exists a permanent dipole due to the fact that positive and negative charges within the molecule rarely perfectly overlap. This makes most covalent molecules at least slightly polar. For IR radiation and matter to interact, the matter must have a permanent dipole. Homonuclear diatomic molecules, by contrast, have no permanent dipole, therefore are not IR active. With the absorption of IR radiation, there is a change in the permanent dipole of a chemical bond. The normal modes of vibration include symmetrical stretching, asymmetrical stretching, twisting, scissoring, rocking, and wagging (Mayo, Miller, and Hannah, 2004). When IR radiation is absorbed by a molecule the permanent dipole (normal vibration) of that molecule changes. The larger the change in the molecular dipole of the molecule, the greater the intensity of the peak (commonly referred to as an absorption band) on the IR spectrum at that wavenumber will be. Peak intensity, however, can also be attributable to the amount of a functional group within a sample, in accordance with Beer's law ($A=\varepsilon bc$). Where A is absorption, ε (molar absorptivity) is dipole dependent, b is path length, and c is concentration. Relative intensities of peaks at different wavenumbers cannot be considered quantitatively, but can be compared qualitatively. However, comparisons of intensities at a particular wavenumber between related spectra may be considered quantitatively if sufficient information is known about the sample (Mayo *et al.*, 2004).

The infrared region is divided into the near-IR (14,000-4,000 cm^{-1}), the mid-IR (4,000 – 400 cm^{-1}), and the far-IR (400-10 cm^{-1}). The mid-IR is the most commonly used region in IR spectroscopy. The region below 1500 cm^{-1} (1500-400 cm^{-1}) is known as the fingerprint region.

Many functional groups absorb IR radiation in this range, resulting in a unique, characteristic spectrum (fingerprint) of a pure substance. Therefore, this region is central in determining compositional information about complex biological mixtures.

Fourier transform infrared (FTIR) spectroscopy is based on the principle of interference between two infrared beams producing an interferogram. It utilizes mathematics (the Fourier transform) to convert the interference pattern into a spectrum, and therefore requires an interferometer in the IR bench. The interferometer produces the interferogram that contains all of the spectral information about the sample. The Michelson interferometer consists of two perpendicular mirrors, one of which is capable of movement, and a beamsplitter (Fig. 1). Ideally, 50% of the IR radiation passes through the beamsplitter to the moving mirror, while 50% is reflected to the stationary mirror. The two mirrors then reflect these beams back to the beamsplitter, where they combine and interfere. The beam that is reflected from the non-moving mirror is transmitted through the beamsplitter, but 50% is reflected back to the source. This beam that is transmitted through the beamsplitter (from the stationary mirror) is the beam that will interact with the sample and subsequently be detected. The most common IR detector is DTGS (deuterium triglycine sulphate), but the IR microscope detector is MCT (mercury cadmium telluride) which requires liquid nitrogen. (Stuart, George, and McIntyre, 1996)

The moving mirror plays a key role in forming the interference pattern, and as such must be properly aligned. As the mirror moves back and forth, there is a highly sensitive laser (often helium-neon) that is used to control and measure the mirror movement precisely (Stuart *et al.*, 1996). It is these measurements that are used when computing an infrared spectrum using the Fourier transform.

There is a selection of sampling techniques available using FTIR spectroscopy. In the studies that follow three different methods were utilized.

i. Transmission spectra were obtained using potassium bromide (KBr) pellets, consisting of <5% sample and >95% KBr ground together then pressed. The IR beam passes through the pellet resulting in transmission spectra.

ii. Reflection spectra were obtained using Attenuated total reflectance (ATR) microscopy using a single point of contact. FTIR-ATR (attenuated total reflectance) microscopy utilizes a microscope in conjunction with a traditional FTIR bench. This enables the infrared spectrum to be obtained from a point located under the microscope approximately 10 x 10 microns in size. There is a crystal (in this case, germanium-Ge) attached to the rotating nosepiece of the microscope. This crystal is brought into contact with the sample, where the beam of IR radiation penetrates it and is reflected back into the crystal. The depth of penetration of the IR beam is dependent upon the refractive indices of the Ge crystal and the sample; it varies with wavelength. The reflected IR beam is then sent to the detector (MCT) in the head of the microscope. This process generates an average FTIR spectrum of the area in contact with the ATR crystal.

iii. ATR microscopic imaging using a focal plane array (FPA) detector that generates a chemical map at a single point. Micro-ATR-FTIR imaging utilizes a similar microscope, but with a focal plane array detector in conjunction with a traditional FTIR bench. This enables the infrared spectrum to be obtained from an image area located under the microscope, composed of 64 x 64, 1.1 μm^2 pixels, resulting in a spectral map composed of 4096 spectra. Each pixel, therefore, is its own spectrum, not an average of spectra over the entire contact area. Micro-ATR-FTIR imaging has recently been used as a tool to investigate chemical composition of biological samples (surface of skin, cross-section of blood vessels, hair) with higher resolution than was previously allowed using traditional IR methods. (Kazarian and Chan, 2010)

The transmission spectra were obtained using an FTIR bench as described above with no additional attachments, whereas ATR and ATR imaging require specialized microscopes.

The chemical composition of leaves is an array of complex biopolymers including pectin, lignin, cellulose and hemicelluloses. During decomposition these polymers are attacked by a variety of fungi capable of breaking the bonds found within these recalcitrant biological compounds. As the compounds in the leaf material are decomposed, the type of functional groups present and their relative ratios will change, thus leading to temporal changes in the IR spectrum. FTIR-ATR microscopy will allow the tracking of those changes occurring at the scale of the fungal hyphae.

FTIR and FTIR-ATR have been utilized in investigating leaf litter changes under the influence of enzymatic degradation (Mascarenhas, Dighton, and Arbuckle, 2000) and under the influence of burning (Lammers, Dighton, and Arbuckle-Keil, 2009). FTIR-ATR has recently been used to successfully distinguish between leaf species (Ribeiro da Luz, 2006).

Atomic Force Microscopy

The atomic force microscope is an imaging and analysis tool that operates by 'feeling' with a probe, as opposed to 'looking' with lenses on an optical microscope (Morris, Kirby, and Gunning, 2010). The AFM probe is a small tip (nm in size) suspended from a cantilever (microns in size). Probes (tips) and cantilevers vary in size, composition, and flexibility; some of which are specially made for an intended purpose (e.g. biological samples) and others are general purpose.

In tapping mode, the probe taps transversely across the surface, as a laser is reflected off the top of the cantilever and onto a photodiode screen, allowing for generation of a height image based on the deflection of the cantilever (Fig. 2). This height image can then be analyzed to measure surface roughness of different areas of the image by utilizing the root mean squared

(RMS) values. In addition to producing images of the surface and measurements of surface roughness, the AFM also has the capability to measure other physical properties of the surface through a series of force curves. Force curves are plots produced as the AFM probe goes through one cycle of down and up (Fig. 3). These curves provide data on the hardness, elasticity, and adhesion of a small area of the sample. When a number of force curves are taken in adjacent regions, a pixelated force map may be generated, where each pixel represents a different force curve (Fig. 4).

Atomic force microscopy is a physical microscopy technique that can be used for measuring surface topography, adhesion, and elasticity in living cells (Kaminskyj and Dahms, 2008). AFM has been used to visualize changes in shape and surface structure of germinating *Aspergillus fumigatus* spores (Dague *et al*., 2008) and to test adhesive properties of *Beauveria bassiana*'s different reproductive cell types: aerial conidia, blastospores and submerged conidia (Holder and Keyhani, 2005).

Using the atomic force microscope in conjunction with the FTIR- ATR microscope, we now have the capability of observing changes in substrate chemistry at or near the resolution of action of a single fungal hypha. The results of these experiments may be the first record of the effects of fungal activity on the chemical structure of leaf material at the scale of resolution of fungal hyphae. The unique combination of data that can be generated using these microscopy methods will allow integration of tools traditionally used in the chemical and physical sciences to determine changes occurring at the micro scale on a substrate during decomposition.

Figures

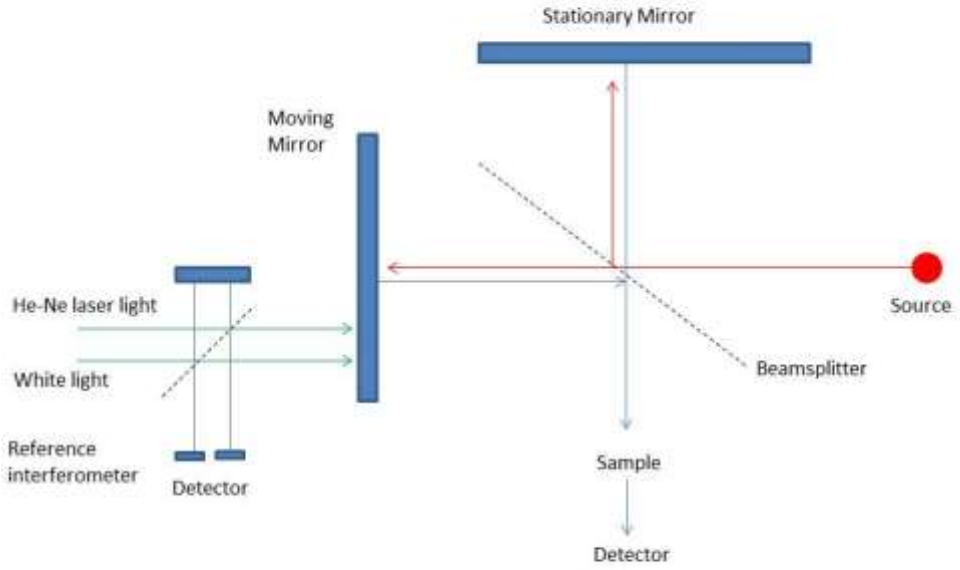

Figure 1. A Michelson interferometer of an IR spectrometer, including major components and beam pathways (after Stuart *et al*.,1996). Essentially, the source emits a beam of IR radiation that is split, reflected off mirrors at 90 degrees, and then recombined. When they recombine, they interfere with one another. This beam is then directed at the sample. In transmission mode it is transmitted through the sample to a detector; in reflection mode the beam is reflected off the sample to a detector.

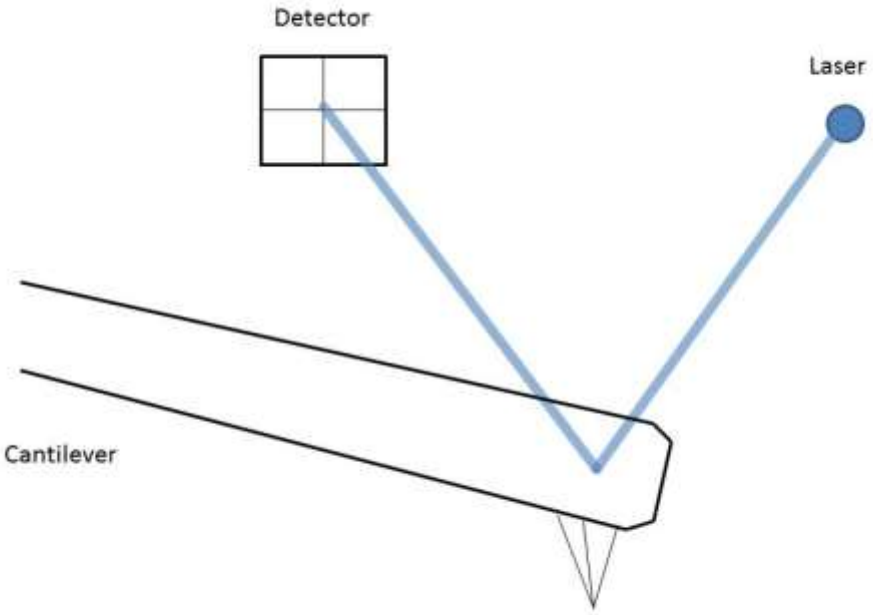

Figure 2. The optical lever sensor of an atomic force microscope. As the cantilever bends (during contact with the sample), the position of the laser spot on the detector (photodiode) will change, generating a height image of the sample (after Eaton and West, 2011).

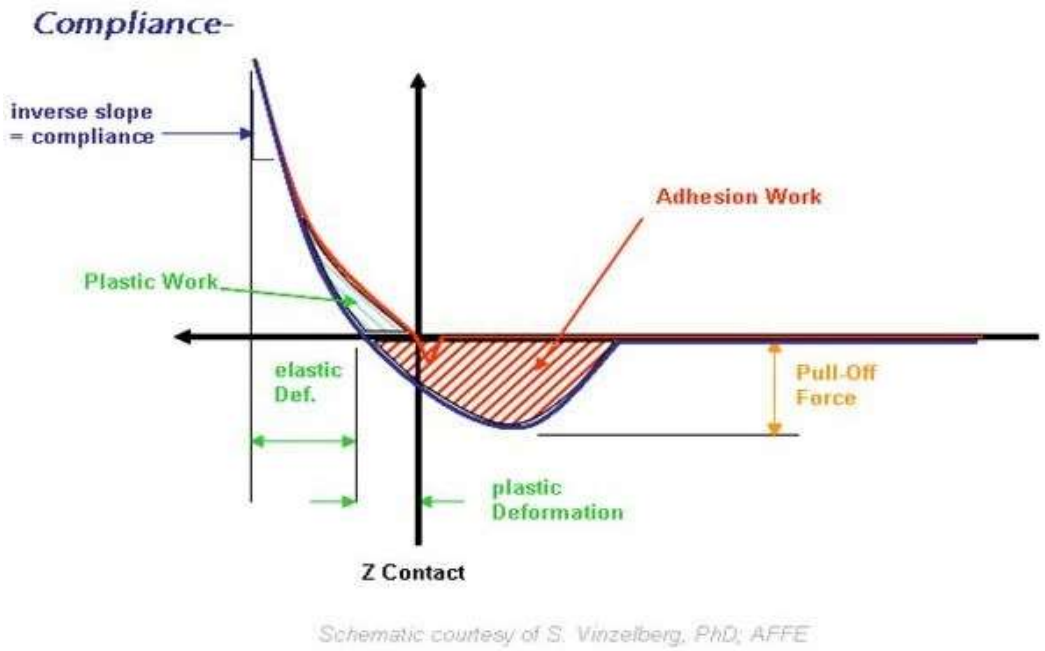

Figure 3. A force curve generated by atomic force microscopy. The area of adhesion work, the red area between the curve and the x-axis, allows for quantitative analysis between varying pixel shading in the force map (Fig. 4) (after Asylum Research Manualette, courtesy of S. Vinzelberg, PhD, AFFE)

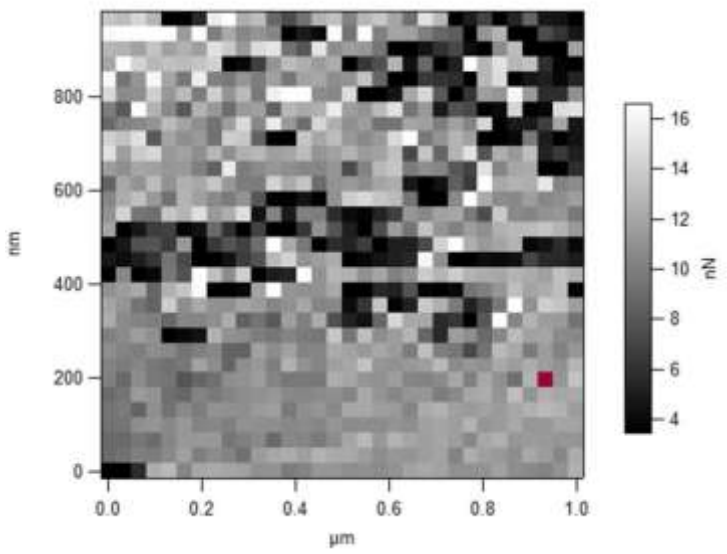

Figure 4. Adhesion force map of the biopolymer polyhydroxyalkanoate (PHA) measuring 1x1 micron. Each pixel represents a force curve similar to the schematic diagram shown on the above. The extent of shading represents the adhesion work of the sample in nanoNewtons.

References

Boyd H. 1991. Field Guide to the Pine Barrens of New Jersey. Plexus Publishing, Medford, NJ

Cahill JF, McNickle GG. 2011. The behavioral ecology of nutrient foraging by plants. *Annual Review of Ecology, Evolution, and Systematics* 42:289-311.

Charnov EL. 1976. Optimal foraging, the marginal value theorem. *Theoretical Population Biology* 9(2):129-136.

Dague E, Alsteens D, Latge JP, and Defrene YF. 2008. High resolution cell surface dynamics of germinating *Aspergillus fumigatus* conidia. *Biophysical Journal 94*:656-660.

Dix NJ, Simpson AP. 1984. Decay of leaf litter by *Collybia peronata*. *Transactions of the British Mycological Society* 83:37-41.

Duygu DY, Baykal T, Acikgoz I, Yildiz K. 2009. Fourier transform infrared (FT-IR) spectroscopy for biological studies. *Gazi University Journal of Science* 22(3):117-121.

Eaton P, West P. 2010. Atomic Force Microscopy. Oxford University Press, Oxford, UK pp 116-117.

Emlen JM. 1966. The role of time and energy in food preference. *American Naturalist* 100:611-617.

Estell RE, Havstad KM, Fredrickson EL, Gardea-Torresdey JL. 1994. Secondary chemistry of the leaf surface of *Flourensia cernua*. *Biochemical Systematics and Ecology* 22(1):73-77.

Frankland JC. 1998. Fungal Succession - unravelling the unpredictable. *Mycological Research 102*(1):1-15.

Gavito ME, Olsson PA. 2008a. Foraging strategies of the external mycelium of the arbuscular mycorrhizal fungi *Glomus intraradices* and *Scutellospora calospora*. *Applied Soil Ecology* 39: 282-290.

Gavito ME, Olsson PA. 2008b. Foraging for resources in arbuscular mycorrhizal fungi: what is an obligate symbiont searching for and how is it done? In: A. Varma (Ed) Mycorrhiza, Springer-Verlag, Berlin – Heidelberg, Germany.

Gleason SK, Fry JE. 1997. Root proliferation and marginal patch value. *Oikos* 79:387-393.

Holder DJ, Keyhani NO. 2005. Adhesion of the entomopathogenic fungus *Beauveria* (*Cordyceps) bassiana* to substrata. *Applied and Environmental Microbiology* 71:5260-5266.

Jensen V. 1974. Decomposition of Angiosperm Tree Leaf Litter. In C. Dickinson, and G. Pugh, *Biology of Plant Litter Decomposition Volume 1* (pp. 69-104). Academic Press, London, UK.

Johnson NC. 2009. Resource stoichiometry elucidates the structure and function of arbuscular mycorrhizas across scales. *New Phytologist* 185: 631-647

Jumpponen A, Egerton-Warburton LM. 2005. Mycorrhizal fungi in successional environments - a community assembly model incorporating host plant, environmental and biotic filters. In J. W. Dighton, *The Fungal Community* (pp. 139-180). CRC Press, New York, NY.

Kaminskyj SG, Dahms TE. 2008. High spatial resolution surface imaging and analysis of fungal cells using SEM and AFM. *Micron* 39: 349-361.

Kazarian S, Chan KLC. 2010. Micro- and macro- attenuated total reflection Fourier transform infrared spectroscopic imaging. *Applied Spectroscopy* 64: 135A-152A.

Kelly CK. 1990. Plant foraging - a marginal value model and coiling response in *Cuscuta subinclusa*. *Ecology* 71:1916–1925.

Kendrick B. 2001. The Fifth Kingdom, 3rd ed. Focus Publishing, R. Pullins Co., Newburyport, MA. pp 184-190.

Klemm D, Heublein B, Fink HP, Bohn A. 2005. Cellulose: a fascinating biopolymer and sustainable raw material. *Angewandte Chemie International Edition* 44: 3358 – 3393.

Lammers K, Arbuckle-Keil G, Dighton J. 2009. FT-IR study of the changes in carbohydrate chemistry of three New Jersey pine barrens leaf litters during simulated control burning. *Soil Biology and Biochemistry* 41: 340-347.

Leisola M, Pastinen O, Axe DD. 2012. Lignin – designed randomness. *BIO-Complexity* 3: 1-11.

MacArthur RH, Pianka ER. 1966. On optimal use of a patchy environment. *American Naturalist* 100:603-609.

Mascarenhas M, Dighton J, Arbuckle GA. 2000. Characterization of plant carbohydrates and changes in leaf carbohydrate chemistry due to chemical and enzymatic degradation measured by microscopic ATR FT-IR spectroscopy. *Applied Spectroscopy* 54: 681-686.

Mayo DW, Miller FA, Hannah RW. 2004. Course Notes of the Interpretation of Infrared and Raman Spectra. John Wiley and Sons, Hoboken, NJ.

Morris VJ, Kirby AR, Gunning AP. 2010. Atomic Force Microscopy for Biologists, 2nd ed. Imperial College Press, London.

Movasaghi Z, Rehman S, Rehman I. 2008. Fourier transform infrared (FTIR) spectroscopy of biological tissues. *Applied Spectroscopy Reviews* 43(2): 134-179.

Oberle-Kilic J, Dighton J, Arbuckle-Keil G. Atomic force microscopy and micro-ATR-FT-IR imaging reveals fungal enzyme activity at the hyphal scale of Resolution. *Mycology: An International Journal on Fungal Biology* DOI:10.1080/21501203.2012.759631

Osono T, Takeda H. 2002. Comparison of litter decomposing ability among diverse fungi in a cool temperate deciduous forest in Japan. *Mycologia* 94(3): 421-427.

Osono T, Hirose D, Fujimaki R. 2006. Fungal colonization as affected by litter depth and decomposition stage of needle litter. *Soil Biology and Biochemistry* 38: 2743-2752.

Ponge, J. 1991. Succession of fungi and fauna during decomposition of needles in a small area of Scots pine litter. *Plant and Soil* 138: 99-113.

Pyke GH, Pulliam HR, Charnov, EL. 1977. Optimal foraging: a selective review of theory and tests. *The Quarterly Review of Biology* 52: 137-154.

Pyke GH. 1984. Optimal foraging: a critical review. *Annual Review of Ecology and Systematics* 15: 523-575.

Rayner, ADM. 1991. The challenge of the individualistic mycelium. *Mycologia* 83:48-71.

Ribeiro da Luz B. 2006. Attenuated total reflectance spectroscopy of plant leaves: a tool for ecological and botanical studies. *New Phytologist* 172: 305-318.

Ritz K. 1995. Growth responses of some soil fungi to spatially heterogenous nutrients. *FEMS Microbiology Ecology* 16: 269-280.

Romani AM, Fischer H, Mille-Lindeblom C, Tranvik LJ. 2006. Interactions of bacteria and fungi on decomposing litter: differential extracellular enzyme activities. *Ecology* 87: 2559-2569.

Sinsabaugh RL. 2005. Fungal Enzymes at the Community Scale. In J. Dighton, J. J. White, and P. Oudemans, *The Fungal Community: Its Organization and Role in the Ecosystem* (pp. 349-361). CRC Press, New York, NY.

Smart KA, Jackson CR. 2009. Fine scale patterns in microbial extracellular enzyme activity during leaf litter decomposition in a stream and its floodplain. *Microbial Ecology* 58:591-598.

Stuart B, George B, McIntyre P. 1996. Modern Infrared Spectroscopy. John Wiley and Sons, Chichester, UK.

Swift MJ, Heal OW, Anderson JM. 1979. Decomposition in Terrestrial Ecosystems. Oxford, Blackwell Scientific, Oxford, UK.

Van Nest B, Moore, D. 2012. Energetically optimal foraging is emergent property of time-keeping behavior in honey bees. *Behavioral Ecology* 23: 649-658.

CHAPTER TWO

Characterization of fungal isolates using Fourier transform infrared (FTIR) spectroscopy and Fourier transform infrared-attenuated total reflectance (FTIR-ATR) microspectroscopy

Introduction

Fourier Transform Infrared (FTIR) spectroscopy involves the absorption of infrared radiation by the sample resulting in several molecular vibrations within each atom or group of atoms. Microscopic FTIR-ATR (attenuated total reflectance) utilizes a microscope in conjunction with a traditional FTIR spectrometer, allowing an infrared spectrum to be obtained from a point approximately 10 x 10 microns in size (Salzer and Siesler, 2009).

When IR radiation is absorbed, each functional group in a molecule vibrates at specific frequency regions depending on its chemical structure and the structures to which the functional group is bound. It should be recognized that different functional groups may vibrate at similar frequencies, making them indistinguishable during IR spectral analysis. This is often the case in complex molecules and mixtures, such as those found in living organisms; however, useful compositional data may still be obtained.

In addition to the ability to examine biological samples at the microscopic scale using transmission techniques (Stewart 1996), numerous advances have occurred in FTIR micro-spectroscopy over the past two decades, and a number of methodologies have been developed to observe or differentiate microbes using FTIR or FTIR-ATR. Kansiz *et al.* (1999) used FTIR micro-spectroscopy to discriminate between different strains of cyanobacteria. Naumann *et al.* (2005) were able to differentiate two fungi: *Trametes verisicolor* and *Schizophyllum commune* growing in wood blocks. Dogan *et al.* (2007) observed changes in mouse liver tissue infected with

candidiasis, and Johnson *et al.* (2009) were able to differentiate between vegetative cells and sporulated cells of *Bacillus* bacteria based on their unique IR signatures.

The use of FTIR in the biological sciences has recently been reviewed by Movasaghi, Rehman, and Rehman (2008) and Duygu *et al.* (2009). Mowasaghi *et al.* (2008) published a 25 page correlation table in their review assigning peak numbers to only biological functional groups, and made tentative assignments to distinct biological molecules in some cases (*e.g*. 1419 cm^{-1} is attributable to (COO^{-}) found in polysaccharides and pectin).

Using synchrotron FTIR micro-spectroscopy, Szeghalami, Kaminskyj, and Gough (2007) identified differences in IR spectra between hyphae of *Aspergillus*, *Neurospora* and *Rhizopus* and slight spectral changes in each of these when grown in sub-optimal conditions. Jilkine *et al.* (2008) similarly used synchrotron FTIR to develop methods for whole-cell biochemical composition using spores of *Neurospora* and *Rhizopus*. Synchrotron FTIR differs from traditional IR in that it utilizes a powerful synchrotron source, which enables the user to overcome resolution problems at the lower wavenumbers. According to Jilkine *et al*. (2008), the most distinctive carbohydrate signatures are found at the longer infrared wavelengths, but the diffraction limit is 5-10 microns, resulting in poor resolution using a traditional IR source.

In this study, traditional FTIR and FTIR-ATR methods were used to determine significant differences in spectral properties of a number of fungal species analyzed using three different methods. FTIR-ATR allows for investigation into surface chemistry; this was used to determine the surface chemistry of (i) living fungal hyphae versus (ii) dried fungal hyphae. The use of transmission FTIR required the (iii) grinding of dried hyphal cells with KBr, allowing the internal cellular chemistry to be investigated. Thus, the ground samples were a mixture of surface (cell wall) and internal material. An in depth statistical analysis was performed, examining minute

differences between fungal spectra using full-spectrum IR analysis. Unique differences were found for both transmission and reflectance (ATR) mode IR spectra.

Methods

Sample Preparation

Twenty species of fungi were obtained as either stock cultures from the laboratory of Dr. Jim White (Rutgers SEBS Department of Plant Pathology) or through direct culture and isolation from NJ Pinelands leaf litter (Table 1). The species or descriptions are given as well as the abbreviations which will be used for simplicity. Selection of fungal species was targeted at those similar to fungi found on decomposing leaf material, primarily Ascomycetes and Basidiomycetes. Therefore, there is not a broad taxonomical range of fungi represented in this study.

Oak and huckleberry leaves were collected from upper and lower layers of the forest floor leaf litter. Leaves were placed on potato dextrose agar (PDA)(Fisher Scientific, Pittsburgh, PA) plates, malt extract agar (MEA) plates, and in damp chambers. After one week at room temperature, colonies that could be sub-cultured from the PDA and MEA were transferred to new PDA and MEA plates. If any contaminants remained, these were then sub-cultured again to isolate.

Damp chambers were prepared by lining empty petri plates with moist paper towels and sterilizing in an autoclave. Damp chambers were moistened as necessary using 1.0 ml of sterile water. After 30 days, leaves were removed and moved to PDA and MEA plates. After one week at room temperature bacterial contaminants were present. Colonies were then transferred to tap water agar to attempt to separate out the fungal colonies from bacterial

colonies, as the fungal hyphae will grow out allowing isolation. After two weeks of growth on tap water agar, fungal colonies were isolated and transferred back to PDA.

After isolation, fungi were kept in pure culture on PDA plates. They were transferred to potato dextrose broth, a liquid media composed of potato infusion and dextrose (Fisher Scientific, Pittsburgh, PA). Once a pure broth culture was maintained, three broth sub-cultures were made per fungal isolate. After the colonies reached approximately 1 cm in diameter, they were removed from the broth culture and rinsed thrice in sterile water to remove excess broth. The colonies were placed on MirrIR™ slides (Kelvey Technologies, Chesterland, OH) and allowed to slightly air dry for 30 minutes. This was enough time to allow excess water to evaporate while leaving the colony slightly moist and alive.

The three replicates of the living samples were analyzed using the FTIR-ATR microscope. All ATR spectra were obtained on an Agilent (formerly Bio-Rad) FTS 6000 infrared spectrophotometer with an attached UMA 500 microscope with a germanium (Ge) ATR crystal. Sixty-four scans were averaged at a resolution of 4 cm^{-1} with air as the background spectrum. Between collections of each average spectrum, the Ge crystal was cleaned with isopropanol.

After collecting spectra from the surface of the living hyphae, the sample slides were placed on a metal block partially submerged in liquid nitrogen (-190 C), freezing the fungus quickly to preserve the intracellular components. Following thirty minutes on the metal block, samples were placed in a drying oven at 25 C for 24 hours to remove excess water (Heike Bucking, personal communication of methods). Once the colonies dried, they were analyzed on the FTIR-ATR microscope using the same settings as the live fungal samples (outlined above).

Following FTIR-ATR spectra collection from living and dried colonies, the dried material of each sample replicate was individually scraped from the MirrIR™ slide and added to ground KBr in approximately a 1:20 ratio of sample:KBr. The mixture was finely ground using a mortar

and pestle, transferred to a KBr press, and pressed into a transparent pellet. Each pellet was placed in the internal sample compartment of the Agilent FTS 6000 and transmission FTIR spectra were obtained.

Spectral Analysis

Spectral databases were created using KnowItAll® (Bio-Rad, Hercules, CA) spectral analysis software. Each database consists of the three replicate spectra of each of the 20 species of fungi (9 identified species and 11 unidentified samples). The three primary spectral databases were created for each treatment: ATR spectra of living fungi, ATR spectra of dried fungi, and KBr transmission spectra of dried-ground fungi.

Upon importing the databases into KnowItAll®, all spectra were normalized and baseline corrected (linear fit). Additionally, the spectra from the KBr samples were smoothed (linearly over 5 points) to remove noise as a result of water in the sample spectra. Following creation of the databases, principal component analysis (PCA) was performed in KnowItAll®. The PCA was mean-centered with 3 factors and included only the CH-region (3050-2800 cm^{-1}) and the fingerprint region (1800 – 700 cm^{-1}) of the spectra. The region above 3050 cm^{-1} is a very large, broad band due to OH vibrations. This region is present in all spectra, but the band itself can shift by 50 or so wavenumbers between spectra. Using such a large band in a full-spectrum analysis causes it to outweigh the smaller, more significant bands in the CH-region and fingerprint regions. The region between 2800 and 1800 consists of few spectral vibrations, except for the CO_2 bands 2390-2285 cm^{-1}, present in air. Below 700 cm^{-1}, there is another CO_2 band that must be excluded at 672-664 cm^{-1}, as well as considerable noise in this region. Additionally, the germanium crystal cannot be used at wavelengths below ~570 cm^{-1}.

The databases were then exported to another informatics software package, Pirouette® (Infometrix, Inc. Bothell, WA). Pirouette® is not exclusively a spectroscopy software package, but it offers the ability to generate spreadsheets of the PCA coordinate scores (KnowItAll does not). The coordinate scores on axes 1, 2, and 3 from the PCA analysis in Pirouette® were imported into SAS® (SAS Institute, Inc.) and one-way ANOVA was performed with a Tukey's post hoc test on the coordinate scores on each of the three primary PC axes. In all data sets, axis three did not contribute significantly to spectral separation, and therefore, it was not analyzed in detail. The coordinate scores were then entered into Graphpad Prism®(GraphPad Software, Inc.) to generate each PCA plot including error bars.

The spectra of each species deemed to be significantly different from the PCA analysis were further analyzed using their x-residuals to determine which spectral peaks were causing separation in the analysis. For example, in the living fungi database, the ANOVA resulted in samples *D* and *S* pulling in the positive direction and *R* pulling in the negative direction on axis 1 – the x axis (Fig. 1).

The x-residual is a result of subtracting each spectrum from the average of all the spectra in the database. These are plotted together with residuals from all 60 spectra on the same graph (Fig. 2). The spectra with the most deviation from the group at certain wavenumbers coincide with the species of fungi responsible for the most separation in the PCA analysis, as they are most different from the average of all the spectra.

The x-residuals of each replicate of these key fungi were then analyzed. Any peak, positive or negative, that separated out from the dark black center of overlapping spectra of the plot was recorded (Fig. 2). A peak on the x-residual was determined to be relevant if 5 or fewer spectra of other species extended further from the zero line (Fig. 3). If a peak separated in all replicates of the same species, this was considered a significant peak for that data set. If two of

the three replicates had a distinct peak, that wavenumber was considered important. This list of significant and important peaks was then compared to the factor loading plots generated in KnowItAll®.

The factor loading plots are essentially line graphs centered on a zero line. They are generated from the PCA analysis in KnowItAll, and reflect the peaks that contribute to separation in the overall analysis of all 20 species' spectra. If there is deviation on the positive side (upward peak) at a wavenumber, then that wavenumber is responsible for "pulling" positively along that axis in the PCA analysis. Conversely, if there is a negative deviation (downward peak) at a specific wavenumber, then that wavenumber is responsible for "pulling" in the negative direction along that axis (Fig. 4).

The important and significant IR peaks identified from analysis of the x-residuals should be present on the factor loading plots. It is important to recognize that the factor loading plots include the entire database of 60 spectra, so there will be other peaks on the plots that are not found on the x-residuals of the species that ANOVA deemed statistically different from the others, for example*, D, S,* and *R* in the living fungi dataset.

Following analysis of the PCA scores, x-residuals, and factor loading plots, these results were compared to the actual IR spectra. The three IR spectral replicates for each fungal species that separated using the ANOVA analysis were averaged to result in one IR spectrum. The CO_2 region was flattened, and peaks with a minimum intensity of 8% and maximum noise of 1% were identified by the software (Fig. 5). Peaks within 5 wavenumbers of each other are considered to be essentially the same peak for the purpose of this analysis.

A comparison of the peaks present in each average IR spectrum was cross-checked with the list of significant and important peaks for that dataset based on the x-residual and factor loading analyses. All significant peaks (those present in all replicates) and important peaks

(those present in two of the three replicates) from axis 1 were included, whereas only significant peaks from axis 2 are included.

Results

FTIR-ATR of living fungi

Spectral collection of living fungal hyphae using FTIR-ATR and subsequent statistical analysis resulted in a Principal Component Analysis (PCA) in which axis 1 accounted for 72.2% of the variability, axis 2 for 18.5%, and axis 3 for 8.1%. ANOVA of the PCA scores determined species *D* and *S* to be significantly different from 7 out of 20 other fungal species and species *R* to be significantly different from 5 out of20 other species along axis 1 (see ANOVA and Tukey's post hoc report in the Appendix). Species *D* & *S* separated in the positive direction and species *R* separated in the negative direction. On axis 2, *An* was significantly different from 5 out of 20 species, separating in the positive direction, and *Tv* was significantly different from 4 out of 20 species, separating in the negative direction. In contrast to the ANOVA results, the PCA plot (Fig. 1) visually indicates a different pattern of separation. On the plot, it appears that: (i) *D, S, Q, E, Tv,* and *M* may form a group; (ii) *Af* and *P* another group; (iii) *Pi, Pc, N, A, Cc,* and *Cg* form a third group; (iv)*O, R, Th,* and *Flf* may form a fourth group; (v)and *An* and *Po* are probably unique. Although ANOVA recognized *D, S,* and *R* as significantly different, the clustering of the PCA plots indicate otherwise.

Analysis of the x-residuals obtained from species previously selected by the ANOVA analysis on axis 1 resulted in 5 significant and 2 important peaks for species *D*, 4 significant and 1 important peaks for species *S*, and 1 important peak for species *R* (Table 2). X-residuals of important species on axis 2 resulted in 2 significant and 3 important peaks for *An* and no significant or important peaks for *Tv* (Table 3).

In evaluating the IR spectra for the 3 species listed (*D, S,* and *R*) on axis 1, it was found that it may be the presence, absence, and/or intensity of significant peaks, and whether those peaks are shared, that is responsible for the separation in the PCA. The average IR spectrum of species *D* has IR peaks at 1738 and 1407 which are not present in any of the other species; it also lacks peak 1380, which is present in the other 2 species. The average IR spectrum of species *S* has peaks 2980, 2970, and 2890, which are not present in the average spectra of other ANOVA-selected species. Species *R* has peaks at 1655 and 1080 in its average spectrum; these peaks are not present in any of the other ANOVA-selected species. Peaks 1596, 1458, 1276, 1174, and 1116 were not picked on any of the spectra using criteria described above (Table 4). However, it is possible that the absence of these peaks separates them from some of the other 17 out of 20 species that did not statistically exhibit high levels of separation on axis 1. In evaluating the spectra for the 2 species pulling on axis 2, none of the peaks identified are present on the average IR spectra of either species.

FTIR-ATR of dried fungi

The PCA resulted in axis 1 accounting for 67.2% of the variability, axis 2 for 15.5%, and axis 3 for 6.5%. ANOVA of the PCA scores determined species *Cc* and *E* to be significantly different from 2 out of 20 other species and species *Q* and *Po* to be significantly different from 2 out of 20 other species along axis 1. Species *Cc* and *E* separated in the positive direction, and species *Q* and *Po* separated in the negative direction on axis 1. On axis 2, species *O* and *Flf* were significantly different from 5 out of 20 species, separating in the positive direction, and species *E* and *P* were significantly different from 6 out of 20 species, separating in the negative direction (Fig. 6). Visual interpretation of the PCA plot (Fig. 6) indicates that: (i) *Cc, E,* and *P* may form a

cluster; (ii) *Cg, Po,* and *Q* may form a group; (iii) *Flf* may cluster with *Th* and *Tv*; (iv) and An appears to be unique.

Analysis of the x-residuals of ANOVA-selected fungal species on axis 1 (*Cc, E, Q, Po*) resulted in 6 significant and 4 important peaks for species *Cc,* 2 significant and 0 important peaks for species *E*, 0 significant and 2 important peaks for species *Q*, and 3 significant and 5 important peaks for species *Po* (Table 5). X-residuals of ANOVA-selected species on axis 2 (*O, Flf, E, P*) resulted in 0 significant and 2 important peaks for species *O*, 1 significant and 3 important peaks for species *Flf*, 2 significant and 0 important peaks for species *E*, and 0 significant and 2 important peaks for species *P* (Table 6).

In evaluating the average IR spectra for the 4 species listed (*Cc, E, Q, Po*), it may be the presence, absence, and/or intensity of significant peaks and whether those peaks are shared that is responsible for the separation in the PCA. The average IR spectrum for *Cc* has peaks at 2980, 2885, and 933 which are not present in any of the ANOVA-selected species; *Cc* also shares peak 1156 with *E*. Species *Cc* lacks peaks at 2930 and 772, which are present in *E, Q,* and *Po*. The average IR spectrum for species *E* has peaks 1745 and 1265 which are not present in *Cc, Q,* and *Po*. Species *E* shares 1628 with *Po*, 1156 with *Cc*, and 2930 and 772 with *Q* and *Po*. Species *Q* shares 2930 and 772 with *E* and *Po* and 1410 with *Po*. Species *Po* shares 2930 and 772 with *E* and *Q*, 1410 with *Q*, and 1628 with *E.* Peaks at 1770, 1721, 1658, 1583, 1520, 1242, 1060, 1010, 986, and 960 were not picked based on the criteria used (explained above) on any of the spectra. However, it is possible that the absence of these peaks separates them from some of the other 16 out of 20 fungi that did not exhibit high levels of separation on axis 1.

Evaluation of the average IR spectra for the 4 species selected by ANOVA (*O, Flf, E, P*) on axis 2 found that it may be the presence, absence, and/or intensity of significant peaks, and whether those peaks are shared, that is responsible for the separation in the PCA. The average

IR spectrum of species *O, E,* and *P* share the same significant and important peaks with peaks present at 2850 and 1745. They exhibit no unique or unshared peaks. Species *Flf* has a peak at 2980 (unshared), 1745 (shared) and lacks the shared peak at 2850. Peaks at 1776, 1520, 1119, and 1012 were not identified on any of the spectra using the criteria noted above. However, it is possible that the absence of these peaks separates them from some of the other species that did not exhibit high levels of separation on axis 2 (Table 8).

KBr Transmission IR of dried fungi

The PCA of dried, KBr-ground fungi resulted in axis 1 accounting for 57.8% of the variability, axis 2 for 20.5% , and axis 3 for 6.8%. ANOVA of the PCA scores determined species *Q* to be significantly different from 4 out of 20 other species and species *E* to be significantly different from 2 out of 20 other species along axis 1, with species *Q* pulling in the positive direction, and species *E* pulling in the negative direction. On axis 2, no species were significantly different than any others. Visual interpretation of the PCA plot (Fig. 7) indicates high levels of overlap between many species, as there are high levels of variability within species in this data set. However, it appears that: (i) *E, Flf,* and *S* may form a group (possibly including *D*); (ii) *Th* and *Af* may form a cluster; (iii) and *Q* is probably unique.

Analysis of the x-residuals of important species on axis 1 (*Q, E*) resulted in 2 significant and 7 important peaks for species *Q*, and 0 significant and 2 important peaks for species *E* (Table 9).

Upon evaluation of the average IR spectra for species *Q* and *E*, it was found that it may be the presence, absence, and/or intensity of significant peaks, and whether those peaks are shared, that is responsible for the separation in the PCA. The average IR spectrum of species *Q*

and *E* share a peak at 2925. All other selected peaks were not found on either spectrum (Table 10).

Discussion

Among the three data sets (living FTIR-ATR, dried FTIR-ATR, and dried-KBr-transmission FTIR) of fungal spectra, there is considerable variation in which fungal species' spectra statistically separate as being different from the others. In the living FTIR-ATR data set, species *D, S, R, An* and *Tv* are responsible for separation in the PCA analysis. In the dried FTIR-ATR data set, an entirely different group of fungal spectra account for the separation on the PCA plot: *Cc, E, Q, Po, O, FLF,* and *P*. In the dried-KBr-ground fungal data set, *Q* and *E* are responsible for differences in the spectra. The only species that cause separation in more than one data set are *Q* and *E*, both in the dried treatment and the dried-KBr-ground transmission spectra. This may be attributable to the similar chemistry of fungal wall materials and internal cellular components across all fungi, whereas living fungi will often produce unique secondary metabolites, particularly when stressed.

Further, there does not appear to be any grouping together of morphologically similar fungi (i.e. species *M* and *S*). Fungi isolated from the leaf litter, whether it was oak or huckleberry or from the upper or lower layer of litter, did not separate distinctly from one another or the known species obtained from lab cultures. There appears to be no pattern to the separation in any of the three data sets that is attributable to macroscopic features or microhabitat (upper or lower leaf litter). However, statistical analysis provides evidence that in each treatment, there are fungi whose spectra are significantly different from the others. If there is no macroscale pattern to account for these differences, perhaps it is at the microscale that the differences are important.

In addition to general differences in spectra between the treatments, there is considerable variation within each treatment with 5 (living FTIR-ATR) and 7 (dried FTIR-ATR) species being significantly different on the first 2 axes. The exception is the dried-KBr-ground transmission IR data set, which resulted in only 2 significantly different fungal species on axis one and no significantly different species on the second axis. This lack of separation may be explained by the process of KBr sample preparation and similarity of internal cellular components. During the FTIR-ATR sample collection procedure, only the external surface of the hyphae was being analyzed. This should result in chemical signals originating from exudates, cell wall material, and plasma membrane components. In the preparation of KBr sample pellets the fungal mycelium is ground, releasing the intracellular components.

When analyzing the results of all three datasets and determining the significant and important peaks within each data set, it became clear that the absence of peaks within spectra was as critical to separation of PCA results as the presence of particular peaks. Therefore, it is not only a matter of the peaks present on an IR spectrum, but also a matter of the peaks that are not present on an IR spectrum in comparison to the entire dataset that determines its uniqueness.

The factor loading plots generate an overall view of which peaks caused the PCA separation across all species, but the x-residuals identify what peaks were key in causing separation of specific species. Although the factor loading plots are informative, one of the major drawbacks is the relative commonness of very large band widths. For example, in figure 4 there is a large section of the factor loading plot between 1733 cm^{-1} and 835 cm^{-1} that is entirely above the zero line. It is impossible to tell from the loading plot alone which sections of this were actually meaningful in separation of species spectra without deconvolution. Essentially, there are peaks within peaks that cannot be distinguished (Fig. 8).

By examining the x-residuals, it is possible to determine which peaks are specifically responsible for the uniqueness of the species' spectra that did separate using ANOVA. When these peaks are compared with the factor loading plots, they are present, but not necessarily as distinct peaks. Figure 4 represents the factor loading plot of axis 1 for the dried-KBr-ground transmission IR data set. ANOVA interpretation indicates that species *Q* and *E* (positive and negative, respectively) are responsible for separation along that axis. Upon x-residual analysis of the *Q* replicates, all 3 replicates have a positive peak at 1776 and all 3 replicates have a negative peak at 1610. The x-residuals from species *Q* also indicate that 2 out of 3 replicates have positive peaks at 1184, 1140, and 935 and negative peaks at 1636, 1586, 1427, and 1220. All of these peaks, except 1776 fall within the range of 1733 cm^{-1} – 835 cm^{-1}, and many of them are located WITHIN other broader peaks. X-residual analysis of *E* resulted in 2 wavenumbers, 2925 and 2980, both present in 2 out 3 replicates pulling in the positive direction. Both are present as distinct peaks on the factor loading plot, however, the 2925 peak is essentially at the zero line. Even more interesting, 2925 is the ONLY peak of the selected wavenumbers that is present on the actual IR spectra of both *Q* and *E*.

Recall that positive peaks on the x-residuals indicate a higher intensity of that peak is present on the actual IR spectrum than the other 59 spectra and negative peaks on the x-residual indicate a lower intensity of that peak on the actual IR spectrum compared to the other 59 spectra in the data set. This leads to the incorrect assumption that if a peak is positive on the x-residual it will be present on the actual IR spectrum. For both *Q* and *E*, none of the positive peaks from the x-residual analysis were present on the actual IR spectrum except 2925 cm^{-1}. This is an indication that separation may be more an artifact of peaks that are not distinctly present, but differ in intensity. A difference in intensity (absorbance, y-axis) on the original IR

spectrum may be present due to slopes, shoulders, or distinct peaks being obscured within broader peaks.

Most fungal spectra within all the datasets were remarkably similar along a continuum in their major peaks (those with high intensities); however, it was the minute differences at particular wavenumbers in the extreme spectra that resulted in separation of spectra of specific species. For example, figure 9 shows two average spectra from the ATR-Living data set: average *D* and average *R*. Spectra are shown overlaid (Fig. 9a) and stacked (Fig. 9b) for ease of viewing peak numbers. There are clear differences between the average spectra of these two species, however when the average spectrum of each of the twenty fungi are overlaid (Fig. 10), it is clear that there is a continuum connecting one extreme to the other. It is this range of spectral overlap that accounts for the little variation found in whole-spectrum analysis of fungal species.

The functional groups represented by the IR peaks that resulted in separation in all datasets are fairly common in organic compounds, making it nearly impossible to determine specific compounds responsible for the differences between fungal spectra (Table 11). The structures for the most common fungal compounds, chitin, trehalose, and ergosterol (Figs. 11-13) are evidence of this similarity. All three compounds include ring structures and OH groups. Chitin and trehalose contain ether linkages (C-O-C), but ergosterol does not. Chitin also contains NH groups and carbonyls, trehalose and ergosterol do not. Many fungi are known to have melanin in their cell walls, a brown or black pigment that protects from UV radiation or may aid in pathogenicity. Fungal melanin structures have been difficult to precisely determine (Casadevall *et al.*, 2012), however it is known that they form by the oxidation of phenolic precursors, for example 3, 4-dihydroxyphenylalanine (Hanson, 2008). Without clear, known structures of the fungal melanins produced by the species being investigated, it is not possible to compare their structure with those of chitin, ergosterol, and trehalose in terms of presence

or absence of major functional groups. However, Paim *et al.* (1990) investigated the FTIR spectra of fungal melanin obtained directly from the cell or culture medium. Cell-derived melanin was obtained from 3 species of fungi. The results of this experiment indicated (i) a strong band at 1650 cm^{-1} (C=O of Amide I) was present in 2 out of 3 species' cell melanin; (ii) a band at 2940-2870 cm^{-1} (aliphatic CH) was strong in 2 out of 3 and weak in 1 out of 3 species' cell melanin; (iii) a band at 1530 cm^{-1} (NH of Amide II) was strong in 2 out of species' cell melanin; and (iv) a band at 1020-1030 cm^{-1} (C-O of carbohydrates) was strong in 2 out of 3 and weak in 1 out of 3 species' cell melanin. This study indicates that fungal melanins may contain carbonyl groups (as does chitin), aliphatic CH groups (as do many organics), NH groups (as does chitin), and C-O groups, most likely the C-O bond found in *O*-glycosidic linkages (C-O-C) of carbohydrates (as found in chitin and trehalose). Unfortunately, the bands of most organics are far from unique, and this information does not aid in indicating which fungal compounds are present or deciding what the similarities and differences are between species.

ATR of Living Fungi

Comparing published correlation charts with the peaks determined as significant or important produces information about what functional groups are meaningful in the ANOVA separation of the key species. In the living fungi treatment, species *D, S,* & *R* separated on axis one and *An* and *Tv* separated on axis two. The significant peaks on the first axis include those for carbonyls (C=O), amides I & II (C=O, NH), aliphatic alkanes (CH, CH_2, CH_3), end ethyls and methyls of lipids (CH_2, CH_3) and carboxylic acids (COOH). The peaks with lesser impact, important on axis one and significant on axis two, include those for esters of aromatic acids (C-O-C), aromatics (CH), and amide III (NH). These functional groups are consistent with

compounds expected to be found in a living fungus, such as lipids, chitin, and proteins (including enzymes).

The ANOVA analysis provides interesting information in terms of the statistical separation of species, however, visual analysis of the PCA plot (Fig. 1) highlights additional species that may be notable despite the lack of separation using ANOVA. In this data set, *D* and *S* separated in the positive direction of axis one, and *R* separated in the negative direction. On the PCA plot, species *D* and *S* are the furthest species on the right of axis one, however, they appear to form a group with *E* and *Q* along that axis. Additionally, *M* and *Tv* also appear to form a group close to the *D-S-E-Q* group, as do *P* and *Af*. In the negative direction on axis one, *R* is one of two species found furthest to the left, joined by *Flf*. Interestingly, the mean of *Flf* is slightly further to the left than *R*, however ANOVA does not recognize *Flf* as significantly different, although they appear to group together on the PCA plot.

The ANOVA resulted in *An* pulling in the positive direction on axis two and *Tv* in the negative direction. On the PCA plot, *An* is the largest positive on axis two, however *Tv* is not the lowest. *Tv* is positioned clearly above *M* and at the same level as *Po*. On axis two, there appears to be a higher level of overlap than axis one in all groups, yet *An* and *Po* appear to be unique.

There also appears to be a high level of variance between the replicates of some species, particularly *E, Cg,* and *Af*, whereas, species *N* exhibits very little variability between replicates.

ATR of dried fungi

The peaks that are observed to be significant on axis 1 for the dried treatment include the following functional groups: carbonyls (C=O), amides (II and III) (NH), aliphatic alkanes (CH, CH_2), carboxylic acid salts (COO^-), amine salts (NH_2^+), carboxylic acids (COOH), and esters of

aromatics (C-O-C). The peaks with lesser impact, those important on axis one or significant on axis two, include functional groups as follows: amide I (C=O), carbonyls, including those of γ-lactones (C=O), esters of aromatic esters OR saturated aliphatic ethers (C-O-C), aromatic ring vibrations (CH ring), aromatic-bound methyl group (Ar-CH_3), and interestingly vinyls (CH), trans (CH), and alkyl phosphates (P-O-C).

It is possible that during the drying process, some of the proteins formed carboxylic acid salts and amine salts, thus explaining their importance in this particular treatment group, but their lack of importance in the living fungi. There also appears in this group the carbonyl of γ-lactones, cyclic esters that are said to form spontaneously in the presence of a dilute acid at room temperature through condensation due to the stability of their 5-membered ring. Many fungi are known to produce polyketide lactones, including *Penicillium* and *Cladosporium* species (Hanson, 2008). The appearance of a vinyl CH band was also interesting in this group, however, further investigation revealed fungal secondary metabolites may possess a vinyl ether functional group, including griseofulvin (Hanson, 2008).

The ANOVA analysis resulted in *Cc* and *E* pulling in the positive direction on axis one and *Q* and *Po* on axis two. Visual interpretation of the PCA plot indicates that *Cc* and *E* are the most positive representative on axis one, however, *Po* and *Q* are both less negative than *Cg*. It appears that *Po, Q*, and *Cg* form a cluster on the plot. Further, species *P* seems to be unique, but near the *Cc-E* group.

Visual separation on the axis two of the PCA plot supports the ANOVA results with *O* and *Flf* being the most positive and *E* and *P* being the lowest. In addition to the cluster formed by *Po, Q,* and *Cg*, several other distinct groups seem to form. *Cc, E,* and *P* may be a group, as may *Flf, Th,* and *Tv*. This would be the first example of a group clustering that included two individuals of the same genus, *Trichoderma*. *An* and *O* are probably unique, although *O* and *Flf*

separated together in ANOVA. Although they do not cluster exclusively with one another, it is important to note that *Pi* and *Pc* are near one another on the PCA plot; both are representatives of the genus *Penicillium*. In this data set, *A, M, P,* and *E* all exhibit high levels of variance between replicates, and species *S* exhibits very little variance.

Dried-KBr-ground transmission IR fungi

Peaks observed as important or significant on axis one indicate the importance of the following functional groups in this dataset: carbonyl of γ-lactones (C=O) and primary amines (NH). The peaks of lesser significance found to be important on axis one or significant on axis two include carboxylic acids (COOH), carboxylic acid salts (COO^{-}), amine salts (NH_2^{+}), amide III (NH), benzenes or higher esters (CH, C-O of R(C=O)OC, respectively), esters of aromatic acids (C-O-C), aromatic ring vibrations (CH ring), aromatic-bound methyl group (Ar-CH_3), and aliphatic alkanes (CH).

In the dried-KBr-ground dataset, γ-lactones, carboxylic acid salts, and amine salts are all considered important based on analysis. This is not surprising considering this sample is merely the dried sample pulverized. However, the appearance of a large number of aromatic groups (esters of aromatic acids, aromatic rings, and aromatic-bound methyl groups), and the smaller number of carboxylic acids, amides, alkanes, and carbonyls compared to the living and dried datasets is interesting, if not confounding.

On the PCA plot, *Q* is the most positive on axis one (in accordance with ANOVA results), however *D* is the most negative. The ANOVA results indicate that *E* is most responsible for separation in the negative direction*; E* is closely clustered with *D* and *Flf* on the negative side. The ANOVA resulted in no separation on axis two in this data set; however the PCA plot indicates that *Af, Th, S, Flf*, and perhaps *E* may form a group on the positive side of this axis.

All species have relatively high variance between replicates, however species *Pi, Af, Pc,* and *Tv* have very high levels. No species exhibit the low levels of variance seen in *N* (ATR-Living set) or *S* (ATR-Dried set).

Conclusions

When visually comparing the FTIR spectra of different fungi, they are remarkably similar, although statistical analysis of the spectra does indicate subtle differences. There is little congruence in the separation of species between each of the methods used, suggesting that different chemistries are being exposed and detected by each method. It is possible that the slight drying of the living fungi triggered a stress response causing the production of unique secondary metabolites. The method of freezing the fungi in liquid nitrogen would not allow for the fungus to respond to the stress in a timely manner. This would require the fungus to sense the change in temperature then activate the gene expression pathways to produce stress-mediated secondary metabolites. There was simply not enough time before the organism was completely frozen. Considering this, and the known structures of chitin, ergosterol, and trehalose, these two treatments were expected to group similarly, yet they did not. Perhaps the drying process caused salts to form, as evidenced by their presence in this treatment group, and perhaps the removal of water from the system concentrated any small amounts of organic acids produced by the fungus, enough for γ-lactones to form spontaneously. The ground samples offered less separation between species, again, most likely due to the similarities of the internal cellular components. However, the separation of ground samples was more dependent on aromatic structures than others. Perhaps this is a result of greater membrane material (including ergosterol) being exposed upon pulverizing the cells.

FTIR and FTIR-ATR are excellent tools for determining components of molecular compounds; however, their use in investigating complex mixtures of biological compounds (whole organisms, in this case) is hindered by the sheer variety of carbon-based molecules. Based on the above analysis, it is clear that there are unique and interesting chemistries occurring on the surface and within different fungal species, but FTIR and FTIR-ATR may not be the best option for separating out these differences.

Tables

Table 1. Fungal Isolates used for spectral analysis, including their description or species name (if known), abbreviation used, and source.

Isolate Abbreviation	Species or Description	Source
An	*Aspergillus niger*	JW stock
Af	*Aspergillus fumigatus*	JW stock
Cc	*Cladosporium cladosporoides*	JW stock
Cg	*Curvularia geniculate*	JW stock
Pc	*Penicillium citreonigrum*	JW stock
Pi	*Penicillium implicatum*	JW stock
Po	*Pleurotus ostreatus*	JW stock
Th	*Trichoderma harzianum*	JW stock
Tv	*Trichoderma viride*	JW stock
Flf	Fusarium-like fungus	JW stock
A	Small white colonies, covered in green conidia, thin light edges, dense, non-aerial, does not penetrate the agar, fast growth rate on PDA	Huckleberry leaf Upper litter layer
D	Pink colony, light edges, dense hyphae, non-aerial, penetrates the agar slightly, average growth rate on PDA	Oak leaf Lower litter layer
E	Brown colony, light edges, dense, non-aerial, penetrates the agar slightly, average growth rate on PDA	Oak leaf Upper litter layer
M	White colony, diffuse hyphae, somewhat aerial, does not penetrate agar, fast grower on PDA	Oak leaf Lower litter layer
N	White hyphae, green conidia isolated to very center of colonies, dense, non-aerial, does not penetrate the agar, fast grower on PDA	Oak leaf Upper litter layer
O	White colony, diffuse hyphae, somewhat aerial, does not penetrate agar, fast grower on PDA	Oak Leaf Lower litter layer
P	White and tan colony, slightly diffuse, aerial, penetrates agar slightly, fast grower on PDA	Oak Leaf Lower litter layer
Q	Appearance of A. niger. White colony, dense hyphae, slightly aerial, penetrates agar slightly, fast grower on PDA, black conidia	Huckleberry leaf Lower litter layer
R	Light pink/yellow colony, white edges, dense, aerial, penetrates agar slightly, causes PDA to change to a dark magenta, fast grower on PDA	Huckleberry Lower litter layer
S	White colony, diffuse hyphae, somewhat aerial, does not penetrate agar, fast grower on PDA	Huckleberry Lower litter layer

Table 2. FTIR-ATR analysis of living fungal samples significant on axis 1 of the PCA. Significant (present in all replicates) and important (present in 2 out of 3 replicates) IR peaks are listed. (+) denotes pulling in the positive direction on the x-residual, meaning the residual spectrum has a higher intensity at that wavenumber than the average of all the spectra. (-) denotes pulling in the negative direction on the x-residual, meaning the residual spectrum has a lower intensity at that wavenumber than the average of all the spectra.

Fungal Species	Significant IR Peaks (present in all 3 replicates)	Important IR Peaks (present in 2 out of 3 replicates)
D	1738 (+)	1174 (+)
	1655 (-)	1276 (+)
	1596 (+)	
	1458 (-)	
	1407 (+)	
S	2980 (+)	1596 (-)
	2970 (+)	
	2890 (+)	
	1380 (+)	
R		1080 (+)
		1116 (+)

Table 3. FTIR-ATR analysis of living fungal samples significant on axis 2 of the PCA. Significant (present in all replicates) and important (present in 2 out of 3 replicates) IR peaks are listed. (+) denotes pulling in the positive direction on the x-residual, meaning the residual spectrum has a higher intensity at that wavenumber than the average of all the spectra. (-) denotes pulling in the negative direction on the x-residual, meaning the residual spectrum has a lower intensity at that wavenumber than the average of all the spectra.

Fungal Species	Significant IR Peaks (present in all 3 replicates)	Important IR Peaks (present in 2 out of 3 replicates)
An	1600 (-)	1662 (+)
	1405 (-)	1067 (-)
		965 (-)

Table 4. Presence or absence of significant and important peaks in the living fungus dataset found in the FTIR spectra of *D, S,* and *R* (species separated on axis 1 of PCA) . X denotes the peak is present in the average IR spectrum of each species. Several peaks identified as causing separation were not present on any of the average spectra; these peaks have been included in the table with all three columns blank.

Peak	Present in *D* Avg. spectrum	Present in *S* Avg. spectrum	Present in *R* Avg. spectrum
2980		X	
2970		X	
2890		X	
1738	X		
1655			X
1596			
1458			
1407	X		
1380		X	X
1276			
1174			
1116			
1080			X

Table 5. FTIR-ATR analysis of dried fungal samples significant on axis 1 of the PCA. Significant (present in all replicates) and important (present in 2 out of 3 replicates) IR peaks are listed. (+) denotes pulling in the positive direction on the x-residual, meaning the residual spectrum has a higher intensity at that wavenumber than the average of all the spectra. (-) denotes pulling in the negative direction on the x-residual, meaning residual the spectrum has a lower intensity at that wavenumber than the average of all the spectra.

Fungal Species	Significant IR Peaks (present in all 3 replicates)	Important IR Peaks (present in 2 out of 3 replicates)
Cc	2980 (+)	1658 (+)
	1583 (+)	1628 (+)
	1410 (-)	1156 (+)
	1265 (+)	933 (+)
	1242 (+)	
	1060 (-)	
E	1745 (+)	
	1520 (+)	
Q		1770 (+)
		1721 (+)
Po	2885 (+)	2930 (-)
	1745 (-)	1010 (+)
	1156 (+)	986 (+)
		960 (-)
		772 (+)

Table 6. FTIR-ATR analysis of dried fungal samples significant on axis 2 of the PCA. Significant (present in all replicates) and important (present in 2 out of 3 replicates) IR peaks are listed. (+) denotes pulling in the positive direction on the x-residual, meaning the residual spectrum has a higher intensity at that wavenumber than the average of all the spectra. (-) denotes pulling in the negative direction on the x-residual, meaning the residual spectrum has a lower intensity at that wavenumber than the average of all the spectra.

Species	Significant IR Peaks (present in all 3 replicates)	Important IR Peaks (present in 2 out of 3 replicates)
O		2980 (+)
		1776 (+)
Flf	2850 (-)	1745 (+)
		1119 (-)
		1012 (-)
E	1745 (+)	
	1520 (+)	
P		1458 (-)
		1032 (+)

Table 7. Presence or absence of significant and important peaks of the dried fungi dataset found in the FTIR spectra of *Cc, E, Q* and *Po* (species separated on axis 1 of PCA). X denotes the peak is present in the average spectrum. Several peaks identified as causing separation were not present on any of the average spectra; these peaks have been included in the table with all three columns blank.

Peak	*Cc* Average	*E* Average	*Q* Average	*Po* Average
2980	X			
2930		X	X	X
2885	X			
1770				
1745		X		
1721				
1658				
1628		X		X
1583				
1520				
1410			X	X
1265		X		
1242				
1156	X	X		
1060				
1010				
986				
960				
933	X			
772		X	X	X

Table 8. Presence or absence of significant and important peaks found in the FTIR spectra of *O, Flf, E* and *P* (species separated on axis 2 of PCA) . X denotes the peak is present in the average spectrum. Several peaks identified as causing separation were not present on any of the average spectra; these peaks have been included in the table with all three columns blank.

Peak	*O* Average	*Flf* Average	*E* Average	*P* Average
2980		X		
2850	X		X	X
1776				
1745	X	X	X	X
1520				
1119				
1012				

Table 9. FTIR analysis of dried-KBr ground fungal samples significant on axis 1 of the PCA. Significant (present in all replicates) and important (present in 2 out of 3 replicates) IR peaks are listed. (+) denotes pulling in the positive direction on the x-residual, meaning the residual spectrum has a higher intensity at that wavenumber than the average of all the spectra. (-) denotes pulling in the negative direction on the x-residual, meaning the residual spectrum has a lower intensity at that wavenumber than the average of all the spectra.

Species	Significant IR Peaks (present in all 3 replicates)	Important IR Peaks (present in 2 out of 3 replicates)
Q	1776 (+)	1636 (-)
	1610 (-)	1586 (-)
		1427 (-)
		1220 (-)
		1184 (+)
		1140 (+)
		935 (+)
E		2925 (+)
		2980 (+)

Table 10. Presence or absence of significant and important peaks found in the FTIR spectra of *Q* and *E* (species separated on axis 1 of PCA. X denotes the peak is present in the average spectrum. Several peaks identified as causing separation were not present on any of the average spectra; these peaks have been included in the table with all three columns blank.

Peak	*Q* Average	*E* Average
2925	X	X
2980		
1776		
1636		
1610		
1586		
1427		
1220		
1184		
1140		
935		

Table 11. Band assignments for peaks thought to be responsible for PCA/ANOVA separation of spectra, includes all three data sets.

Wavenumber (cm^{-1})	Significant functional group(s) responsible for vibrations	Proposed band assignment	Reference	Data set including this wavenumber
2980	CH	Aliphatic alkane	Socrates (2001)	ATR Living ATR Dry KBr
2970	CH	Aliphatic alkane	Pretsch *et al.* (1983); Socrates (2001)	ATR Living
2930, 2925	Ar-CH_3	Aromatic-methyl group	Pretsch *et al.* (1983); Socrates (2001)	ATR Dry KBr
2890, 2885	CH	Aliphatic alkane	Socrates (2001)	ATR Living ATR Dry
2850	CH_2	Aliphatic alkane	Socrates (2001)	ATR Dry
1770, 1776	C=O	γ-lactones	Socrates (2001)	ATR Dry KBr
1745	C=O	Saturated aliphatic ketones	Socrates (2001)	ATR Dry
1738	C=O	Aliphatic aldehydes, conjugated carbonyl structures	Socrates (2001)	ATR Living
1721	C=O	Saturated aliphatic ketones or aldehydes	Socrates (2001);	ATR Dry
1655, 1658	C=O	Amide I	Mantsch & Chapman (1996)	ATR Living ATR Dry
1628, 1636	C=O	o-Hydroxy- and o-amino-aryl aldehydes	Socrates (2001);	ATR Dry KBr
1610	NH C=C	Primary amine aromatic	Socrates (2001) Socrates (2001)	KBr
1596, 1600	NH C=C	Primary amine aromatic	Socrates (2001) Socrates (2001)	ATR Living
1583, 1586	NH_2^+ CO_2^-	Amine salts Carboxylic acid salts	Socrates (2001) Socrates (2001)	ATR Dry KBr
1520	NH	Amide II	Socrates (2001)	ATR Dry
1458	CH_2 or CH_3	Aliphatic alkane	Pretsch *et al*. (1983); Vane (2003)	ATR Living

1427	CH	carboxylic acid, aliphatic aldehyde	Socrates (2001)	KBr
1407, 1405, 1410	OC-OH CH_3	Carboxylic acid Lipids (bending of end ethyl groups and branched methyl groups of lipids)	Pretsch *et al*. (1983) Erukhimovitch *et al*.(2007)	ATR Living ATR Dry
1380	CH_3	End methyl	Pretsch *et al*. (1983); Mantsch & Chapman (1996)	ATR Living
1276	C-O C-O-C NH	Carboxylic acid dimers Aromatic ester Amide III	Pretsch *et al*. (1983); Socrates (2001)	ATR Living
1265	C-O C-O-C NH	Carboxylic acid dimers Ester Amide III	Pretsch *et al*. (1983); Socrates (2001)	ATR Dry
1242	C-O C-O-C NH	Carboxylic acid dimers Ester Amide III	Pretsch *et al*. (1983); Socrates (2001)	ATR Dry
1220	C-O NH	Carboxylic acid dimers Amide III	Pretsch *et al*. (1983); Socrates (2001)	KBr
1184	CH C-O	p-substituted benzenes propionates and higher esters, formates	Socrates (2001)	KBr
1174	CH C-O	aromatic propionates and higher esters, formats	Pretsch *et al*. (1983); Socrates (2001)	ATR Living
1156	C-O-C	Esters of	Socrates (2001)	ATR Dry

		aromatic acids Saturated aliphatic ethers		
1140	C-O-C	Esters of aromatic acids Saturated aliphatic ethers	Socrates (2001)	KBr
1116	CH C-O	p-substituted benzenes Esters of aromatic acids Saturated aliphatic ethers	Pretsch *et al*. (1983); Socrates (2001)	ATR Living
1080	CH C-O C-O, C-C, COH	aromatic Esters of aromatic acids Saturated aliphatic ethers Carbohydrates	Pretsch *et al*. (1983);Mantsch & Chapman (1996); Socrates (2001) Erukhimovitch *et al*. (2007)	ATR Living
1060	C-O	Esters of aromatic acids Saturated aliphatic ethers	Socrates (2001)	ATR Dry
1010	P-O-C C-O	Alkyl phosphates Carbohydrate (at 1020, shifted)	Socrates(2001)	ATR Dry
986	CH	vinyls	Socrates (2001)	ATR Dry
960	CH	Trans	Socrates(2001)	ATR Dry
933, 935	CH ring	aromatic	Socrates (2001)	ATR Dry KBr
772	CH ring	Aromatic, o-substituted benzenes, monosubstituted benzenes	Socrates (2001)	ATR Dry

Figures

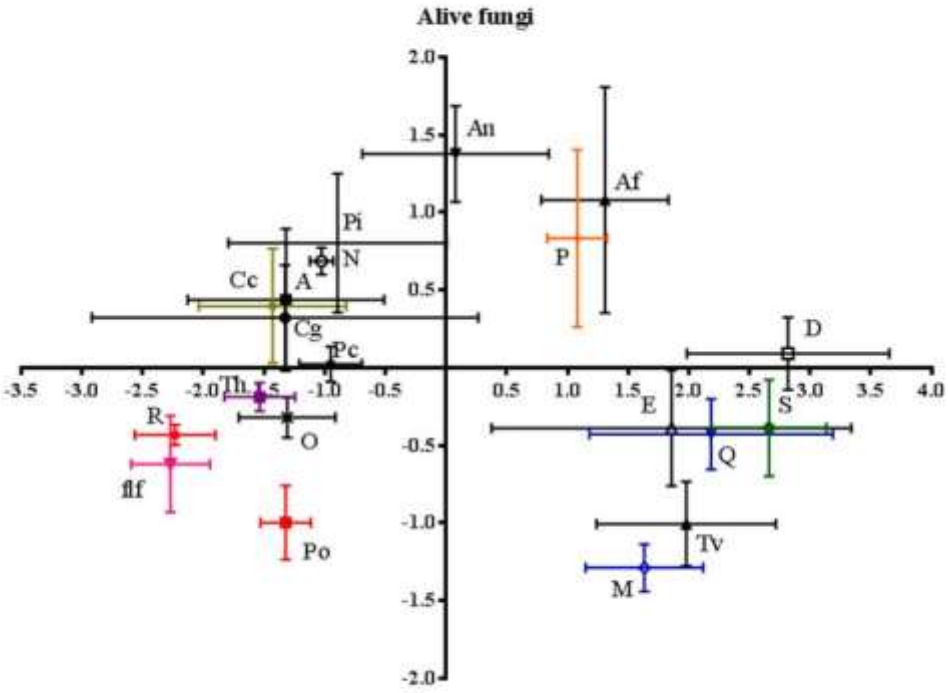

Figure 1. PCA plot of coordinate scores of living fungi in microscopic ATR FT-IR spectral space dataset. Error bars represent standard errors. For Axis 1 $F=5.56$, $P < 0.0001$. For Axis 2 $F=4.76$, $P<0.0001$.

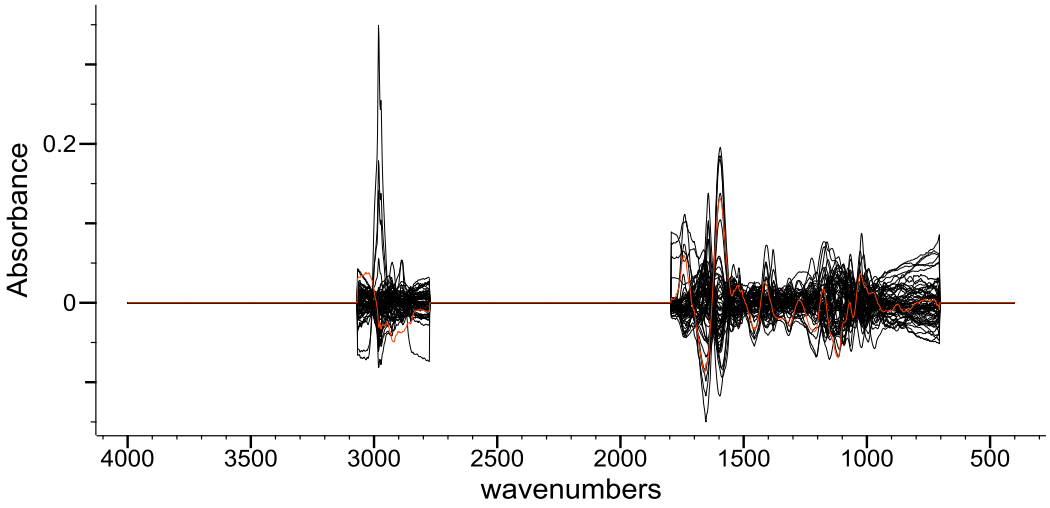

Figure 2. A sample x-residual with one spectrum highlighted for contrast. The black background is formed from overlapping the other 59 spectra in the dataset.

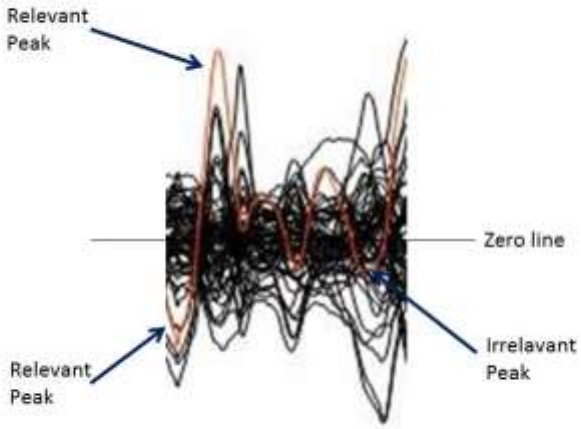

Figure 3. A region of an x-residual illustrating how relevant peaks were determined. Relevant peaks for a spectrum are those exceeding in intensity at a given wavenumber by 5 or fewer different spectra.

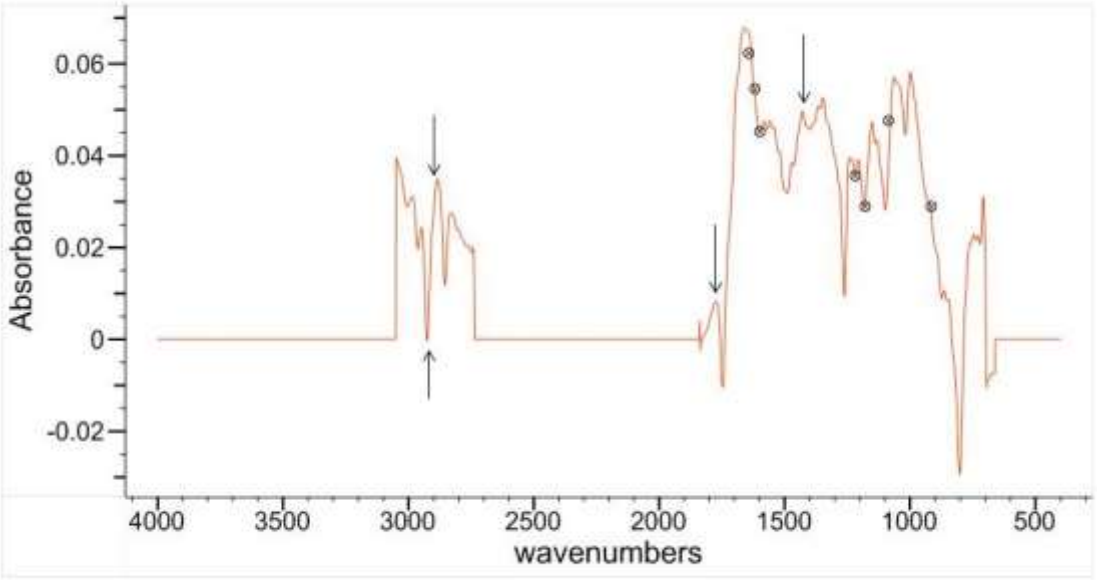

Figure 4. The factor loading plot of axis 1 generated using the ATR-Living data set in KnowItAll®. Deviation on the positive side (upward peak) at a specific wavenumber indicates "pulling" positively along the axis in the PCA analysis, whereas a negative deviation (downward peak) at a specific wavenumber indicates pulling in the negative direction along that axis. The arrows indicate distinct peaks that were identified as either significant or important wavenumbers during x-residual analysis of the 2 species responsible for separation on this axis (Q and E, positively and negatively, respectively). The circles also indicate wavenumbers deemed important upon x-residual analysis, yet they do not form distinct peaks in the factor loading plot.

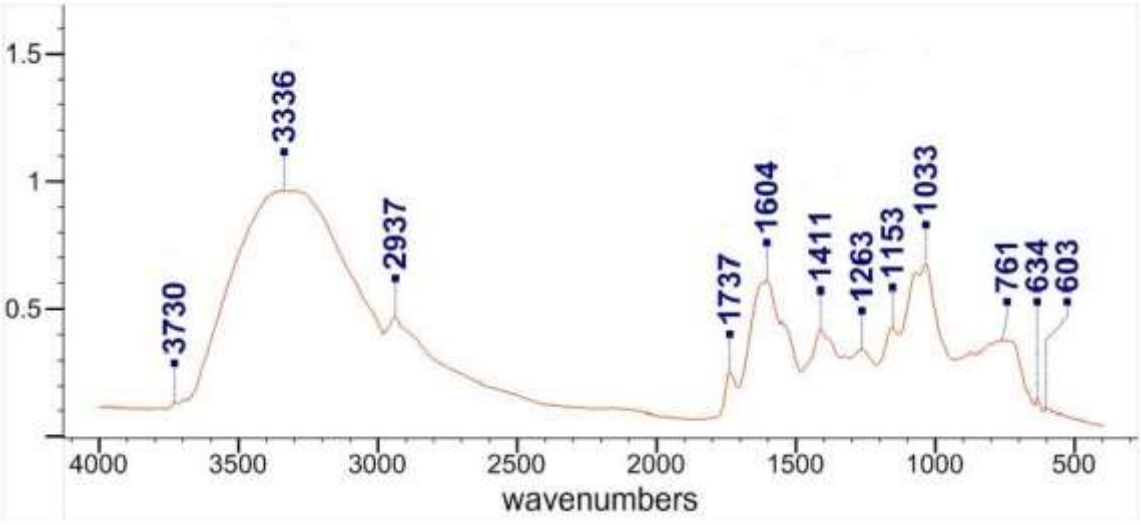

Figure 5. The average spectrum for species D; peaks selected by KnowItAll software. Peaks with a minimum intensity of 8% and maximum noise of 1% are labeled.

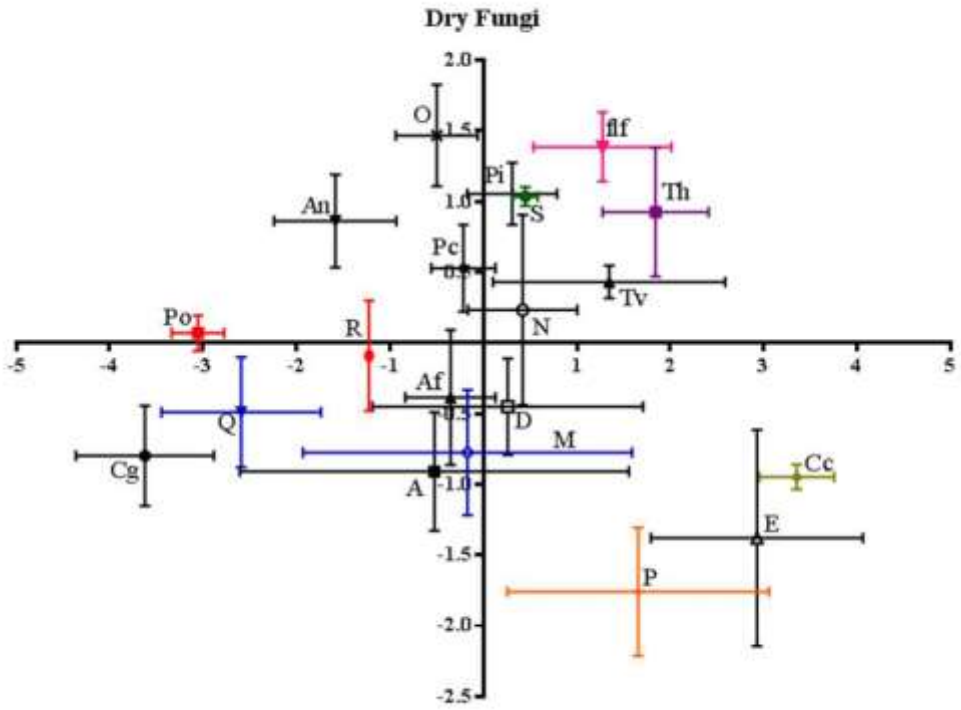

Figure 6. PCA plot of coordinate scores of dried fungi in microscopic ATR-FTIR spectral space. Error bars represent standard errors. For Axis 1 F=3.68, P = 0.0003. For Axis 2 F=5.79, P<0.0001.

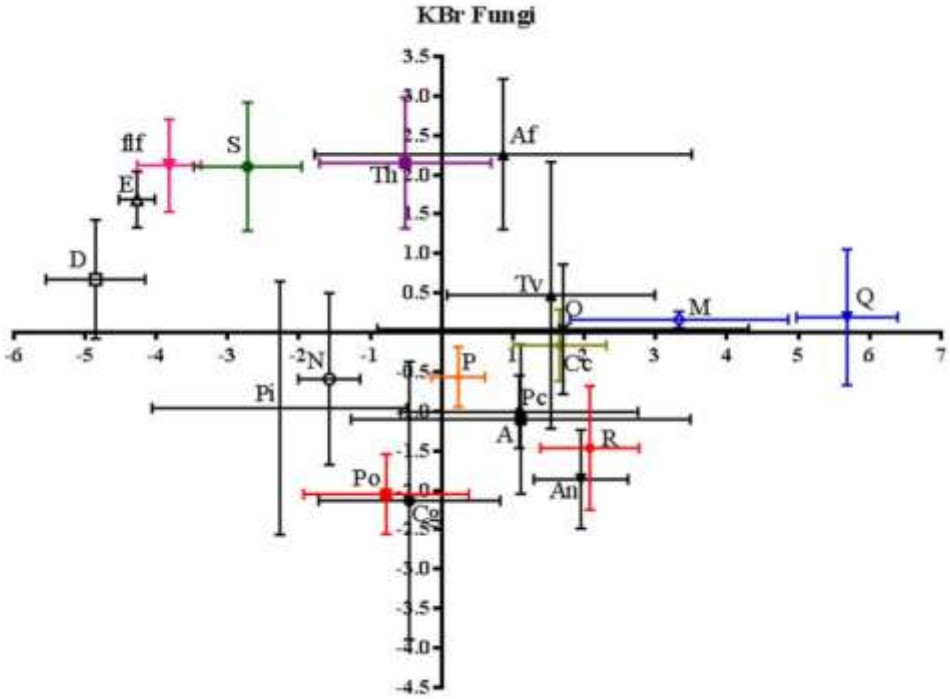

Figure 7. PCA plot of coordinate scores of dried-KBr-ground fungi in transmission FTIR spectral space. Error bars represent standard errors.For Axis 1 F=3.77, P = 0.0002. For Axis 2 F=2.47, P=0.0080.

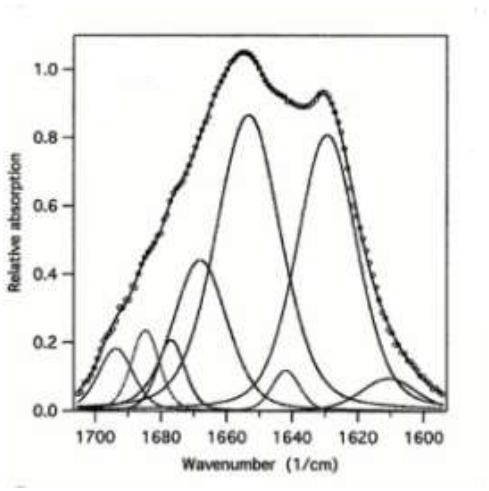

Figure 8. An example showing how large, broad peaks may obscure smaller, more distinct peaks on a FTIR spectrum, from Ahting *et al*. (2001).

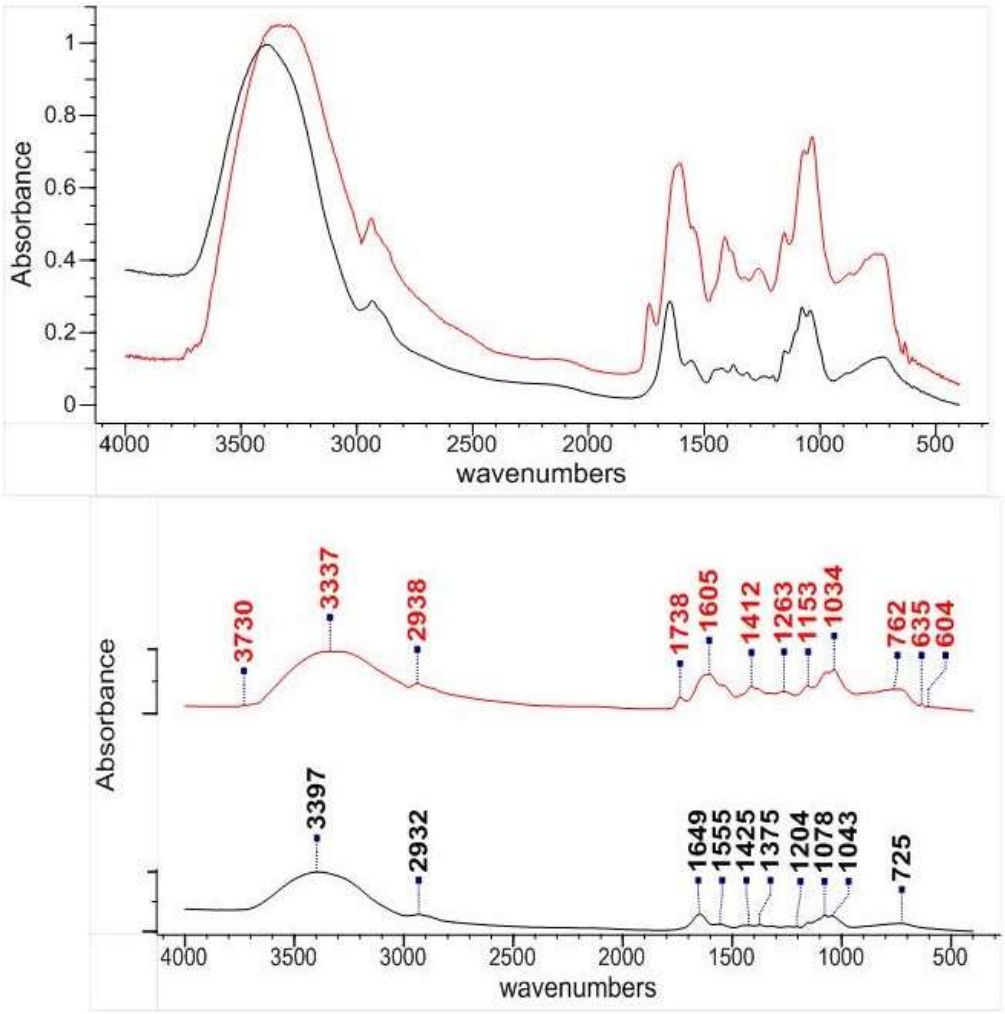

Figure 9. A comparison of the average IR spectra of D and R from the ATR-Living data set. This illustrates the overall similarities of spectra, even those that are statistically the most different. Spectra are shown overlaid (Fig. 9a) and stacked (Fig. 9b) for ease of viewing peak numbers. There are clear differences between the average spectra of these two species, however when the average spectrum of each of the twenty fungi are overlaid (see Fig. 10), it is clear that there is a continuum connecting one extreme to the other.

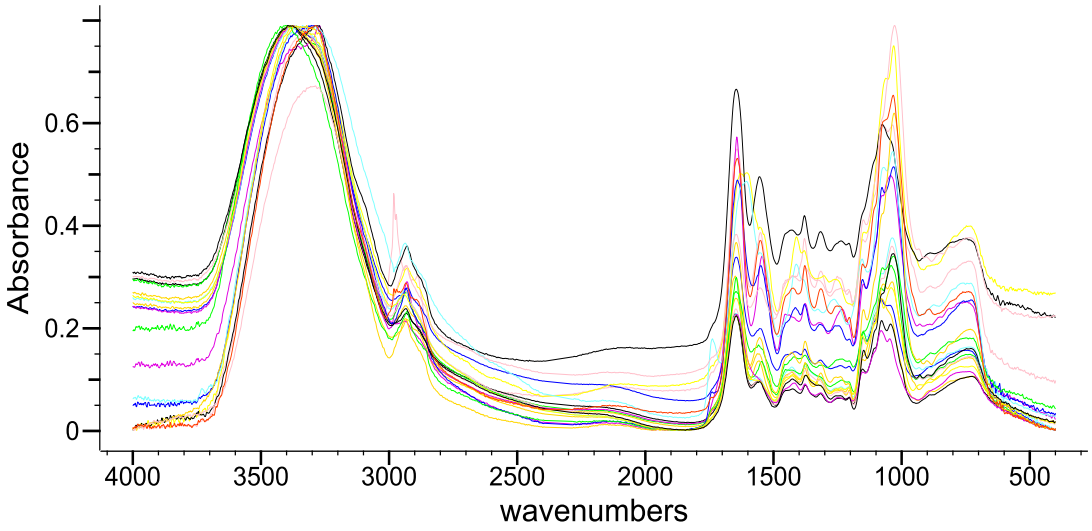

Figure 10. The three replicates for each species of fungi were averaged together to produce one average spectrum per species. This figure shows the twenty average spectra overlaid with one another. Although there are clearly spectra that represent the extremes, there is a steady continuum connecting those extremes.

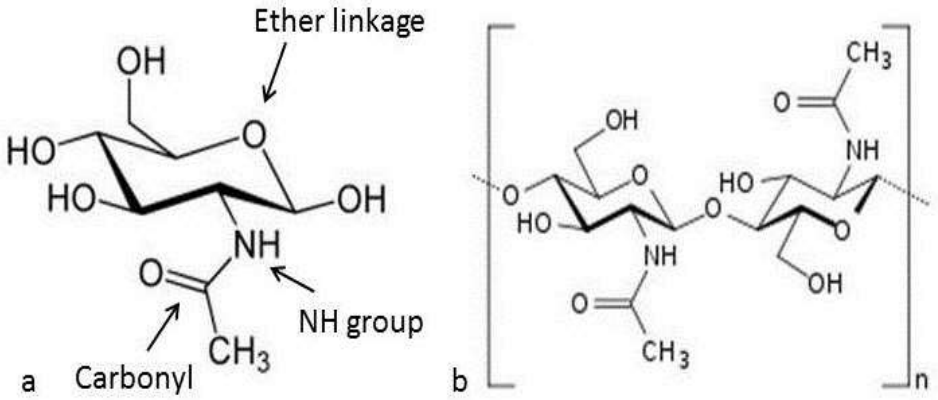

Figure 11. (a)The chemical structure of *N*-acetylglucosamine, the monomer of chitin. (b) Two monomers of *N*-acetylglucosamine linked together through an ether linkage to form the chitin polymer. Note the presence of ether linkages, carbonyls, NH groups in chitin.

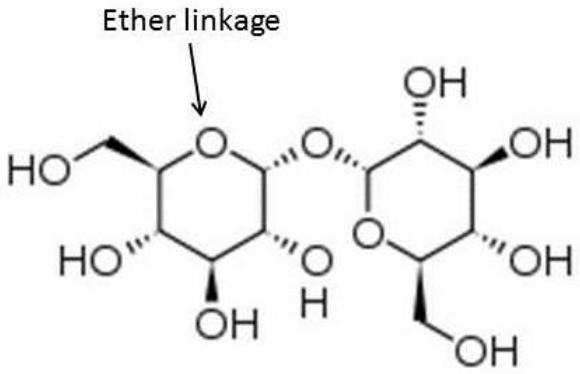

Figure 12. The chemical formula of trehalose, a common sugar produced by many species of fungi. Note that trehalose lacks carbonyl groups and NH groups that are present in chitin.

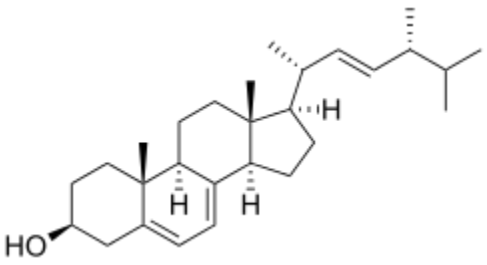

Figure 13. The chemical formula of ergosterol, a sterol found exclusively in the plasma membranes of nearly all fungi. Note the structure is primarily CH groups; ergosterol lacks ether linkages (as found in chitin and trehalose) and carbonyl and NH groups (as found in chitin).

References

Ahting U, Thieffry M, Engelhardt H, Reiner H, Neupert W, Nussberger S. 2001. Tom40, the pore-forming component of the protein-conducting TOM channel in the outer membrane of mitochondria. *The Journal of Cell Biology*, 153(6): 1151-1160.

Casadevall A, Nakouzi A, Crippa PR, Eisner M. 2012. Fungal melanins differ in planar stacking distances. *PLoS ONE* 7(2): e30299.doi:10.1371/journal.pone.0030299

Dogan A, Ergen K, Budak F, Severcan F. 2007. Evaluation of disseminated candidiasis on an experimental animal model: a Fourier transform infrared study. *Applied Spectroscopy* 61: 199-203.

Duygu DY, Baykal T, Acikgoz I, Yildiz K. 2009. Fourier transform infrared (FT-IR) spectroscopy for biological studies. *G.U. Journal of Science* 22(3): 117-121.

Erukhimovitch V, Tsror L, Hazanovsky M, Talyshinsky M, Souprun Y, Huleihel M. 2007. Early and rapid detection of potato's fungal infection by Fourier transform infrared microscopy. *Applied Spectroscopy* 61: 1052-1056.

Hanson JR. 2008. The Chemistry of Fungi. RSC Publishing, Cambridge, UK.

Jilkine K, Gough KM, Julian R, Kaminshyj SGW. 2008. A sensitive method for examining whole-cell biochemical composition in single cells of filamentous fungi using synchrotron FTIR spectromicroscopy. *Journal of Inorg. Biochem.* 102: 540-546.

Johnson TJ, Su YF, Valentine NB, Kreuzer-Martin HW, Wahl KL, Williams SD. 2009. The infrared spectra of *Bacillus* bacteria part I: vegetative *Bacillus* versus sporulated cells and the contributions of phospholipids to vegetative infrared spectra. *Applied Spectroscopy* 63: 899-907.

Kansiz M, Heraud P, Wood B, Burden F, Beardall J, McNaughton D. 1999. Fourier transform infrared microspectroscopy and chemometrics as a tool for the discrimination of cyanobacterial strains. *Phytochemistry* 52: 407-417.

Mantsch HH, Chapman D. 1996. Infrared Spectroscopy of Biomolecules. Wiley-Liss, New York, NY.

Movasaghi Z, Rehman S, Rehman I. 2008. Fourier transform infrared (FTIR) spectroscopy of biological tissues. *Applied Spectroscopy Reviews* 43(2): 134-179.

Naumann A, Navarro-Gonzalez M, Peddireddi S, Kues U, Polle A. 2005. Fourier transform infrared microscopy and imaging: detection of fungi in wood. *Fungal Genetics and Biology* 42: 829-835.

Paim S, Linhares LF, Mangrich AS, Martin JP. 1990. Characterization of fungal melanins and soil humic acids by chemical analysis and infrared spectroscopy. *Biology and Fertility of Soils* 10: 72-76.

Pretsch E, Clerc T, Seibl J, Simon W. 1983. Tables of Spectral Data for Structure and Determination of Organic Compounds. Springer-Verlag, Berlin, Germany.

Salzer R, Siesler HW. 2009. Infrared and Raman Spectroscopic Imaging. Wiley-VCH, Weinheim, Germany.

Socrates G. 2001. Infrared Characteristic Group Frequencies, 3rd ed. John Wiley & Sons, West Sussex, UK.

Stewart D. 1996. Fourier-transform infrared microspectroscopy of plant tissues. *Applied Spectroscopy* 50: 357-365.

Szeghalami A, Kaminskyj S, Gouch KM. 2007. A synchrotron FTIR microspectroscopy investigation of fungal hyphae grown under optimal and stressed conditions. *Anal. Bioanal. Chem.* 387: 1779-1789.

Vane CH. 2003. Monitoring decay of black gum wood (*Nyssa sylvatica*) during growth of shiitake mushroom (*Lentinula edodes*) using diffuse reflectance infrared spectroscopy. *Applied Spectroscopy* 57: 514-517.

CHAPTER THREE

Temporal changes in chemical composition of three litter species during field decomposition using Fourier transform infrared-attenuated total reflectance microspectroscopy

Introduction

Decomposition of leaf litter is the primary process for nutrient cycling in terrestrial ecosystems, with a large proportion of the products of primary productivity being respired by the decomposer food chain (Satchell, 1974). Litter quality (i.e. composition of the litter) has long been known to influence decomposition rates (Dickinson and Pugh, 1974; Cadish and Giller, 1997), and different species of plant produce leaf litter of varied quality (Daubenmire and Prusso, 1963; Johansson, 1995; Melillo, Aber, and Muratore, 1982). The decomposition of leaves has been observed in bulk studies of litter bags or individual leaves. In these studies, the compositional changes within the leaf and the successive changes in the decomposer community within and on the leaf are well documented (Ponge, 1991; Frankland, 1998; Jensen, 1974; McTiernan *et al*., 2003, Fioretto *et al*., 2005).

White oak (*Quercus alba*), pitch pine (*Pinus rigida*), and black huckleberry (*Gaylussacia baccata*) are common plant species found in the NJ Pinelands. Although the *exact* chemical composition (and ratios) of their leaf litters are not known, it can be inferred that each species produces a distinct complement of organic molecules that vary in relative quantities based on previous studies. Lammers, Dighton, and Arbuckle-Keil (2009) used FTIR to investigate the chemical composition of these exact species during thermal decomposition as part of a larger study on the effects of prescribed burning in the NJ pine barrens. That study found that unburned leaves of these species produced FTIR spectra with several shared chemical signatures, but were overall chemically different from one another. In addition to differences

between species, there is heterogeneity within a species and within individual leaves or needles. This multi-tier chemical heterogeneity renders them perfectly suited to act as variable substrate choices for the assembly of a decomposer community.

Fourier Transform Infrared (FTIR) spectroscopy and microscopic FTIR-ATR (attenuated total reflectance) were utilized in chapter 2 to investigate fungal chemical signatures. In this chapter, FTIR-ATR is applied to leaf litter decomposition over a 12 month period. There exists a large body of research using FTIR or FTIR-ATR to produce spectra of plant-produced macromolecules or plant tissues. Xiao, Sun, and Sun (2001) extracted lignin and hemicelluloses from de-waxed maize stems, rye straw, and rice straw to determine chemical structure of those compounds. Kubo and Kadla (2005) obtained commercially produced hardwood and softwood lignin to investigate differences in the lignin of different wood types. Michell (1990) studied celluloses from algae, bacteria, cotton, ramie, and wood, and found those celluloses separated into two primary chemical groups, algal-bacterial cellulose and cotton-ramie-wood cellulose.

In addition to studies using plant extracted macromolecules, a number of studies have been performed on whole plant tissues. Stewart (1996) used FTIR to analyze flax (*Linum usitatissimum*) hypocotyls, potato tubers (*Solanum tuberosum*), bamboo (*Thamnocalamus spathaceus*) stems, and several species of nutshells. Gorgulu, Dogan, and Severcan (2007) ground leaves of the genera *Astragalus* and *Ranunculus* to characterize higher plants using FTIR. In contrast to these studies, but similar to the research of Lammers *et al.* (2009), the research presented here attempts to characterize the macromolecular components of leaves at the level of the individual fungal hypha and track changes in those components during a 12-month field decomposition study. Determining the chemical changes occurring within leaves during natural field decomposition using microscopic FTIR-ATR lays the ground work for the potential to relate

microscale heterogeneity and serial changes in the resource (the leaf) to changes in the decomposer community (particularly, the fungal community) of the NJ Pinelands.

Methods

Sample Preparation

White Oak (*Quercus alba*), pitch pine (*Pinus rigida*), and black huckleberry (*Gaylussacia baccata*) leaves were collected from trees just before senescence in a mixed pine-oak section of the NJ Pinelands. Individual leaves were collected, placed in brown paper bags and transported to Rutgers Camden for analysis. A random number table was generated and gridded transparency paper was used to number quadrats on a microscope slide. This was used to randomly select sample areas on the leaves. Leaves were mounted to a slide, oak and huckleberry leaves were mounted with the abaxial side exposed.

Initially, fifteen individual leaves from each species were analyzed using the FTIR-ATR microscope. On each oak and huckleberry leaf, three replicate regions of the vein and three of the lamina were processed using the FTIR-ATR microscope. Three locations on each pine needle were analyzed, as there are no separate lamina and vascular regions on the needle. All spectra were collected using an Agilent (formerly Bio-Rad) FTS 6000 infrared spectrophotometer with an attached UMA 500 microscope with a germanium (Ge) ATR crystal. Sixty-four scans were averaged at a resolution of 4 cm^{-1} with air as the background spectrum. Between collections of each spectrum, the Ge crystal was cleaned with isopropanol to remove any residual material.

Following the initial collection of spectra, leaves were placed individually in litter bags constructed of aluminum 1mm mesh screen (unbranded) purchased at a local hardware store. Bags measured approximately 15 x 15 cm and were sealed with standard staples. The litter bags were placed within the litter in a mixed oak-pine section of the forest. Litter bags were collected

every 60 days for 15 months, placed in plastic bags to prevent drying, and taken to Rutgers Camden for IR spectral analysis. In the laboratory, leaves were removed from the litter bags and spectra were collected using the same methods as at the initial collection. Spectra were obtained within the first 1-2 days and leaves were returned to the litter within 48 hours of collection. After 15 months, many of the leaves had considerable degradation, were possibly eaten by invertebrates or otherwise, and were no longer in the mesh bag. At 12 months, 5 leaves of each species remained intact for analysis (for this reason, the spectra at 15 months were not included in this analysis). Spectra at 0 months, 6 months, and 12 months were used in the analysis.

Spectral Analysis

Six spectral databases were created using KnowItAll® (Bio-Rad) spectral analysis software. Five databases were created based on leaf species/location on leaf: huckleberry lamina spectra, huckleberry vein spectra, oak lamina spectra, oak vein spectra, and pine needle spectra. Each database consisted of the average spectrum of three replicate spectra of each leaf species/location on an individual leaf. This resulted in 15 average spectra per database. The sixth database combined the other five into one large database consisting of 75 spectra (5 sample average spectra x 3 times x 5 species/location).

Upon importing the databases into KnowItAll®, all spectra were ATR-corrected, smoothed to 5 points, normalized, and baseline corrected (linear fit). Following creation of the databases, principal component analysis (PCA) was performed in KnowItAll®. The PCA was mean-centered with 3 factors and excluded the wavenumber ranges 2800-1800 cm^{-1} and 700-400 cm^{-1} of the spectra. The former region was excluded due to the lack of spectral vibrations in this range and the presence of the CO_2 band at 2390-2285 cm^{-1}. The latter was excluded due to

a second CO_2 band at 672-664 cm^{-1} and the presence of excess noise in the region (Fig. 1). The databases were then exported to another informatics software package, Pirouette® (Infometrix, Inc.). Pirouette® is not exclusively a spectroscopy software package, but it offers the ability to generate spreadsheets of the PCA coordinate scores (KnowItAll does not). The coordinate scores on Axes 1, 2, and 3 from the PCA analysis in Pirouette® were imported into SAS® (SAS Institute, Inc.) and one-way ANOVA was performed with a Tukey's post hoc test on the coordinate scores on each of the three primary PCA axes. In instances where Axis 3 contributed less than 10% to the variance, no further analysis was conducted on data from that axis.

The initial analysis was to review the x-residuals of each dataset to determine which spectral peaks were causing individual spectra to separate from the rest, similar to the analysis performed in chapter 2. However, the datasets were not large enough for this method to be useful, as the sample size was 25% the size.as the larger dataset in chapter 2. The 15 x-residuals of each average spectrum in the database were analyzed. Any peak, positive or negative, that separated out from the dark black center of overlapping spectra of the plot was recorded. A peak on the x-residual was determined to be relevant if it was one of the two furthest from the zero line(see Fig. 3, chapter 2). In the sixth database (with all 75 average spectra), the analysis is solely based on the factor loading plots and coordinate scores generated from the PCA; x-residuals are not included due to the lack of information provided from residual spectra.

The list of x-residual peaks for each leaf/location was then compared to the factor loading plots from the PCA. By cross-checking the factor loading plot peaks with the x-residual-obtained peaks, it was possible to create a list of those peaks that should have contributed significantly to the separation of spectra in the PCA. There were a number of peaks on the factor loading plots that were not identified by x-residual analysis. It is important to note that x-residual analysis may indicate peaks that are different from the average of all the spectra in the

database. If all the spectra have the same peak with similar intensities, or lack the same peak, this peak will not be evident on the x-residuals. However, the factor loading plot is not a comparison of each spectrum to the average. The factor loading plot is a result generated by the PCA which indicates which wavenumbers are responsible for the separation seen along a specific axis; again it does not necessarily indicate peaks that are present. As was found in chapter 2, it may be the presence or absence of particular peaks, or the intensity of those peaks that results in the particular wavenumbers found on a given factor loading plot.

The wavenumbers found on both the x-residuals and factor loading plots were then added to the PCA plot to visualize which wavenumbers were contributing to pulling on each axis. Wavenumbers are listed in decreasing order of importance on the PCA plots. These wavenumbers were then compared to the actual IR spectra in each data set. The five average spectra per leaf species/location/time were overlaid and the listed peaks were selected to compare changes in those peaks between times. Peaks within five wavenumbers of each other are considered to be essentially the same peak for the purpose of this analysis. Additionally, a visual analysis of the spectra was performed to identify other peaks or ranges of peaks that may have changed over time, but were not identified by the statistical analysis. Table 1 lists all of the important wavenumbers (as identified on the six separate PCA plots) and their corresponding functional groups. This table was used to evaluate which functional groups may be changing during decomposition.

Results

Huckleberry Lamina (HL dataset)

The principal component analysis of the huckleberry lamina dataset resulted in Axis 1 accounting for 52.4% of the variability between sampling times, axis 2 for 35.3%, and axis 3 for 3.3%. ANOVA of the PCA scores on Axis 1 resulted in time 0 and 12 months being significantly different from each other, but neither was significantly different from 6 months. On axis 2, ANOVA of the PCA indicated that time 0 and 6 months were both significantly different from 12 months, but not from each other. However, the PCA plot does not appear to represent any overlap on either Axis 1 or Axis 2 between all three times (Fig. 2).

The x-residuals for three leaves at time 0, one leaf at 6 months, and one leaf at 12 months did not possess any peaks that were determined to be relevant, indicating these five spectra were more similar to the average of all spectra in the dataset. The remaining ten leaves all had at least one peak that was one of the two most extreme at a given wavenumber. Sixty specific peaks were determined from the x-residuals and compared to the factor loadings.

On Axis 1 there were twelve strong peaks on the factor loading plot 3430(OH,NH), 2918(CH, CH_2)*, 2850(CH_2)*, 1735(C=O)*, 1600, 1462(CH_2, CH_3)*, 1370, 1322, 1173, 1093*, 1034(C-O, C-OH) *, and 713*), seven of which were on the list of x-residual wavenumbers, denoted by asterisks above (throughout the paper, the asterisk will indicate the peak was found on both the x-residuals and factor loading plots). The absence of the remaining five peaks on the x-residual analysis indicates that at those wavenumbers, all spectra were likely similar. On Axis 2 there were thirteen strong peaks on the factor loading plot (3360*, 2918(CH, CH_2)*, 2850(CH_2)*, 1735(C=O)*, 1650(C=O)*, 1530*, 1462*, 1300*, 1167, 1128*, 1034(C-O, C-OH)*, 950*, and 746), eleven of which were found on the list of x-residual wavenumbers. Table 2 lists the peaks that were found on both the x-residual analysis and factor loading plots and the sampling times at which each peak appeared on the x-residual.

The wavenumbers determined above were added to the axes of the PCA plot ranked in order from most important to least important on each axis (positive and negative sides) as determined by the factor loading plots. The PCA plot illustrates the direction of influence on each axis and which sampling times were being influenced by these peaks. On Axis 1, wavenumber 713 was important in the positive direction, and wavenumbers 2918(CH, CH_2), 2850(CH_2), 1034(C-O, C-OH), 1093, 1462, and 1735(C=O) were important peaks in the negative direction (in order of decreasing importance). On Axis 2, 2918(CH, CH_2), 2850(CH_2), 1034(C-O, C-OH), 1735(C=O), and 1462 were the important peaks in the positive direction, and wavenumbers 1650(C=O), 3360, 1530, 1300, 1128, and 950 were important in the negative direction. Based on the location of the 3 sampling times on this plot, it appears that wavenumbers 2918(CH, CH_2), 2850(CH_2), 1034(C-O, C-OH), 1093, 1462, and 1735(C=O) strongly influenced time 0 on both axes. Time 6 months appears to be weakly influenced on Axis 1 by 713, and weakly influenced by 2918(CH, CH_2), 2850(CH_2), 1034(C-O, C-OH), 1735(C=O), and 1462 on axis 2. Time 12 months was weakly influenced by 2918(CH, CH_2), 2850(CH_2), 1034(C-O, C-OH), 1093, 1462, and 1735(C=O) on Axis 1, but strongly influenced on axis 2 by 1650(C=O), 3360, 1530, 1300, 1128, and 950. Although there does not appear to be overlap of the error bars of the sampling times, the weak influence of Axes 1 and 2, and the large variability on Axis 1 at 6 months correlates with the ANOVA results that time 6 months was not significantly different from time 0 or time 12 months.

The wavenumbers pulling on the PCA plots were then compared to the actual spectra. The five average leaf spectra for each sampling time were overlaid, and the peaks listed on the PCA plots were labeled on each (Figs 3-5). At wavenumber 3360, there was an increase in intensity from 0 to 6 months to 12 months. At wavenumbers 2918(CH, CH_2) and 2850(CH_2), there was a clear decrease in intensity from 0 to 6 months to 12 months. At time 0, the intensity

of the peak at 1735(C=O) appeared to be relatively similar between the five spectra, however at 6 months and 12 months, there was more variability at this wavenumber. Wavenumber 1650(C=O) did not appear as a specific peak, but on the slope of another larger peak at time 0 and 6 months, yet at 12 months it appeared as a distinct peak. At 1530, the time 0 spectra did not appear to have a distinct peak, rather a somewhat flat region that became increasingly defined at 6 months and more so at 12 months. Wavenumber 1462 did not appear to change much between times. At 1300, there appeared to be a small peak at times 0 and 6 months, but at 12 months this small peak was no longer visible. The peak at 1128 increased from time 0 to 6 months, but then decreased from 6 months to 12 months. At 1093, there appeared to be a slight shoulder on the higher-wavenumber side (left slope) of the larger peak at 1034(C-O, C-OH). The peak at 1034(C-O, C-OH) seemed to decrease in intensity and broaden in range from time 0 to 6 months to 12 months. Wavenumber 950 appeared to be a slight shoulder on the lower-wavenumber side (right-side) slope of the large 1034(C-O, C-OH) peak across all three times, however in one spectrum at 12 months, there was a clear, distinct peak. At time 0, there was no peak at 713, but at 6 months and 12 months there appeared to be distinct peaks, despite the presence of considerable noise in the lower wavenumbers of the 6 month spectra. Wavenumbers, their correlating functional groups, and proposed biological assignments are found in Table 1 and addressed in more detail in the discussion.

Huckleberry Vein (HV dataset)

The principal component analysis of the huckleberry lamina dataset resulted in Axis 1 accounting for 51.8% of the variability between sampling times, axis 2 for 22.1%, and axis 3 for 11.8%. ANOVA of the PCA scores on Axis 1 resulted in time 0 and 12 months being significantly different from each other, but neither was significantly different from time 6 months. On Axis 2,

there was no significant difference between times, and on axis 3 times 0 and 6 months were similar, but significantly different from 12 months. The PCA plot does not appear to represent any overlap of the error bars on axis 1, however there is a large amount of variability at 6 and 12 months along Axis 1. On Axis 2 there is a large region of overlap of times 6 and 12 months due to the large amount of variability found within the 6 month samples. Although the ANOVA of PCA coordinate scores indicates no significant difference on axis 2, the PCA plot indicates that time 0 does separate along this axis (Fig. 6).

The x-residuals for two leaves at time 0 and one leaf at 6 months did not possess any peaks that were determined to be relevant, indicating these 3 spectra were more similar to the average of all spectra in the dataset. The remaining twelve leaves all had at least one relevant peak. Fifty-four specific peaks were determined from the x-residuals and compared to the factor loadings.

On Axis 1 there were thirteen strong peaks on the factor loading plot (3460, 2918(CH, CH_2)*, 2850(CH_2)*, 1735(C=O)*, 1650(C=O)*, 1580, 1465, 1364, 1320, 1252, 1167*, 1106(C-O, C-C ring)*, and 1038), however only six of those wavenumbers were on the list of x-residual peaks. The absence of the remaining seven peaks on the x-residual analysis indicates that at those wavenumbers, all spectra were likely similar. On Axis 2 there were sixteen strong peaks on the factor loading plot (2918(CH, CH_2)*, 2850(CH_2)*, 2807*, 1774*, 1735(C=O)*, 1700, 1650(C=O)*, 1632, 1556*, 1542*, 1397, 1288*, 1128*, 1090, 1029(C-O, C-OH)*, and 784), and eleven of which were found on the list of x-residual wavenumbers. For Axis 3, the factor loading plot identified fifteen strong peaks (3640, 2980(CH_3)*, 2918(CH, CH_2)*, 2850(CH_2)*, 1774*, 1735(C=O)*, 1633 1556*, 1520, 1442*, 1307, 1221*, 1128*, 950*, and 817), and ten of those were also selected from the x-residual analysis (Table 2).

The wavenumbers were added to Axes 1 and 2 of the PCA plot (Fig. 6) to better illustrate the direction of influence on each axis and which sampling times were being influenced by these wavenumbers. These values are listed in decreasing order from most important to least, as determined by their intensity on the factor loading plots. On Axis 1, wavenumbers 2918(CH, CH_2), 2850(CH_2), 1167, 1106(C-O, C-C ring), and 1735(C=O) influence the positive side, and wavenumber 1650(C=O) influences the negative side. On Axis 2, in the positive direction 2918(CH, CH_2), 2850(CH_2), 1029(C-O, C-OH), and 1735(C=O) have strong influence, and wavenumbers 1650(C=O), 1556, 1542, 1288, 2807, 1128, and 1774 have a strong influence in the negative direction. This indicates that time 0 is strongly influenced by those wavenumbers positive on Axis 1 and negative on Axis 2. Time 6 months is only slightly influenced by those numbers on the positive side of Axis 1 and the positive side of Axis 2. The error bars for the 6 month samples are quite large, covering both positive and negative regions of both axes, although the sample mean is located slightly positive on both. At 12 months, there appears to be a relatively strong influence by the wavenumbers on the negative side of Axis 1 and the positive side of Axis 2, although there is high variability (large error bar) along Axis 1. The large amount of error within 6 months data supports the ANOVA analysis that does not separate 6 months from either time 0 or 12 months on both Axis 1 and Axis 2.

The peaks influencing Axes 1 and 2 of the PCA plot were then compared to the actual spectra. The five average leaf spectra for each sampling time were overlaid as they were in the huckleberry lamina dataset, and the peaks listed on the PCA plots were labeled (Figs. 7-9). At wavenumbers 2918(CH, CH_2) and 2850(CH_2), there was a clear relative decrease in intensity from time 0 to 6 months to 12 months. No distinct peak could be identified at wavenumber 2807 on any of these spectra. At time 0 and 6 months, no specific peaks were present at wavenumber 1774. At 12 months, one discernible peak appeared in one spectrum at 1774. The

intensity of the peak at 1735(C=O) initially (time 0) appears to be relatively similar between the five spectra; at 6 months the intensities of 1735(C=O) all decreased, however at 12 months, 4 spectra continued to lose intensity, but one increased dramatically, perhaps due to the baseline correction. There was variability at this wavenumber in the huckleberry lamina dataset as well. At time 0, wavenumber 1650(C=O) appeared on the higher wavenumber side of a peak at 1635. At 6 months and 12 months, 1650(C=O) was present in all spectra as an increasingly dominant peak. At wavenumber 1556, one spectrum at time 0 had a very small peak, and two spectra at 12 months had a small peak. No distinct peak could be identified at wavenumber 1556, however at 6 months there may have been a peak obscured by a broader peak. For wavenumber 1542, there were no peaks on the time 0 spectra, but small broad peaks were noted on the 6 months spectra, and narrower, more intense peaks identified on four of the five 12 month spectra. At all three times, no distinct peak could be identified at wavenumber 1288; it was located on the higher-wavenumber side of a small peak, although after 12 months a small shoulder appeared at this wavenumber on all 5 spectra. Wavenumber 1167 was present as a distinct peak at time 0, decreasing in intensity at 6 months and no more than a small peak (on 3 spectra) or shoulder (on 2 spectra) at 12 months. There was no identifiable peak at 1128 on any time 0 or 6 months spectra. At 12 months, there was a slight rise in intensity, and one spectrum had a peak at 1128. Wavenumber 1106(C-O, C-C ring) was present on all spectra at all times as a barely discernible shoulder on the much larger, dominant peak at 1029(C-O, C-OH). All spectra at all times had a large peak at 1029. This peak had similar intensity at times 0 and 6 months and increased considerably (from 0.6 to 0.9) from time 0 to 6 months. At 12 months there was considerable variation at this peak, as all spectra changed intensity differently, resulting in a range of intensities from 0.4-0.9. Wavenumbers, their correlating functional groups, and

proposed biological assignments are found in Table 1 and are addressed in greater detail in the discussion.

Oak Lamina (OL dataset)

The principal component analysis of the oak lamina dataset resulted in Axis 1 accounting for 54.8% of the variability between sampling times, Axis 2 for 26.5%, and Axis 3 for 3.6%. ANOVA of the PCA scores on axis 1 resulted in time 0 and 6 months being significantly different from 12 months but not each other. On axis 2, ANOVA of the PCA indicated that times 6 months and 12 months were significantly different from time 0 but not from each other. However, the PCA plot indicates separation of time between all three times on Axis 1, but time 0 and 6 months overlap on Axis 2 (Fig. 10).

The x-residuals for two leaves at time 0 and two leaves at 6 months did not have any peaks that were determined to be relevant, indicating these four spectra were more similar to the average of all spectra in the dataset. The remaining eleven leaves all had at least one peak that was considered relevant based on the analysis. Fifty-four specific peaks were determined from the x-residuals and compared to the factor loadings.

On Axis 1 there were fifteen strong peaks on the factor loading plot (3407, 2980(CH_3)*, 2918(CH, CH_2)*, 2850(CH_2)*, 2807, 1774*, 1683*, 1542*, 1485, 1390*, 1301, 1180*, 1135, 1043*, and 839), and nine of those wavenumbers were on the list of x-residual wavenumbers. The absence of the remaining six peaks on the x-residual analysis indicates that at those wavenumbers all spectra were likely similar. On Axis 2 there were sixteen strong peaks on the factor loading plot (3450, 3021, 2918(CH, CH_2)*, 2850(CH_2)*, 1774*, 1740, 1650(C=O)*, 1542*, 1458, 1305, 1261*, 1195*, 1106(C-O, C-C ring)*, 1043*, 922*, and 784), and ten of those were found on the list of x-residual wavenumbers (Table 2).

These wavenumbers were added to the axes of the PCA plot (Fig. 10) to better illustrate the direction of influence on each axis and which sampling times were being influenced by these peaks. The wavenumbers were listed in decreasing order of influence. The PCA plot indicates that wavenumbers 2918(CH, CH_2), 2850(CH_2), and 1043 had a strong influence in the positive direction on Axis 1, and wavenumbers 1774, 1542, 1390, 1683, 1180, and 2980(CH_3) had a strong influence in the negative direction on Axis 1. On Axis 2, 2918(CH, CH_2), 2950, 1106(C-O, C-C ring), 1043, 1195, 1261, and 922 had a strong influence in the positive direction and wavenumbers 1650(C=O), 1542, and 1774 in the negative direction. Time 0 was strongly influenced by those peaks influencing positively on Axis 1 and negatively on Axis 2. At 6 months, wavenumbers influencing negatively on Axes 1 and 2 were most important. At 12 months, wavenumbers pulling positively on Axis 2 had the most influence and neither set of wavenumbers (positive or negative)on Axis 1 appeared to have greater influence than the other.

The wavenumbers noted on the PCA plots were then compared to the actual spectra. The five average leaf spectra for each sampling time were overlaid, and the wavenumbers listed on the PCA plots were labeled on each (Figs. 11-13). Wavenumber 2980(CH_3) was not present at time 0, but at 6 months and 12 months was present in 2 spectra. At wavenumbers 2918(CH, CH_2) and 2850(CH_2), there is no change in intensity from time 0 to 6 months, with a small decrease at 12 months. Wavenumber 1774 did not have a peak at time 0 or 6 months, but there was an increase in 1 spectrum at 12 months. The IR spectra had no identifiable peak at 1683 at all three times. The peaks at wavenumbers 1650(C=O) and 1542 were not present at time 0 and are barely discernible at 6 months, but they developed into distinct peaks at 12 months. At time 0, there were no peaks at 1390; at 6 months and 12 months there were 2 and 4 spectra (respectively) with small peaks. At 1261, there were small peaks or shoulders at all times. At wavenumber 1195, there were no peaks at time 0 or 12 months, but one spectrum at 6 months

had a small peak. At 1180, there were no distinct peaks across all spectra at all times. At wavenumber 1106(C-O, C-C ring), there was little change between times, as there were barely discernible shoulders on all spectra at all times. At wavenumber 1043, there was a considerably large peak in all spectra at all times. This peak remained similar in times 0 and 6 months, but increased in intensity at 12 months. At wavenumber 922, only 1 spectrum at 6 months had a small peak, no other spectra at any time had a notable peak at this wavenumber.

Oak Vein (OV dataset)

The principal component analysis of the oak vein dataset resulted in Axis 1 accounting for 64.2% of the variability between sampling times, Axis 2 for 25.1%, and Axis 3 for 3.7%. ANOVA of the PCA scores on both Axis 1 and Axis 2 resulted in time 0 being significantly different from both 6 and 12 months. Time 6 and 12 months are not significantly different from each other. The PCA plot indicates separation between all three times on Axis 2, but time 0 and 12 months appear to overlap on Axis 1 (Fig. 14).

The x-residuals for three leaves at time 0 did not possess any peaks that were determined to be relevant , indicating these three spectra were more similar to the average of all spectra in the dataset. The remaining twelve leaves all had at least one relevant peak. Fifty specific peaks were determined from the x-residuals and compared to the factor loadings.

On Axis 1 there were thirteen strong peaks on the factor loading plot (3440, 2918(CH, CH_2)*, 2850(CH_2)*, 1735(C=O)*, 1584, 1512, 1462*, 1355, 1247, 1166, 1106(C-O, C-C ring)*, 1036, and 718*), however only six of those wavenumbers were on the list of x-residual peaks. The absence of the remaining seven peaks on the x-residual analysis indicates that at those wavenumbers, all spectra were likely similar. On Axis 2 there were eighteen strong peaks on the factor loading plot (3430, 3220, 2980(CH_3)*, 2918(CH, CH_2)*, 2850(CH_2)*, 2790, 1780*,

1735(C=O)*, 1650(C=O)*, 1555(NH)*, 1534, 1462*, 1256, 1175, 1106(C-O, C-C ring)*, 1056*, 950*, and 784), and eleven of those were found on the list of x-residual wavenumbers (Table 2). The wavenumbers were added to the axes of the PCA plot (Fig. 14) to better illustrate the direction of influence on each axis and which sampling times were being influenced by these peaks. The peaks are listed in decreasing order from most important to least for each direction on each axis. Here the PCA plot indicates that wavenumbers 2918(CH, CH_2), 2850(CH_2), 1106(C-O, C-C ring), 1462, and 1735(C=O) had a strong influence on in the positive direction on Axis 1, and wavenumber 718 had a strong influence in the negative direction Axis 1. On Axis 2 wavenumbers 2918(CH, CH_2), 2850(CH_2), 1462, 1056, 1106, and 1735(C=O) influence the positive side, and wavenumbers 1650(C=O), 1555(NH), 1780, 2980(CH_3), and 950 were responsible for separation in the negative direction. At time 0, peaks on the negative sides of both Axes 1 and 2 had a strong influence in separation. At 6 months, the wavenumbers on the positive side of Axis 1 had a strong influence, and the wavenumbers on the negative side of Axis 2 appear to have a slight influence on separation. Time 0 and 6 months have small error bars about the mean, but 12 months had larger error bars indicating more variability between replicates at this time. The samples at 12 months were influenced most strongly by those in the negative direction on Axis 1 and the positive direction on Axis 2.

The wavenumbers noted on the PCA plots were then compared to the actual IR spectra. The five average leaf spectra for each sampling time were overlaid, and the peaks listed on the PCA plots were labeled (Fig. 15-17). At wavenumber 2980(CH_3), there are no identifiably distinct peaks present at time 0, yet at 6 months two of the five spectra and at 12 months four of the five spectra have small peaks at this wavenumber. At wavenumbers 2918(CH, CH_2) and 2850(CH_2), there is a clear decrease in intensity from time 0 to 6 months to 12 months. At 1780, there were no clear peaks on any of the spectra at any of the sampling times, however the

intensity in this region increased from time 0 to 6 months, then fell from 6 months to 12 months. This may be attributable to changes in the baseline intensity. At time 0, the intensity of the peak at 1735(C=O) appeared to be relatively similar between the five spectra, however at 6 months the 1735(C=O) peak had clearly broadened and lessened in intensity. At 12 months, wavenumber 1735(C=O) increased in intensity in three spectra, but lost intensity in two spectra; there was an overall narrowing of the peak in those that had increased intensity. At time 0, wavenumber 1650(C=O) was a barely discernible shoulder on the side of a larger peak, but as time progressed, the peak increased in intensity and became more defined. At 12 months there was a clear strong peak at 1650(C=O). At times 0 and 6 months, there were no clear peaks at 1555(NH), however at 12 months, a small peak had appeared in the spectra. At all three times, there was a peak of moderate intensity present at 1462 which remained relatively unchanged between times. At time 0, two of the five spectra had peaks at 1106 (C-O, C-C ring), but at 6 and 12 months no distinct peaks were found although a broader peak was present in this range. Wavenumber 1056 was obscured by a larger, broad peak (1060-1020) at time 0. At 6 months, this large peak seemed to shift up a bit in wavenumber, as the point at 1056 was nearer the top of this peak. By 12 months, 1056 was very close to the top of this peak on 4 spectra and at the peak tip in one spectrum. Wavenumber 950 was located on the opposite side of this peak; however there was no discernible peak in this region at any of the sampling times. At time 0 there were no peaks at 718; at 6 months there were large distinct peaks that decreased slightly at 12 months. Wavenumbers, their correlating functional groups, and proposed biological assignments are found in Table 1 and addressed further in the discussion.

Pine Needle (P dataset)

The principal component analysis of the pine needle dataset resulted in Axis 1 accounting for 49.4% of the variability between sampling times, Axis 2 for 27.8%, and Axis 3 for

10.0%. ANOVA of the PCA scores on Axes 1 and 2 resulted in times 0 and 6 months being significantly different from 12 months but not each other. On Axis 3, there was no significant difference between times. However, the PCA plot does not appear to represent any overlap of the error bars on either Axis 1 or Axis 2, although on Axis 2, times 0 and 6 months do appear to be very close to overlapping (Fig. 18).

All x-residual spectra had at least one peak that was determined to be relevant. This resulted in seventy-three specific peaks being determined from the x-residuals which were subsequently compared to the factor loading plots.

On Axis 1 there were twenty-three strong peaks on the factor loading plot (3465, 2918(CH, CH_2)*, 2850(CH_2)*, 1787*, 1735(C=O)*, 1665, 1650(C=O), 1560(NH)*, 1550*, 1474, 1413, 1342, 1323, 1300*, 1237*, 1218, 1194*, 1090, 1074*, 1044*, 967*, 942*, 800), and thirteen of those wavenumbers were on the list of x-residual peaks. The absence of the remaining ten peaks on the x-residual analysis indicates that at those wavenumbers, all spectra were likely similar. On Axis 2 there were also twenty-three strong peaks on the factor loading plot (3030, 2918(CH, CH_2)*, 2850(CH_2)*, 2807*, 1787*, 1735(C=O)*, 1630*, 1579*, 1509, 1429*, 1401, 1344, 1329*, 1312*, 1259, 1168*, 1099, 1034(C-O, C-OH)*, 986, 951*, 920, 729*, and 721*), and fifteen of those were found on the list of x-residual wavenumbers. For the third axis, the factor loading plot identified twenty-eight strong peaks (2973, 2918(CH, CH_2)*, 2850(CH_2)*, 2807*, 1735(C=O)*, 1644*, 1579*, 1528, 1489*, 1439, 1429*, 1388*, 1352, 1335*, 1312*, 1288*, 1266, 1249*, 1227, 1207*, 1187, 1133, 1105, 1066*, 967*, 942*, 830*, and 715*), and nineteen of these were also found on the x-residual table of wavenumbers (Table 2). The wavenumbers were added to Axes 1 and 2 of the PCA plot (Fig. 18) to better illustrate the direction of influence on each axis and which sampling times were being influenced by these peaks. Wavenumbers were listed in decreasing order of importance on each direction of each

axis. The PCA plot indicates that wavenumbers 942 and 967 had a strong influence on the positive side of Axis 1 and, wavenumbers 2918(CH, CH_2), 2850(CH_2), 1735(C=O), 1194, 1237, 1300, 1560(NH), 1550, 1787, and 1044 influenced the negative side of Axis 1. Axis 2 was most strongly influenced in the positive direction by wavenumbers 1168, 2918(CH, CH_2), 1735(C=O), 721, 729, 1034(C-O, C-OH), 951, and 2850(CH_2) and in the negative direction by wavenumbers 2807, 1787, 1579, 1630, 1429, 1329, and 1312. Based on the PCA plot, spectra at time 0 were most strongly influenced by those wavenumbers on the negative side of Axis 1 and the positive side of Axis 2. At 6 months, there was strong influence by the wavenumbers on the positive side of Axis 1 and a slight influence by those wavenumbers pulling on the positive side of Axis 2. There was little pull in either the positive or negative direction on Axis 1 at 12 months, but a clear separation in the negative direction on Axis 2 was present at that time. In contrast to the ANOVA analyses, which indicated time 0 and 6 months were not significantly different from each other but were different from 12 months on both axes, the PCA plot indicates that along Axis 1 time 0 and 6 months are very different from one another and 12 months falls between them.

The peaks influencing Axes 1 and 2 of the PCA plot were then compared to the actual spectra. The five average leaf spectra for each sampling time were overlaid, and the peaks listed on the PCA plots were labeled on each (Figs. 19-21). At wavenumbers 2918(CH, CH_2) and 2850(CH_2), there are sharp peaks that are fairly consistent in intensity from time 0 to 6 months. At 12 months, three of the five spectra exhibit a sharp decrease in intensity, while the remaining two spectra still have intense peaks. There is no distinct peak at wavenumber 2807on any of the spectra. At time 0 and 6 months, no peaks are present at wavenumber 1787, but at time 12, at least 3 spectra have a small, yet discernible peak. At wavenumber 1735(C=O) there are sharp, intense peaks at time 0 and 6 months. At 12 months, 1 spectrum has a considerably smaller

peak, but the four remaining spectra maintain a large intense peak. At wavenumbers 1630, there are broad peaks at time 0 that decrease in intensity at time 6 months. At 12 months, the intensity increases, but the wavenumber value is on the shorter-wavenumber (right) side of a peak at 1650(C=O). At wavenumber 1579, there are no peaks at time 0 and 6 months, but at 12 months small peaks are present. At 1560(NH), there are small peaks at time 0, no peaks at 6 months, and small peaks again at 12 months. There are no peaks at 1550 at any of the times, however, it appears that this peak in found on the larger peak at 1560(NH). At wavenumbers 1429, 1329, and 1312 there are small peaks at time 0, but no peaks at 6 or 12 months. At wavenumber 1300 there are small peaks at time 0 and 6 months, but at 12 months only 2 of the 5 replicate spectra still have clear peaks, 2 have small shoulders, and 1 has neither. At wavenumbers 1237 all three times exhibit small peaks. Wavenumber 1194 at time 0 and 6 months has clear peaks, but at 12 months only 2 of the 5 replicates have clear peaks. The remaining 3 spectra have what appear to be small peaks or shoulders on the side of the peak at 1168. Wavenumber 1168 has intense, sharp peaks at time 0 and 6 months that are relatively consistent in intensity across replicates. At 12 months, there is more variability at this wavenumber with 2 replicates maintaining intense peaks, 2 with rather weak, broad peaks, and 1 with a moderate-intensity peak. At wavenumber 1074 there are shoulders at time 0, 1 peak and 1 shoulder at 6 months, and 3 shoulders and 2 peaks at 12 months. The presence of a peak or shoulder at this wavenumber becomes more apparent over time, but it appears to be somewhat hidden by the presence of the broad neighboring peak at 1034. (C-O, C-OH) Wavenumber 1044 is almost completely indiscernible on the spectra across all three times, as it is also located on the longer-wavelength side of the large, broad peak at 1034(C-O, C-OH). This peak at 1034(C-O, C-OH) is intense but broad at time 0, less intense at 6 months, yet increases in intensity again at 12 months. At wavenumber 967 there are no peaks at time 0, 1 shoulder and

no peaks at 6 months, and 3 peaks and 1 shoulder at 12 months. There is a small peak at 951 at all times which seems to include wavenumber 942 on the longer-wavelength (right) side of the peak. The peak at 951 decreases in clarity at 12 months; it appears on four of the five spectra. At time 0, there is no peak at 721 or 729. At 6 months a large broad peak is present with 729 and 721 at the top on all spectra. At 12 months, this peak broadens in 4 of the 5 replicates, increases in intensity in 3 of those 4, and is lost in 1 replicate. Wavenumbers, their correlating functional groups, and proposed biological assignments are found in Table 1 and are addressed in greater detail in the discussion.

All Spectra (ALL dataset)

The principal component analysis of all leaves together, resulted in Axis 1 accounting for 58.0% of the variability between sampling times, Axis 2 for 22.1%, and axis 3 for 8.2%. The PCA plot of the coordinate scores resulted in clear clustering together of HL, HV, OL, and OV at time 0. Within each cluster, the lamina and vein of the same species also appear closer together than to the others in that cluster. Pine at time 0 appears to be unique from all other species and times. All 5 datasets (HL, HV, OL, OV, and P) at 6 months clustered together, as did all the 12 month datasets (Fig. 22).

ANOVA of the PCA indicated that on Axis 1, P at time 0 and OV and OL at 6 months were statistically the most different. This corroborates with the actual PCA plot, whereas P at time 0 is the most extreme in the positive direction on Axis 1 and OL and OV are the most extreme means on the negative side of Axis 1. Scores on Axis 1 resulted in P at time 0 being statistically different from all of the 6 month samples, as well as from P and OL at 12 months. OL and OV at 6 months were also highly separated, being statistically different from all time 0 samples and OV at 12 months. On Axis 2, ANOVA of the PCA indicated that HL, HV, OL, and OV at time 0 and HL

at 12 months were statistically the most different. This also correlates with the PCA plot of coordinate scores in which HL, HV, OL, and OV are the most positive on Axis 2, and HL at 12 months is the most negative on Axis 2. HL, HV, OL, and OV at time 0 were significantly different from all the 12 months samples and P at time 0. HL at 12 months was found to be significantly different from all the time 0 and all the 6 month samples, being only similar to the other 12 month samples.

The wavenumbers obtained from the factor loading plots were added to the axes of the PCA plot and ranked in order from most important to least important on each axis (positive and negative sides) as determined by the intensity of the significant, distinct peaks on the factor loading plots. The PCA plot illustrates the direction of influence on each axis and which sampling times/locations on the leaf/species combinations were being influenced by these wavenumbers. On Axis 1, wavenumbers 2918(CH, CH_2), 2850(CH_2), 1174, 1195, 1040, 1101(C-O, C-C ring), 1467, 1735(C=O), 1323, and 1574 were important in the positive direction, and wavenumbers 3460, 721, 809, 704, and 1650(C=O) were important peaks in the negative direction (in order of decreasing importance). On Axis 2, 2918(CH, CH_2), 2850(CH_2), 1040, 1101(C-O, C-C ring), and 1170 were the important peaks in the positive direction, and wavenumbers 778, 809, 751, 1650(C=O), 713, 704, 1560(NH), 1537, 2810, 1780, 1394, 951, 936, 1297, and 1242 were important in the negative direction. Based on the PCA plot, spectra at time 0 were most strongly influenced by those wavenumbers on the positive side of Axis 1 and the positive side of Axis 2 except pine. At time 0 on Axis 2, pine appears to be slightly influenced in the negative direction. At 6 months, there was influence by the wavenumbers on the negative side of Axis 1 and a slight influence by those wavenumbers pulling on the positive side of Axis 2. At 12 months, there was pulling in both the positive and negative direction on Axis 1, but only in the negative direction

on Axis 2. Wavenumbers, their correlating functional groups, and proposed biological assignments are found in Table 1 and addressed in more detail in the discussion.

Discussion

The investigation of the fine-scale changes in leaf litters during decomposition, using FTIR spectroscopy, has demonstrated that three contrasting litter types have similar overall chemistries throughout, with small differences being most notable. Only freshly fallen pine needles appeared to have different spectral attributes than freshly fallen oak or huckleberry, and these differences tended to be lost as decomposition proceeded over a 12 month period. Despite this general observation, specific chemical signatures, indicated by particular wavenumbers on the FT-IR spectra, were identified from the spectral analysis using principal component analysis. Using these wavenumbers, it is possible to determine general trends in the changing chemistry as decomposition progresses and identify slight differences in the process of decomposition for pine litter compared to huckleberry and oak litters, particularly during the early stages of decomposition.

Pine needles at the initial time were a clear outlier in the ALL dataset; this corroborates with the large number of unshared wavenumbers found only in the pine needle spectral analysis. The last column of Table 1 indicates the datasets in which each wavenumber was found on the factor loading plots and the x-residuals. Each dataset (excluding pine) possess a small number of unique wavenumbers that are unshared in the other datasets. There are 3 wavenumbers unique to HL, 2 to HV, 4 to OL, and 2 to OV. In contrast, there are 17 wavenumbers found only in the pine analysis.

To determine general trends within all litter types, peaks shared by three, four, or five of the five litter types investigated were identified. The vein and lamina regions of the same

species (e.g. huckleberry vein vs huckleberry lamina) are considered different litter types as they are discussed below. All five litter types shared peaks 2918(CH, CH_2) and 2850(CH_2). Four of the five datasets shared peaks 1735(C=O) and 1650(C=O), and three of the five datasets shared peaks 2980(CH_3), 1555-1560(NH), 1101-1106(C-O, C-C ring), and 1029-1034(C-O, C-OH). Of these eight wavenumbers, seven were present on the factor loading plots in the compiled "ALL" database (1029-1034 range was not).

In all litter types, peaks 2918 and 2850 change similarly. Both bands are found in the CH region of the spectrum (3000-2800 cm^{-1}), but are more specifically linked to aliphatic methylenes (straight chain molecules with -CH_2- units). Smidt *et al.* (2005) reported these bands decreased during decomposition of biowaste as the macromolecules' aliphatic skeletons were breaking down. In both huckleberry lamina and vein and the oak vein, these peaks decreased in intensity from time 0 to 6 months to 12 months. In the oak lamina and pine, there was little to no change in intensity from time 0 to 6 months, but a decrease in intensity from 6 to 12 months. Considering these wavenumbers both represent CH bonds, particularly aliphatic methylenes, it is not surprising that they trend similarly within each dataset.

Wavenumbers 1735 and 1650 were present in four of the five litter types. Although both bands represent C=O, it is important to realize that the band at 1735 probably represents the carbonyl of saturated esters (C-C(=O)-O) of phospholipids, hemicellulose, or pectin (Gorgulu *et al*., 2007), whereas 1650 most likely represents the carbonyl of a protein or polypeptide (known as the amide I band) (Socrates, 2001) or possibly of fatty acids or aldehydes. This band is only considered to represent fatty acids or aldehydes if bands at 1000-700 are also present (Stewart, 1996). Bands in this region are present in some spectra, but not all. This leads to the conclusion that the band at 1650 (at least in some spectra) is a result of different, diverse substances with the same functional group, the carbonyl (C=O).

Wavenumber 1735 was present in HL, HV, OV, and P, whereas 1650 was present in HL, HV, OL, and OV. The peaks at 1735 were relatively sharp with consistent intensity at time 0 within each dataset, however at 6 months this peak varied in intensity in both huckleberry datasets and became a broad peak in the oak vein data set. At 12 months, all datasets exhibit variability in intensity at 1735. As the intensity changes at this wavenumber, it is likely due to the changes in the amount of phospholipids, hemicellulose, or pectin present. Phospholipids were likely decomposed at a higher rate earlier (between 0 and 6 months), pectin with the next highest decomposition rate in the early months, and hemicelluloses decomposing the slowest of the three. This may explain the increasing variability found at the wavenumbers measured from leaves decomposed for 6 and 12 months. The large amount of variability at 12 months may also be due to a higher concentration of biological contaminants on the leaf (i.e. bacteria, protozoa, fungi, invertebrate fecal material, etc.)

The peak at 1650(C=O) was either not present or was noted as a very small, barely discernible shoulder on a larger peak at time 0 in all datasets. From time 0 to 6 to 12 months, the peak increased in intensity consistently. At 12 months, all spectra had a distinct peak at 1650, although they varied in intensity between litter types (not within). This increase at wavenumber 1650 is very interesting, and may help further determine its molecular assignment. The appearance of the band over time implies that either proteins/polypeptides or fatty acids/aldehydes are increasingly present, however, one would expect that during decomposition of the leaf material, these compounds would decrease quickly leaving behind the more recalcitrant polysaccharides (pectin, hemicellulose, cellulose, lignin). Perhaps this increase is due to the presence of the microbial community and microbial decomposer-derived molecules (e.g. enzymes) on the leaves at 6 and 12 months, as living organisms would consist of and produce all of these compounds.

Yet another possibility is the presence of water in the samples. Increased water in the sample would be evident as a large increase in the broad -OH band at 3500-3300cm^{-1} and, according to Socrates (2001), the bands that correlate with the –OH deformation of water occur at 1630 to 1600 (not 1650). However, Xiao *et al.* (2001) attributed a peak at 1645 in both hemicellulose and lignin to be due to residual water absorption in their extractions. Wavenumber correlation charts in Socrates (2001) do not indicate an -OH band at wavenumber 1650, but there are nearby OH bands for crystallized water at 1630-1600 and the weak –OH of cellulose at 1635-1600. The lack of any assigned OH bands at 1650 appears to rule out the possibility that this band is increasing due to the presence of water, cellulose, or the action of hydrolytic enzymes' decomposition of the large macromolecules. During hydrolysis enzymes attach an –OH to one side of the cleavage site, and it is expected that this would increase the –OH signal in the spectra. On the contrary, the large –OH region at 3500-3300 does increase overtime providing evidence of increased –OH in the sample.

To further complicate the issue, hydrogen bonding can cause shifts in wavenumber (Kubo and Kadla, 2005; Socrates, 2001). In the presence of water it is expected that hydrogen bonding would occur in hydroxyl groups (and among others, e.g. carbonyl groups). This could be an explanation of an -OH peak being present at wavenumber 1650. If this is the case, then the source of the –OH may be the presence of water, hydrolysis, or the weak –OH deformation of cellulose growing in intensity. As other less recalcitrant molecules are decomposed, could the signal from cellulose be increasing? Clearly, there are multiple substances that may contribute to this peak.

In addition to the peaks shared by 5/5 and 4/5 litter types, there were four wavenumbers shared by 3/5 litter types (2980(CH_3), 1555-1560(NH), 1101-1106(C-O, C-C ring), and 1029-1034(C-O, C-OH) These wavenumbers do not follow clear patterns in their changes

over time, nor do they occur in the same three databases Wavenumber 2980 appears to follow the general trend of being absent at time 0, but grows in intensity at 6 and 12 months in datasets HV, OL, and OV. This is interestingly in contrast to 2918 and 2850 which decrease in intensity over time. This appears to indicate there is a shifting of the types of CH bonds in the sample. The decreasing peaks at 2918 and 2850 are primarily associated with aliphatic methylenes (-CH_2-), however 2980 is primarily associated with CH_3. This shift in intensity could occur as fatty acids chains are cleaved through β-oxidation. The relative ratios of CH_2:CH_3 should change as the fatty acid chain is shortened (lessening the number of CH_2 groups), but the number of end methyl (CH_3) groups would decrease more slowly. It is possible that this change in the CH_2:CH_3 ratio contributes to the decreasing intensity of the CH_2 bands and increasing the intensity of the CH_3 band.

The 1555-1560(NH) peaks are either very small or not present at both time 0 and 6 months, and are present in only a subset of each dataset (HV, OV, P) at 12 months. This follows a pattern of increasing intensity over time (albeit a less pronounced increase) as is seen for 1650. Recall that among other possibilities, 1650 is the amide I band (present in proteins), and 1555-1560(NH) is the amide II band of proteins. It was previously mentioned that the strong bands at 1650 and their presence in all the spectra are likely due to vibrational contributions from multiple functional groups (not only the amide), however with the presence of both the amide I and amide II bands, this appears to confirm that at least a portion of the amide I band at 1650 is due to the presence of proteins. If the slight increase over time is occurring at both the amide I and amide II bands (as it appears to be), this implies that the presence of proteins in the litter is, in fact, increasing from time 0 to 6 to 12 months. This would not be expected due to the leaf material itself; however, the increased presence of microbial decomposers and their proteinaceous products on the leaf could contribute to the increase in intensity of these bands.

The peak at 1106(C-O, C-C ring) is present on all spectra within the HV and OL datasets as a shoulder on the larger 1029-1034 peak, but in the OV dataset, 2 spectra have peaks at time 0 and none at 6 and 12 months. The ring mode in pectin has been tentatively linked to this wavenumber, as it indicates the presence of aromatics (Wilson *et al.,* 2000). From a biological perspective, the veins of plant leaves should possess lower levels of pectin compared to the lamina. However, it is in the OV litter that peaks decrease over time. In the HV and OL litters, the peak is consistent over time.

At wavenumbers 1029-1034(C-O, C-OH), there is a large peak in all spectra in the HL, HV, and P datasets, and is considered a strong cell wall polysaccharide band (Gorgulu *et al.,* 2007), but also more specifically appearing in cellulose (Ribeiro da Luz, 2006). In the HL dataset, this peak decreases in intensity and broadens from 0 to 6 to 12 months, but in the HV spectra it increases slightly from 0 to 6 months, then becomes quite varied in intensity at 12 months. In the pine dataset, this peak starts as intense and broad, decreasing in intensity at 6 months, but increasing in intensity at 12 months. There is no consistent pattern that appears to be tied to a general increase or decrease over time. As this band has been assigned to several cell wall polysaccharides, perhaps it is also present in non-plant derived polysaccharides, such as those found in bacterial or protozoan cell walls. Based on the wavenumber analysis in chapter 2 of this dissertation, it is not a band dominant in fungi.

Although there are only 8 important wavenumbers that three or more litter types share, 7 of those are found to be important in the PCA analysis of the ALL dataset that includes all the average litter spectra: (2918(CH_2), 2850(CH_2), 1735(C=O), 1650(C=O), 2980(CH_3), 1555-1560(NH), and 1101-1106(C-O, C-C ring). However, this does not imply that these are the only important wavenumbers. The remaining wavenumbers from the factor loading plots, as seen on Fig. 22, must also be considered. In addition to the seven wavenumbers above, the following

were determined to be important in separation on the PCA plot: 3460, 2810, 1780, 1574, 1537, 1467, 1394, 1323, 1297, 1242, 1195, 1174, 1170, 1040, 951, 936, 809, 778, 751, 721, 713, and 704. The overlaid spectra from the ALL dataset and a grid with these wavenumbers and their relative intensities are presented in Figure 23.

The band at 3460 corresponds to the very large –OH stretch between 3500-3300, however there could also be a sharper NH band that is obscured by the large –OH stretch. If present, this NH band correlates with the presence of the amide bands (I, II, & III). Within all litter types, this band increases greatly from time 0 to 12 months. This increase may be attributable to the presence of water, alcohols, polysaccharides or action of hydrolytic enzymes. As hydrolytic enzymes degrade polymers, they add an –OH group to one side, therefore a collection of small oligomers and polymers will have a greater number of –OH groups than groups of large polymers.

The band at 2810 is included in the CH region. As was discussed earlier, there appears to be a shift in the types of CH vibrations over time (i.e. methylene vs end-methyl). The band at 1780 is associated with vinyl and phenyl esters, both of which may be found in the cuticular waxes of plants, particularly in cutins and suberins (Kolattukudy, 1980). The band at 1574 is associated with the C=C vibrations of aromatics and phenols; these may be found in cutins, suberins, as well as lignin. Another band commonly found in cutins, suberins, and lignin is 1467, the CH ring vibrations. Wavenumber 1537 is associated with the amide II band, as 1560(NH) (discussed above). Wavenumbers 1394 and 1323 are both associated with various alkanes (C-H vibrations). Wavenumbers 1297 and 1242 are both associated with the NH Amide III band. Wavenumber 1195 is an unspecified ester band, and the combination of 1174 with 1249 and 1207 is associated with methyl esters of fatty acids. Although 1249 and 1207 are not on the PCA plot, they are present in the spectra of pine needles, perhaps associated with the unique waxes

present in a pine needle. Wavenumbers 1170 and 1040 are both assigned to cellulose; 1170 is the band for the β-1, 4 glycosidic linkage, and 1040 is associated with the C-O and C-C ring vibrations of cellulose. Wavenumbers 951 and 936 are associated with CH ring vibrations as well, but have not been assigned to a particular molecule in the literature. Wavenumbers 809 and 704 are associated with C-O and CH ring vibrations of cellulose, and 713 are associated with the C-OH vibration of cellulose. Wavenumbers 778, 751, and 721 are all associated with fatty acids and aldehydes (in the presence of 1650). Table 1 lists all of the wavenumbers that were determined to be important within all the litter types, comparison of the band assignments, the actual spectral wavenumbers from the 6 datasets, and tentative assignments of the molecules.

Wavenumbers from Table 1 that were specifically identified in the literature as being associated with a particular type of biological molecule were further analyzed for temporal trends in the spectra of each species/location dataset. There appears to be several general trends in the biology of the decomposing litters investigated. There is no clear trend across all polysaccharides, however for the most part, bands associated with i) cellulose and lignin decrease over time; ii)hemicellulose decrease initially, then increase; pectin increase initially, then decrease. The decrease in plant cell wall material over time is easily explained by loss of those compounds; an initial increase then decrease can be explained by the early exposure of more material as the surface waxes are decomposed. In contrast an early decrease is not readily explained, as it would not be expected for the surface waxes to increase nor would it be expected for the amount of hemicellulose in the sample to increase relatively. Presence of microbial decomposers, however, could have impacted those results.

Bands associated with fatty acids all initially decrease, but the 1249, 1207, 1174 combination increases later, again, perhaps due to the colonization of microbial decomposers. Suberin and cutin decreases initially in 1 band, but exhibits no clear pattern in the other. It

would be expected that both bands would decrease with time. The amide I and II bands both increase with time, and the amide III band exhibits no clear pattern. The amide III band is in a region with much overlap of band assignments, whereas the amide II band has fewer potential biomolecular assignments (see discussion of wavenumber 1650 above) and the amide I band is primarily assigned to polypeptides and proteins. This appears to indicate a general trend of increasing proteinaceous material over time, likely due to the colonization of the leaf material by microbial decomposers and their subsequent secretion of products (e.g. enzymes).

This analysis is based on both the existing band assignments for biomacromolecules in the literature, as well as functional group assignment. It is clear, based on the sheer possibilities of band assignments in certain spectral regions, that many of the tentative band assignments to specific molecules in the literature may be attributable to other molecules as well. Several literature sources (Xiao *et al.,* 2001; Kubo and Kadla, 2005; Michell, 1990) utilized isolated extracts of plant cell wall material in their studies. Although one must consider that a band was assigned to a pure extract of a biomolecule, that does not necessarily imply that the presence of that band in a complex sample (such as a leaf) is actually due to the presence of (or solely the presence of) that particular compound. Perhaps, then, the FTIR studies of whole plant tissues would be useful for comparison. However, the fallacy in this is that all of these studies refer to band assignments from the literature based on studies of pure extracted substances (e.g. lignin, cellulose).

FTIR-ATR has enabled the investigation of leaf material at the 10 x 10 micron scale, however the complex nature of a decomposing leaf makes compositional determination indistinct. The attempt to characterize the macromolecular components of leaves at the level of the individual fungal hypha could enable a much greater understanding of that vague area of scale between the truly microbial (at level a bacterium may experience, <1 micron) and the

macroscopic (at level of an entire leaf). Although this attempt to characterize decomposing leaf material at the micro scale was successful in these studies, it did not result in the amount of detail originally planned. However, it will enable others to develop further studies utilizing additional or different methods of micro-scale substrate changes.

Tables

Table 1. List of specific wavenumbers identified in the analyses, their corresponding functional groups, the wavenumber ranges of those functional groups, and tentative band assignments based on the current literature.

Wavenumber Ranges (cm^{-1})	Functional Group	Specific Wavenumbers (cm^{-1})	Tentative band assignments	References
3500-3300	OH	3360, 3460	Polysaccharides, alcohols	Socrates (2001)
3000-2800	C-H (CH, CH_2, and/or CH_3)	2980	Aliphatic alkanes, often associated with hydrocarbon regions of lipids	Socrates (2001), Ribeiro da Luz (2006)
		2918		
		2850		
		2807, 2810		
1850-1590	C=O	1787, 1780, 1774	Vinyl and phenyl esters, such as those found in cutins and suberins	Socrates (2001), Kolattukudy (1980)
		1735	Saturated esters of phospholipids, hemicellulose, and pectin	Gorgulu *et al*. (2007)
		1683	Unconjugated carbonyl, lignin	Kubo and Kadla (2005)
		1650, 1644	Amide I: Primarily proteins and peptides Possibly fatty acids or aldehydes if bands at 1000-700 are also present	Mantsch and Chapman (1996), Movasaghi *et al.* (2008) Stewart (1996)
		1630	Non-esterified carboxyl of pectins	Chatjigakis *et al*. (1998)
1590-1575	C=C ring	1579, 1574	Phenols or aromatics, found cutins, suberins, lignin,	Socrates (2001), Movasaghi *et al.* (2008)

1570-1515	N-H	1560, 1556, 1555, 1550 1542, 1537 1530	Amide II: primarily proteins and peptides	Socrates (2001)
1490-1300	C-H (CH, CH_2, CH_3 or CH ring)	1489, 1394 1390, 1388 1323, 1312	Various alkanes	Movasaghi *et al.* (2008)
		1462, 1467	Lignin cutin/suberin	Boeriu *et al.* (2004), Kubo and Kadla (2005), Xiao *et al.* (2001) Stewart (1996)
		1442	Various plant cell wall polysaccharides	Gorgulu *et al.* (2007)
		1429	Cellulose, other plant cell wall polysaccharides	Movasaghi *et al.* (2008), Wilson *et al.* (2000), *Oh et al.* (2005)
	CH ring	1335	Cellulose, pectin	Wilson *et al.* (2000)
		1329	Phenyl ring Lignin	Movasaghi *et al.* (2008) Kubo and Kadla (2005), Boeriu *et al.* (2004)
1305-1200	N-H, C-N C-O	1300, 1297 1288, 1261, 1249, 1242, 1237	Amide III: primarily proteins and peptides Ester	Socrates (2001) Pretsch *et al.* (1983)
1300-1000	C-O	1194, 1195, 1180	Ester	Pretsch *et al.* (1983)
Three band combination: ~1250, ~1205, and ~1175	C-O	1249, 1207, 1174	Methyl esters of fatty acids	Silverstein and Webster (1998)
1228-1215	C-O, C-C, C=O (combined)	1221	Lignin	Boeriu *et al*. (2004), Xiao *et al.* (2001)

1170-1150	C-O-C	1170	Cellulose, β-1,4 glycosidic link	Michell (1990)
1168	C-O-C	1167, 1168	Hemicellulose	Xiao *et al.* (2001),
1130-1050	Intense Polysaccharide Vibrations C-O, C-C ring	1128, 1093, 1074, 1066	Polysaccharides, primarily cellulose	Stewart (1996), Wilson *et al.* (2000)
~1107	C-O, C-C ring	1106, 1101	Pectin	Wilson *et al*. (2000)
~1055	C-O, C-C, C-OH	1056	Pectin	Wilson *et al.* (2000)
~1042	C-O, C-C, C-OH	1043, 1044, 1040	Hemicellulose	Xiao *et al.* (2001)
1035-1025	C-O, C-OH	1029, 1034	Cellulose and other cell wall polysaccharides	Ribeiro da Luz (2006), Gorgulu *et al.* (2007)
1000-700	CH (out of plane bending)	729, 778, 718, 721	Fatty acids and aldehydes (with 1650 also present)	Stewart (1996)
~963	C-O	967	Cellulose ester	Wilson *et al.* (2000)
900-650	CH ring	950, 951, 942, 936, 922	aromatics	Socrates (2001)
~831	unknown	830	Tentatively assigned to phenolic compounds in Cutin	Ribeiro da Luz (2006)
800-500	C-O CH ring	809, 704	Cellulose	Michell (1990)
~713	C-OH	713, 715	Cellulose	Oh *et al*. (2005)

Table 2. List of peaks identified from both the x-residual analysis and PCA factor loading plots for all 5 datasets (HL, HV, OL, OV, and P). The numbers (0, 1, and 2) indicate if the peak was present on the x-residuals for their respective times (time 0: initial; time 1: 6 months; time 2: 12 months). The final column summarizes which datasets possessed specific peaks; it also indicates if the peak was present in the PCA factor loading plots of the compiled ALL database.

Specific Wavenumbers (cm^{-1})	HL Dataset Times peaks were present	HV Dataset Times peaks were present	OL Dataset Times peaks were present	OV Dataset Times peaks were present	Pine Dataset Times peaks were present	Data sets
3360, 3460	1, 2					HL, ALL
2980		0, 1, 2	1, 2	1, 2		OL, OV, HV
2918	0, 1, 2	1, 2	0, 1, 2	0, 1, 2	1	HL,HV, OL, OV, P, ALL
2850	0, 1, 2	0, 1, 2	0, 1, 2	0, 1, 2	1	HL, HV, OL, OV, P, ALL
2807, 2810		1			0, 1	HV, P, ALL
1787					1, 2	P
1780				1		OV, ALL
1774		1, 2	0, 2			HV, OL
1735	1	1, 2		0, 2	1	HL, HV, OV,P, ALL
1683			2			OL
1650	1, 2	1, 2	0, 1, 2	0, 1		HL, HV, OL, OV, ALL
1644					1	P
1630					0	P
1579, 1574					1	P, ALL
1555, 1556, 1560		1		1	1	HV, OV, P, ALL
1550					0, 1	P
1542, 1537		1, 2	2			HV, OL, ALL
1530	1, 2					HL
1489					0, 1	P
1462, 1467	2			1		HL, OV, ALL
1442		2				HV
1429					1	P
1394						ALL

1390, 1388			1, 2		2	OL, P
1335					1	P
1329					1	P
1323						ALL
1312					1, 2	P
1300, 1297	2				1	HL, P, ALL
1288		2			1	HV, P
1261			2			OL
1249					1, 2	P
1237, 1242					1	P, ALL
1221		1				HV
1207					1	P
1194, 1195			2		1, 2	OL, P, ALL
1180			2			OL
1174						ALL
1167, 1168, 1170		1			0, 1, 2	HV, P, ALL
1128	2	1, 2				HL, HV
1106, 1101		1	1, 2	2		HV, OL, OV, ALL
1093	1					HL
1074					0, 2	P
1066					1	P
1056				1		OV
1043, 1044, 1040			0		0	OL, P, ALL
1029, 1034	1	2			0	HL, HV, P
967					1	P
950, 951	2	2		1, 2	1, 2	HL, HV, OV, P, ALL
942					1, 2	P
936						ALL
922			2			OL
830					2	P
809						ALL
778						ALL
729					1	P
718, 721				1	1	OV, P, ALL
713, 715	0,1, 2				2	HL, P, ALL
704						ALL

Table 3. Summary of the major groups of biological compounds expected in a leaf (Polysaccharides, Lipids/fatty acids, cutin/suberin, and proteins) and subgroups of polysaccharides, the wavenumbers that are unique or highly correlated with that compound-type, and the trends occurring in the spectra at those wavenumbers over time.

Biological Compound	Specific Wavenumbers (cm^{-1})	General Trend of Intensity Over Time
Polysaccharides (general-mixed)	1442	Increases, then decreases
	1130-1050	Increases, then decreases
Pectin	1630	Increases
	1106, 1101	Consistent or decreases
	1056	Increases, then decreases
Hemicellulose	1167, 1168	Decreases, then increases
	1040, 1043, 1044	Decreases, then increases
Cellulose	1170	Decreases then increases
	967	Decreases
	809	Decreases
	704	Decreases
	713, 715	Decreases
Lignin	1683	Decreases
	1329	Decreases
	1221	Decreases, then increases
Lipids/Fatty Acids	1249, 1207, and 1174 combined	Decreases, then increases
	778, 751, 729, 718, 721	Decreases
Cutin/Suberin	1787, 1780, 1774	No clear pattern
	830	Decreases
Proteins	1650, 1644 (Amide I)	Increases
	1555-1560 (Amide II)	Increases
	1305-1200 (Amide III)	No clear pattern

Figures

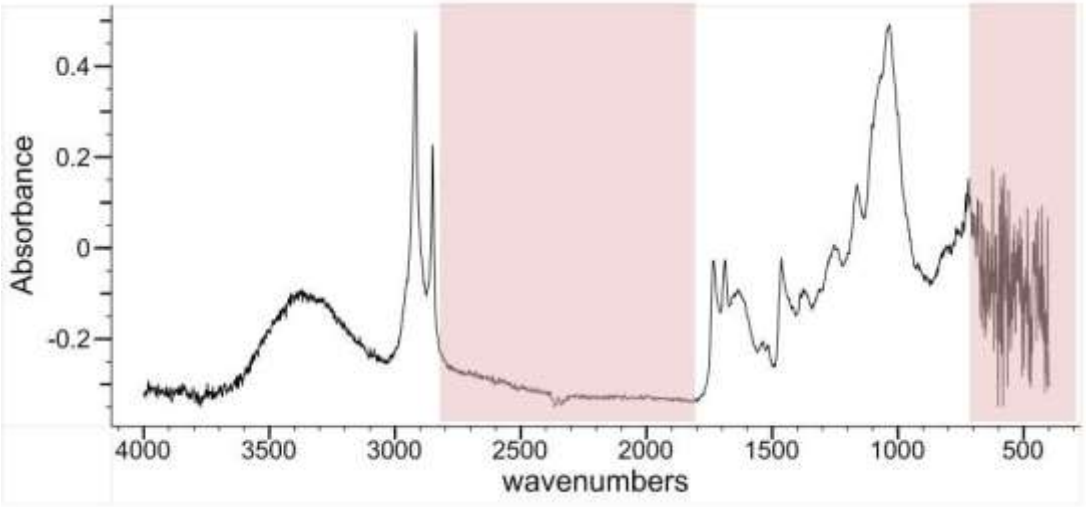

Figure 1. Sample FTIR-ATR spectrum highlighting regions 2800-1800cm^{-1} and 700-400cm^{-1} (respectively) that were excluded from the analysis. The former was excluded due to the lack of spectral information in this region, and the latter was excluded due to intense noise in many spectra probably a result of the functional wavelength range of the germanium ATR crystal, CO_2 signals, and water.

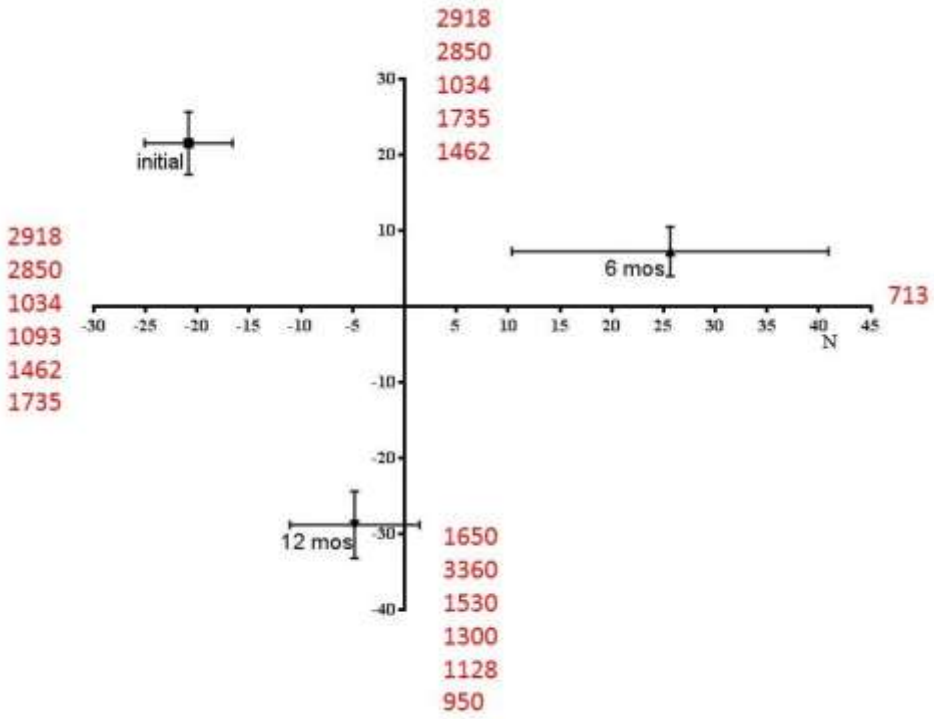

Figure 2. PCA plot of huckleberry lamina data set. Wavenumbers are listed on the axes and direction (positive or negative) on which they influenced the spatial distribution of the data. Wavenumbers are ranked from most important to least. Error bars represent standard errors. For Axis 1 F=5.75, P = 0.0178. For Axis 2 F=42.65, P<0.0001.

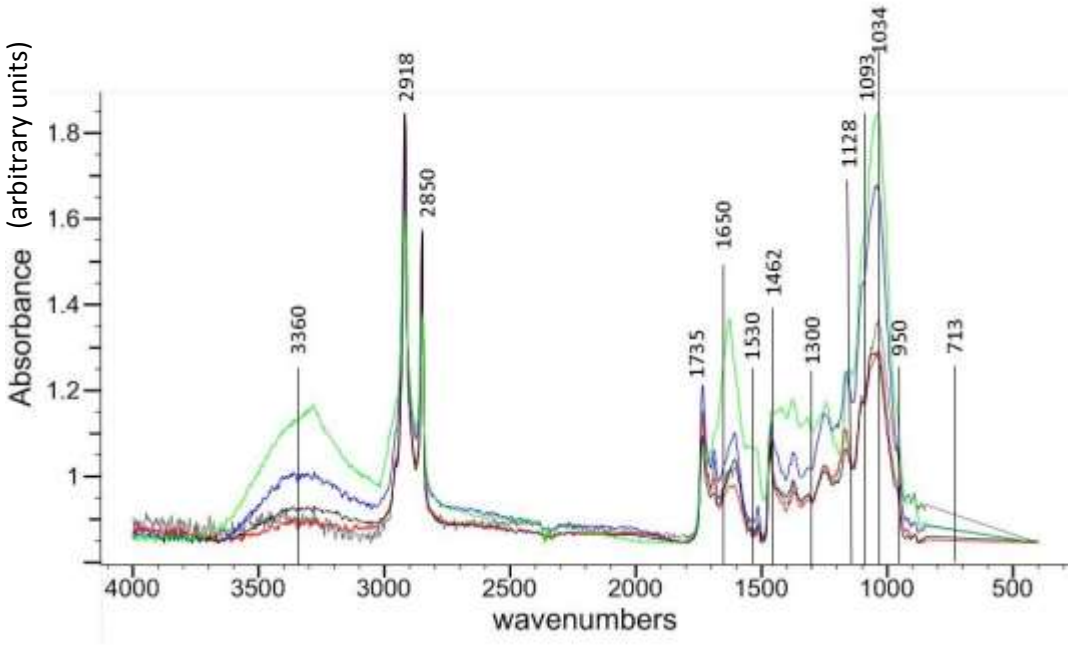

Figure 3. Huckleberry lamina spectra at time 0. Wavenumbers found to be important on the x-residuals and factor loading plots have been labeled.

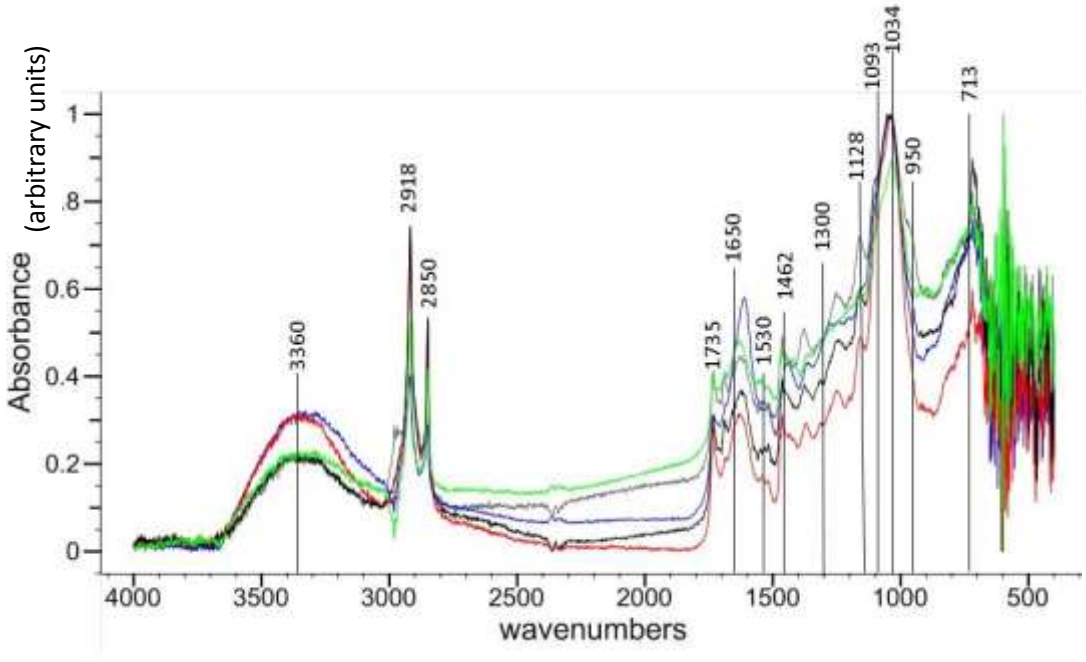

Figure 4. Huckleberry lamina spectra at 6 months. Wavenumbers found to be important on the x-residuals and factor loading plots have been labeled.

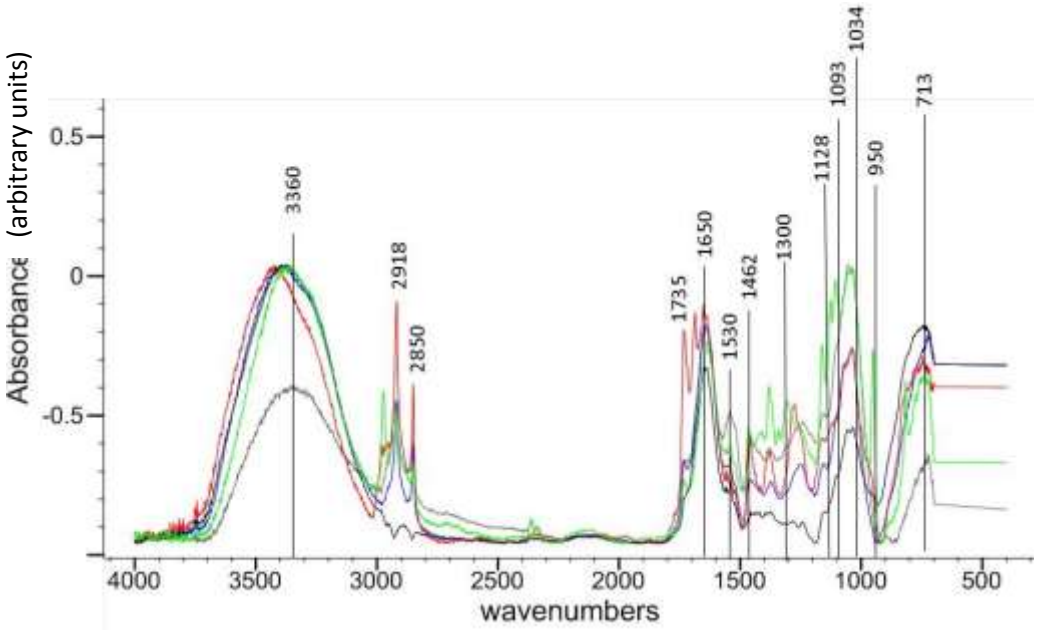

Figure 5. Huckleberry lamina spectra at 12 months. Wavenumbers found to be important on the x-residuals and factor loading plots have been labeled. Negative absorbance values are relative, not empirical.

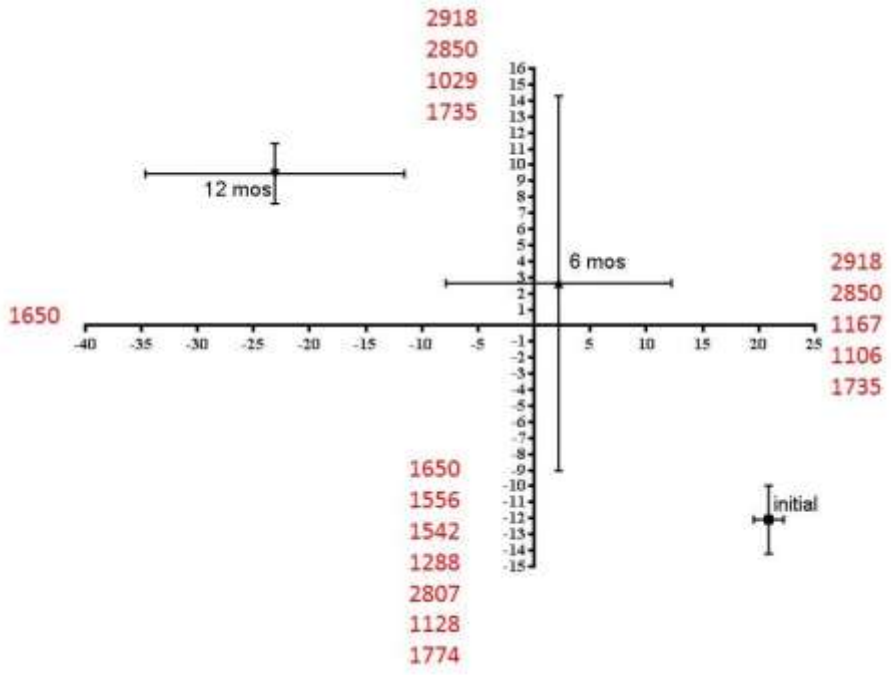

Figure. 6 PCA plot of huckleberry vein data set. Wavenumbers are listed on the axes and direction (positive or negative) on which they influenced the spatial distribution of the data. Wavenumbers are ranked from most important to least. Error bars represent standard errors. For Axis 1 F=6.19, P = 0.0142. For Axis 2 F=2.52, P=0.1222.

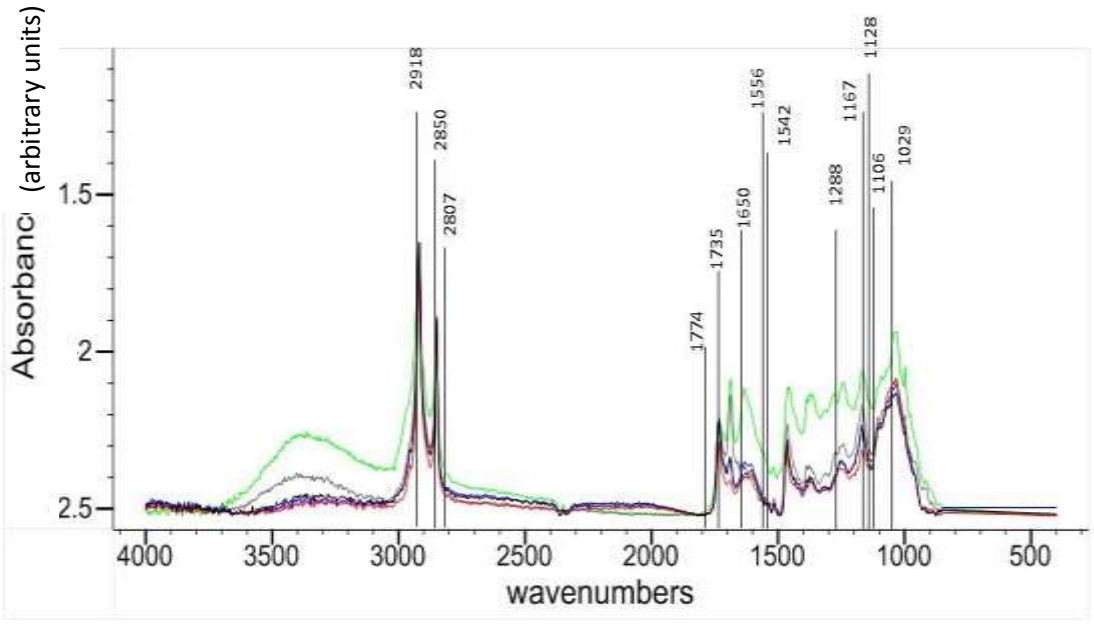

Figure 7. Huckleberry vein spectra at time 0. Wavenumbers found to be important on the x-residuals and factor loading plots have been labeled.

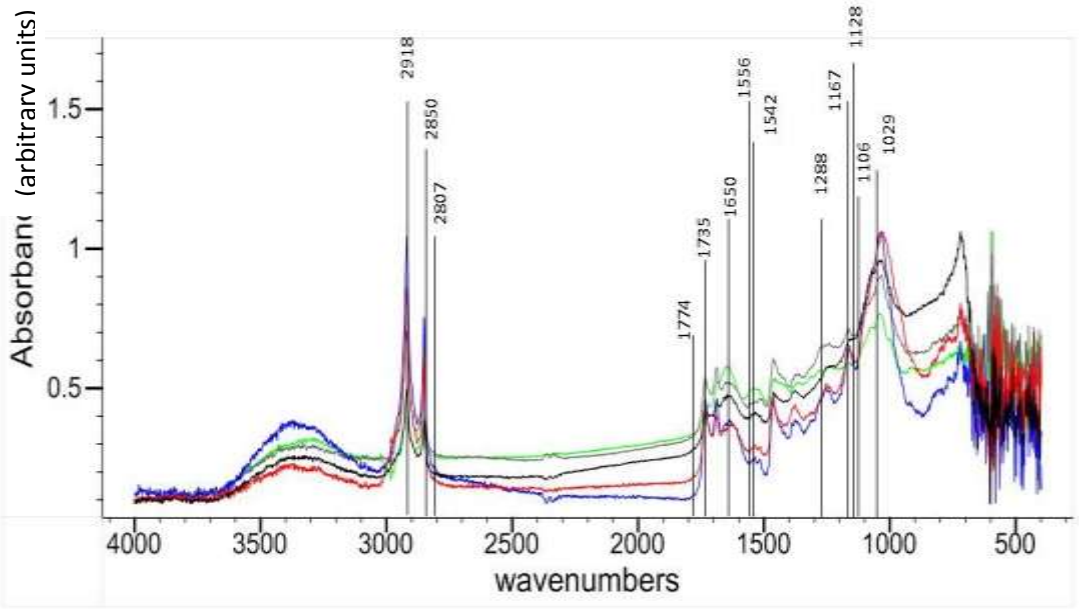

Figure 8. Huckleberry vein spectra at 6 months. Wavenumbers found to be important on the x-residuals and factor loading plots have been labeled.

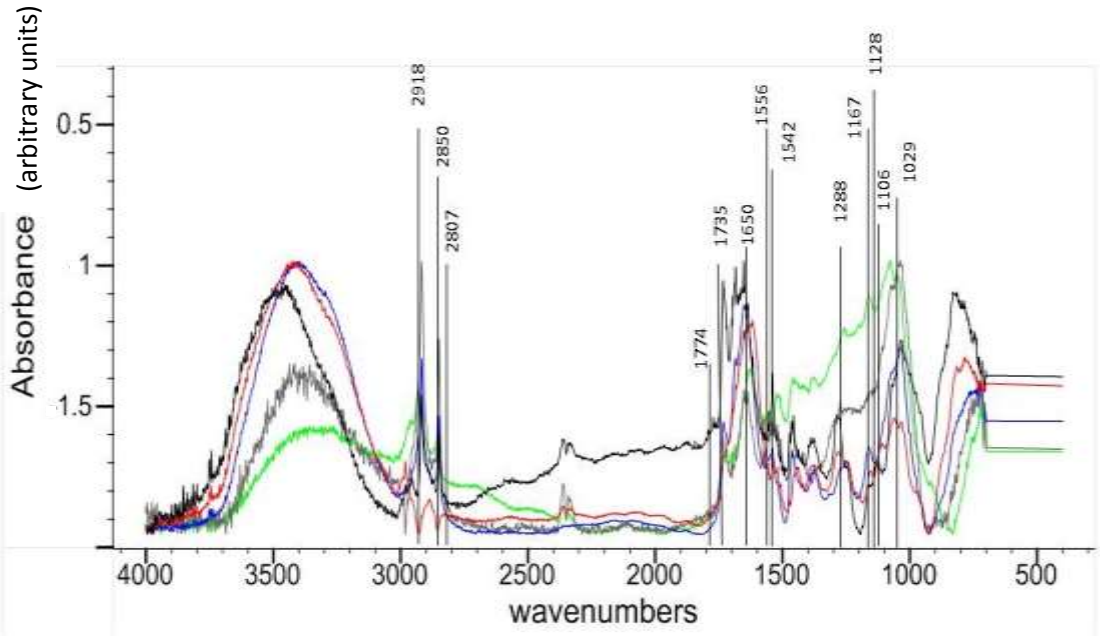

Figure 9. Huckleberry vein spectra at 12 months. Wavenumbers found to be important on the x-residuals and factor loading plots have been labeled.

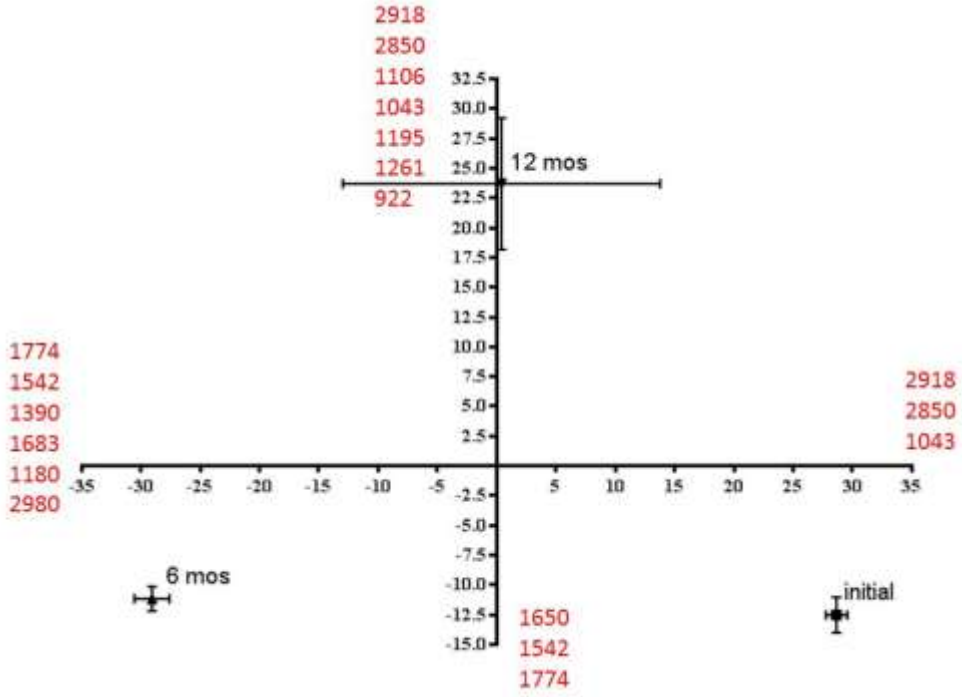

Figure 10. PCA plot of oak lamina data set. Wavenumbers are listed on the axes and direction (positive or negative) on which they influenced the spatial distribution of the data. Wavenumbers are ranked from most important to least. Error bars represent standard errors. For Axis 1 F=13.73, P = 0.0008. For Axis 2 F=37.29, P<0.0001

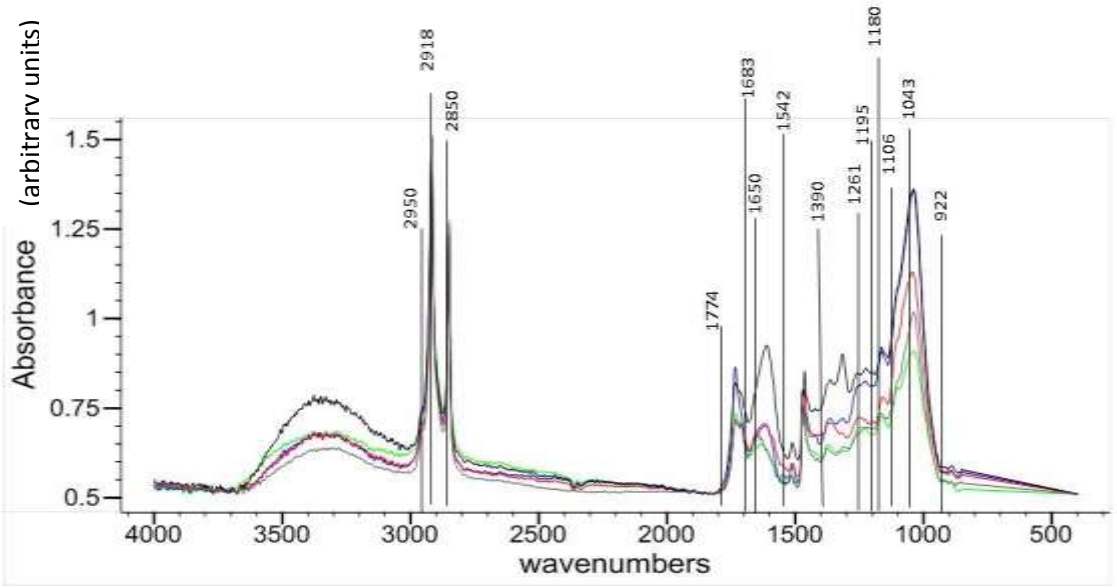

Figure 11. Oak lamina spectra at time 0. Wavenumbers found to be important on the x-residuals and factor loading plots have been labeled.

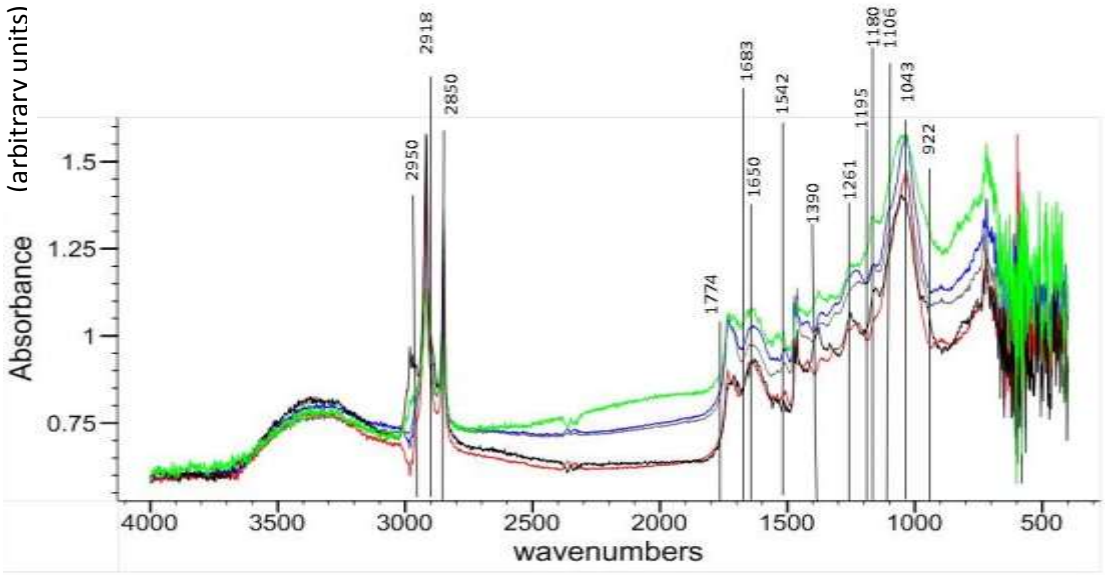

Figure 12. Oak lamina spectra at 6 months. Wavenumbers found to be important on the x-residuals and factor loading plots have been labeled.

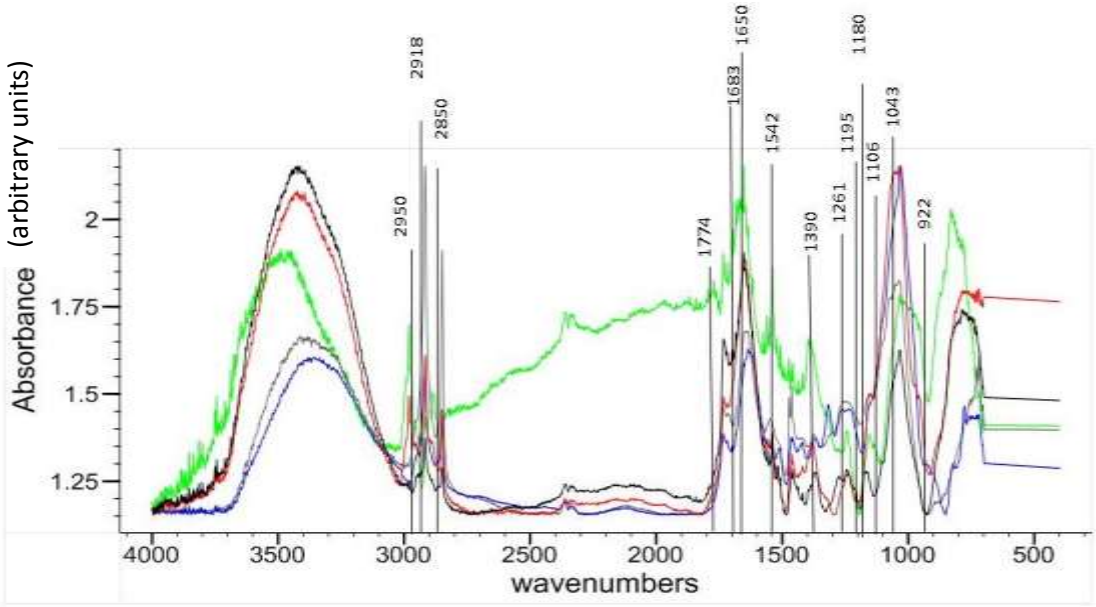

Figure 13. Oak lamina spectra at 12 months. Wavenumbers found to be important on the x-residuals and factor loading plots have been labeled.

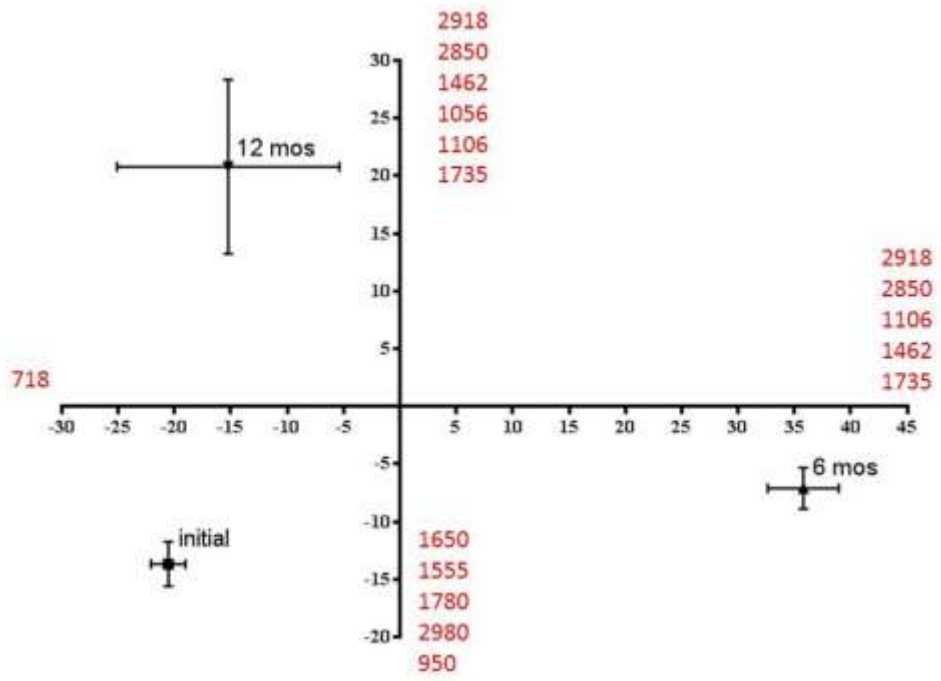

Figure 14. PCA plot of oak vein data set. Wavenumbers are listed on the axes and direction (positive or negative) on which they influenced the spatial distribution of the data. Wavenumbers are ranked from most important to least. Error bars represent standard errors. For Axis 1 F=26.46, P < 0.0001. For Axis 2 F=15.63, P=0.0005.

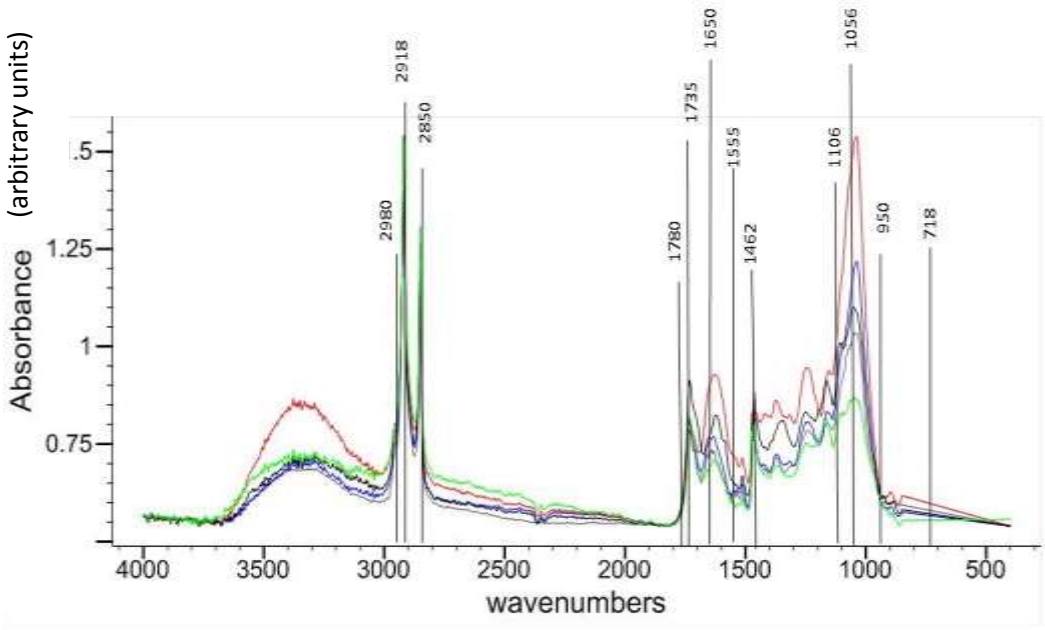

Figure 15. Oak vein spectra at time 0. Wavenumbers found to be important on the x-residuals and factor loading plots have been labeled.

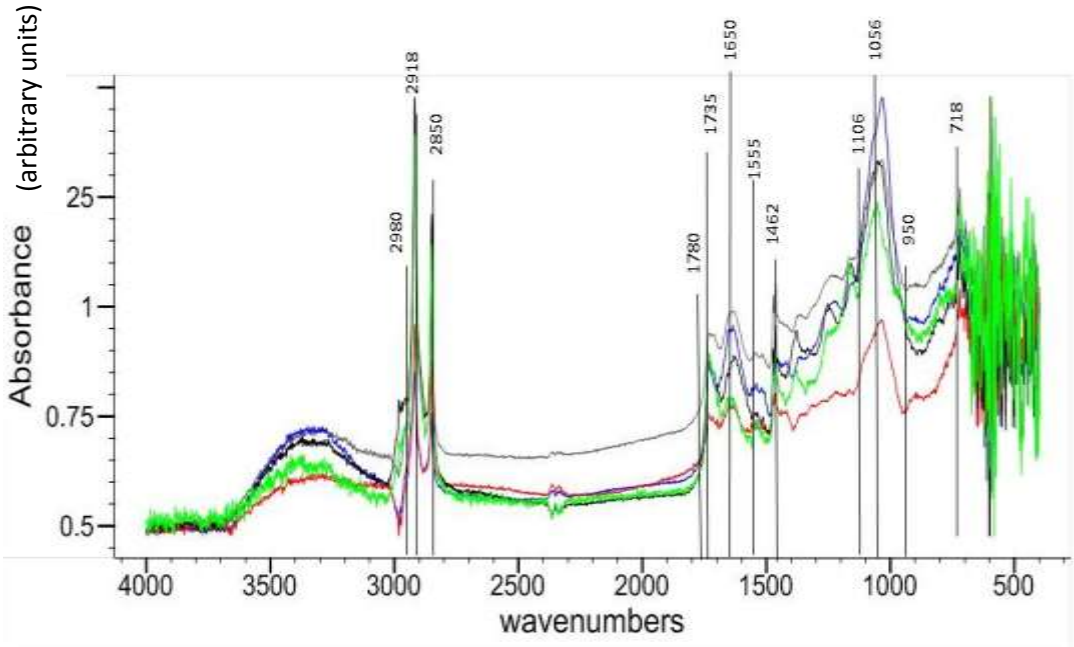

Figure 16. Oak vein spectra at 6 months. Wavenumbers found to be important on the x-residuals and factor loading plots have been labeled.

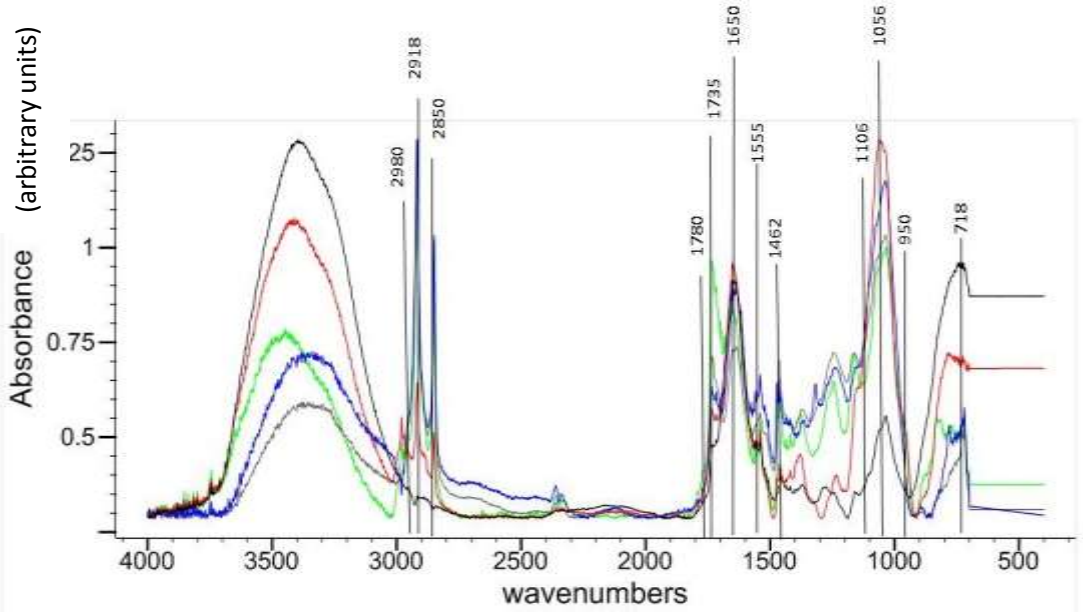

Figure 17. Oak vein spectra at 12 months. Wavenumbers found to be important on the x-residuals and factor loading plots have been labeled.

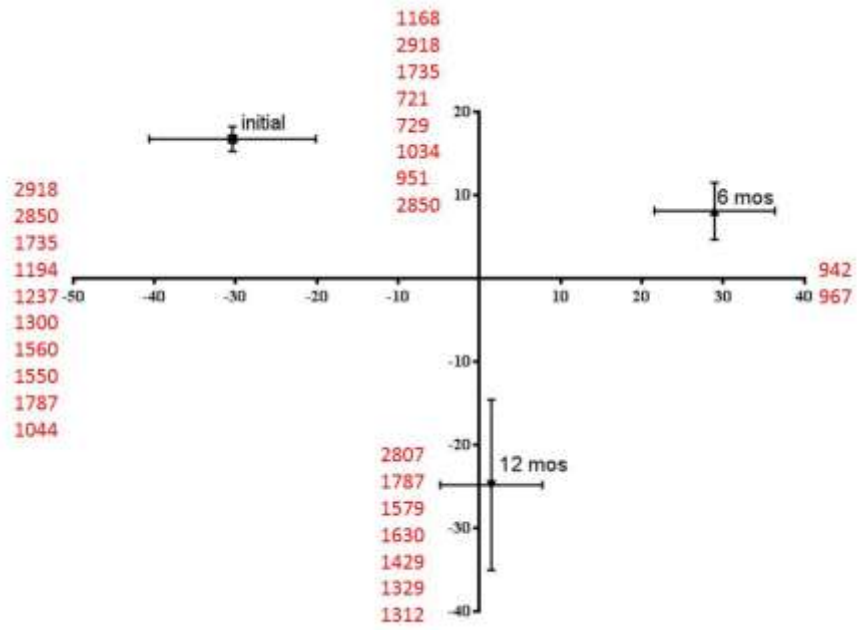

Figure 18. PCA plot of pine needle data set. Wavenumbers are listed on the axes and direction (positive or negative) on which they influenced the spatial distribution of the data. Wavenumbers are ranked from most important to least. Error bars represent standard errors. For Axis 1 F=13.23, P = 0.0009. For Axis 2 F=12.06, P=0.0013.

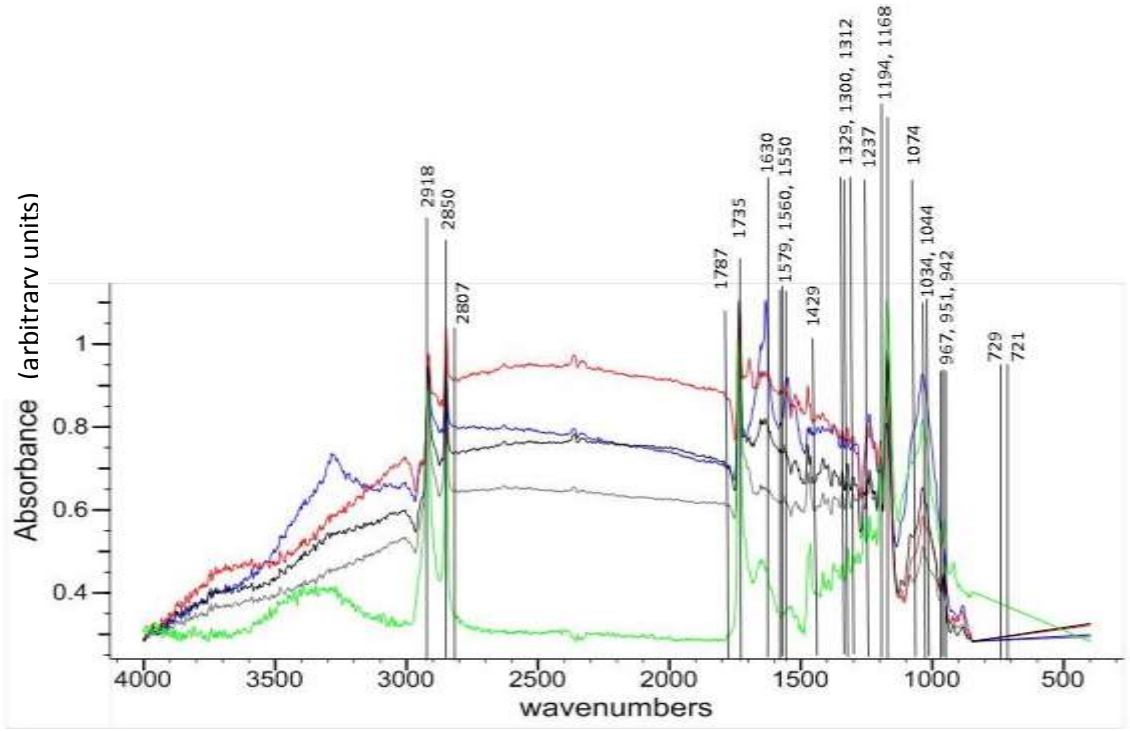

Figure 19. Pine needle spectra at time 0. Wavenumbers found to be important on the x-residuals and factor loading plots have been labeled.

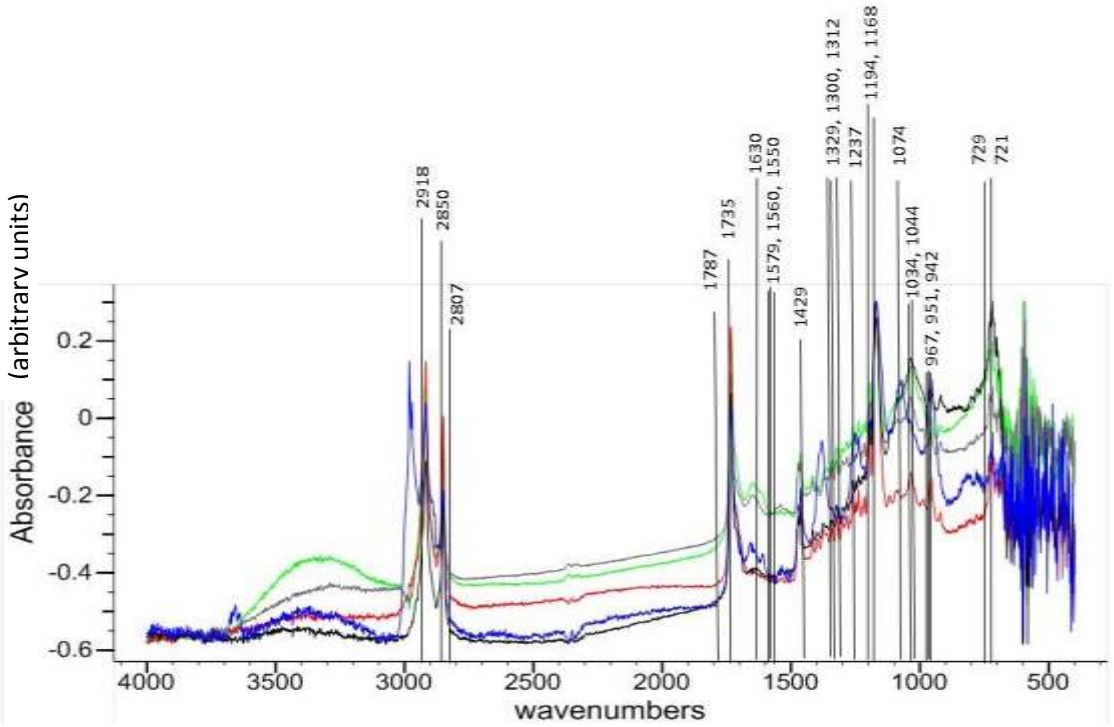

Figure 20. Pine needle spectra at 6 months. Wavenumbers found to be important on the x-residuals and factor loading plots have been labeled. Negative absorbance values are relative, not empirical.

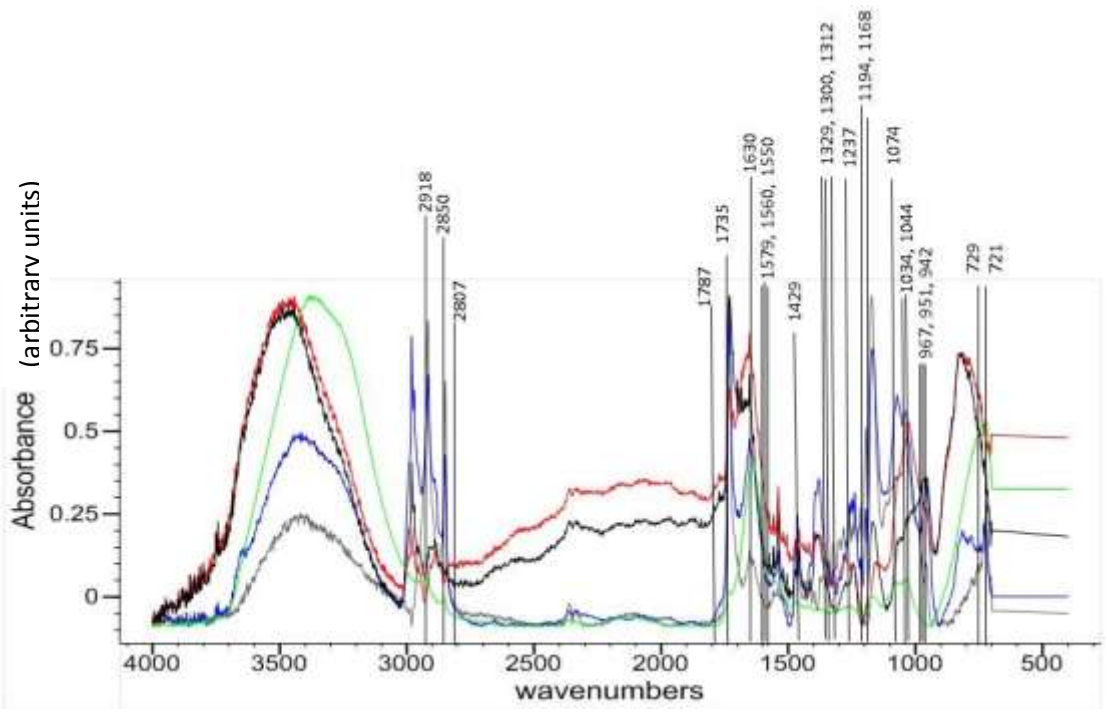

Figure 21. Pine needle spectra at 12 months. Wavenumbers found to be important on the x-residuals and factor loading plots have been labeled.

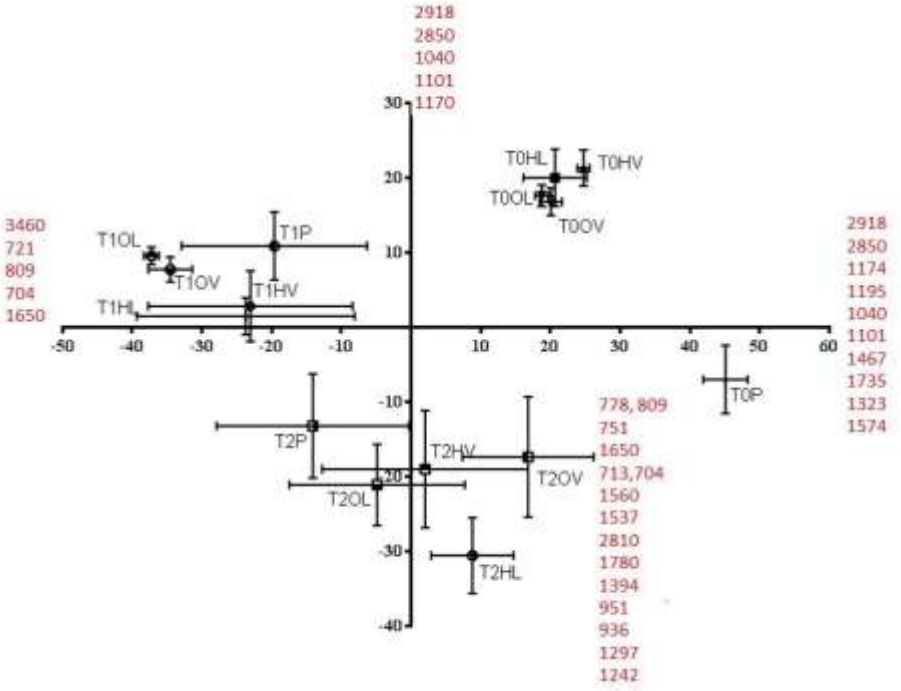

Figure 22. PCA plot of all leaf data sets. Wavenumbers are listed on the axes and direction (positive or negative) on which they influenced the spatial distribution of the data. Wavenumbers are ranked from most important to least. Means are coded as follows: T0=initial, T1=6 months, T2= 12 months; HL=huckleberry lamina, HV=huckleberry vein, OL=oak lamina, OV=oak vein, P=pine. For example, T2HL represents the huckleberry lamina spectra at 12 months. Error bars represent standard errors. For Axis 1 $F=6.61$, $P < 0.0001$. For Axis 2 $F=12.91$, $P<0.0001$.

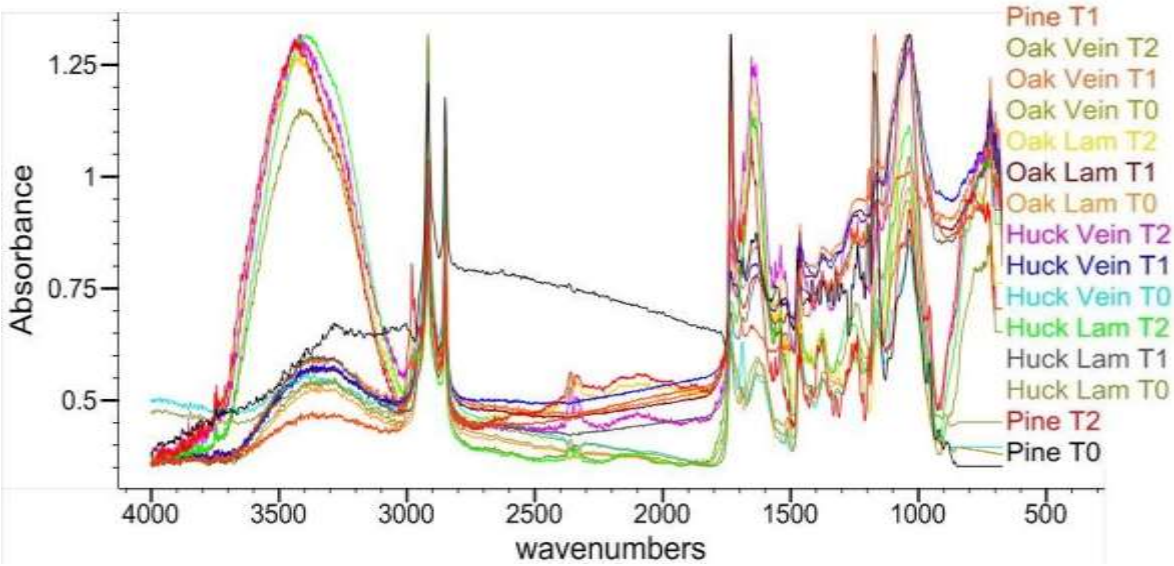

	3460	2810	1780	1574	1537	1467	1394	1323	1297	1242	1195	1174	1170	1040	951	936	809	778	751	721	713	704
Huck Lam T0	0.83	0.80	0.71	0.80	0.76	0.89	0.83	0.84	0.83	0.90	0.87	0.93	0.95	1.23	0.87	0.80	0.78	0.78	0.78	0.78	0.78	0.78
Huck Lam T1	0.35	0.29	0.30	0.46	0.44	0.52	0.51	0.55	0.56	0.62	0.62	0.67	0.69	1.03	0.67	0.63	0.70	0.73	0.76	0.84	0.83	0.81
Huck Lam T2	0.88	0.36	0.34	0.51	0.52	0.49	0.48	0.46	0.50	0.52	0.45	0.49	0.51	0.80	0.47	0.38	0.65	0.71	0.75	0.76	0.73	0.69
Huck Vein T0	1.07	1.04	0.93	1.01	0.98	1.14	1.05	1.06	1.06	1.13	1.11	1.19	1.21	1.33	1.06	1.00	0.96	0.96	0.96	0.96	0.96	0.96
Huck Vein T1	0.42	0.41	0.45	0.55	0.57	0.65	0.61	0.64	0.66	0.72	0.71	0.76	0.78	1.02	0.78	0.76	0.78	0.81	0.82	0.89	0.87	0.85
Huck Vein T2	1.11	0.65	0.67	0.82	0.85	0.82	0.81	0.80	0.85	0.88	0.81	0.85	0.87	1.12	0.73	0.67	0.92	0.97	0.98	0.99	0.96	0.93
Oak Lam T0	0.88	0.83	0.75	0.84	0.80	0.97	0.89	0.93	0.92	0.98	0.98	1.01	1.02	1.38	0.83	0.79	0.78	0.77	0.77	0.77	0.77	0.77
Oak Lam T1	0.56	0.53	0.57	0.70	0.70	0.82	0.80	0.83	0.84	0.92	0.91	0.95	0.97	1.29	0.93	0.90	0.94	0.97	0.99	1.11	1.06	1.05
Oak Lam T2	1.70	1.12	1.19	1.29	1.32	1.24	1.25	1.20	1.17	1.24	1.13	1.20	1.22	1.74	1.26	1.17	1.47	1.54	1.49	1.46	1.41	1.36
Oak Vein T0	1.05	1.00	0.91	1.03	0.99	1.15	1.07	1.08	1.08	1.18	1.14	1.18	1.19	1.50	1.00	0.96	0.93	0.93	0.93	0.93	0.92	0.92
Oak Vein T1	0.53	0.50	0.53	0.66	0.67	0.76	0.73	0.76	0.77	0.84	0.85	0.89	0.90	1.13	0.84	0.81	0.86	0.89	0.91	1.02	0.99	0.97
Oak Vein T2	1.36	0.86	0.85	1.02	1.05	1.03	0.99	0.97	0.98	1.07	1.00	1.07	1.09	1.51	0.93	0.85	1.07	1.13	1.13	1.17	1.12	1.06
Pine T0	0.17	0.28	0.21	0.24	0.24	0.28	0.25	0.27	0.25	0.28	0.32	0.47	0.47	0.31	0.15	0.10	0.07	0.07	0.07	0.07	0.07	0.07
Pine T1	0.45	0.47	0.55	0.61	0.63	0.78	0.76	0.80	0.78	0.87	1.01	1.30	1.32	1.04	0.98	0.90	0.91	0.93	0.93	1.10	1.02	1.00
Pine T2	1.90	1.27	1.35	1.34	1.39	1.37	1.39	1.31	1.31	1.39	1.37	1.62	1.65	1.62	1.44	1.32	1.64	1.66	1.63	1.63	1.54	1.48

Figure 23. The 15 average spectra from the ALL dataset are overlaid. The accompanying chart lists the important wavenumbers from the PCA analysis (columns) and their relative intensities (rows) as found on the y-axis of the spectra (T0=initial, T1=6 months, T2=12 months).

References

Boeriu CG, Bravo D, Gosselink RJA, Van Dam JEG. 2004. Characterization of structure-dependent functional properties of lignin with infrared spectroscopy. *Industrial Crops and Products* 20:205-218.

Cadish G, Giller K. 1997. Driven by Nature: Plant Litter Quality and Decomposition. CAB international, Wallingford, UK.

Chatjigakis AK, Pappas C, Proxenia N, Kalantzi O, Rodis P, Polissiou M. 1998. FTIR spectroscopic determination of the degree of esterification of cell wall pectins from stored peaches and correlation to textural changes. *Carbohydrate Polymers* 37: 395-408.

Daubenmire R, Prusso D. 1963. Studies of the decomposition rates of tree litter. *Ecology* 44(3):589-592.

Dickinson C, Pugh G. 1974. Biology of Plant Litter Decomposition Volume 1. Academic Press, London, UK.

Fioretto A, Di Nardo C, Papa S, Fuggi A. 2005. Lignin and cellulose degradation and nitrogen dynamics during decomposition of three leaf litter species in a Mediterranean ecosystem. *Soil Biology and Biochemistry* 37:1083-1091.

Frankland JC. 1998. Fungal Succession - unravelling the unpredictable. *Mycological Research* 102(1):1-15.

Gorgulu S, Dogan M, Severcan F. 2007. The characterization and differentiation of higher plants by Fourier transform infrared spectroscopy. *Applied spectroscopy* 61(3):300-308.

Jensen V. 1974. Decomposition of angiosperm tree leaf litter. In Dickinson C, Pugh G. Biology of Plant Litter Decomposition Volume 1, pp. 69-104. Academic Press, London, UK.

Johansson MB. 1995. The chemical composition of needle and leaf litter from Scots pine, Norway spruce and white birch in Scandinavian forests. *Forestry* 68(1):49-62.

Kolattukudy PE. 1980. Biopolyester membranes of plants: cutin and suberin. *Science* 208(4447):990-1000.

Kubo S, Kadla JF. 2005. Hydrogen bonding in lignin: A Fourier transform infrared model compound study. *Biomacromolecules* 6: 2815-2821.

Lammers K, Arbuckle-Keil G, Dighton J. 2009. FT-IR study of the changes in carbohydrate chemistry of three New Jersey pine barrens leaf litters during simulated control burning. *Soil Biology and Biochemistry* 41: 340-347.

Mantsch HH, Chapman D. 1996. Infrared Spectroscopy of Biomolecules. Wiley-Liss, New York, NY.

McTiernan KB, Couteaux MM, Berg B, Berg M, Calvo de Anta R, Gallardo A, Kratz W, Piussi P, Remacle J, Virzo De Santo A. 2003. Changes in chemical composition of *Pinus sylvestris* needle litter during decomposition along a European coniferous forest climatic transect. *Soil Biology and Biochemistry* 35:801-812

Melillo JM, Aber JD, Muretore JF. 1982. Nitrogen and lignin control of hardwood leaf litter decomposition dynamics. *Ecology* 63(3): 621-626.

Michell AJ. 1990. Second-derivative FTIR spectra of native celluloses. *Carbohydrate Research* 197:53-60

Movasaghi Z, Rehman S, Rehman I. 2008. Fourier transform infrared (FTIR) spectroscopy of biological tissues. *Applied Spectroscopy Reviews* 43(2): 134-179.

Oh SY, Yoo DI, Shin Y, Kim HC, Kim HY, Chung YS, Park WH, Youl JH. 2005. Crystalline structure analysis of cellulose treated with sodium hydroxide and carbon dioxide by means of X-ray diffraction and FTIR spectroscopy. *Carbohydrate Research* 340: 2376-2391.

Ponge J. 1991. Succession of fungi and fauna during decomposition of needles in a small area of Scots pine litter. *Plant and Soil* 99-113.

Pretsch E, Clerc T, Seibl J, Simon W. 1983. Tables of Spectral Data for Structure and Determination of Organic Compounds. Springer-Verlag, Berlin, Germany.

Ribeiro da Luz B. 2006. Attenuated total reflectance spectroscopy of plant leaves: a tool for ecological and botanical studies. *New Phytologist* 172: 305-318.

Satchell JE. 1974. Introduction: litter – interface of animate/inanimate matter. In Dickinson C, Pugh G. Biology of Plant Litter Decomposition Volume 1, pp. 13-44. Academic Press, London, UK.

Silverstein RM, Webster FX. 1998. Spectroscopic Identification of Organic Compounds, 6th ed. John Wiley and Sons, New York, NY.

Smidt E, Eckhardt K, Lechner P, Schulten H, Leinweber P. 2005. Characterization of different decomposition stages of biowaste using FT-IR spectroscopy and pyrolysis-field ionization mass spectrometry. *Biodegradation* 16:67-79.

Socrates G. 2001. Infrared Characteristic Group Frequencies, 3rd ed. John Wiley & Sons, West Sussex, UK.

Stewart D. 1996. Fourier-transform infrared microspectroscopy of plant tissues. *Applied Spectroscopy* 50: 357-365.

Wilson RH, Smith AC, Kacurakova MS, Willner M, Waldron, KW. 2000. The mechanical properties and molecular dynamics of plant cell wall polysaccharides studied by Fourier-transform infrared spectroscopy. *Plant Physiology* 124: 397-405.

Xiao B, Sun XF, Sun RC. 2001. Chemical, structural, and thermal characterizations of alkali-soluble lignins and hemicelluloses, and cellulose from maize stems, rye straw, and rice straw. *Polymer Degradation and Stability* 74:307-319.

CHAPTER FOUR

Chemical characterization of starch and starch: lignin films using micro-attenuated total reflectance Fourier transform infrared spectroscopy (micro-ATR FTIR)

Previously published *Trends in biomaterials and artificial organs* (2012) 26(2):107-109

Abstract

Micro-attenuated total reflectance Fourier transform infrared spectroscopy (micro-ATR FTIR) was used to investigate the chemical composition of biodegradable films produced from starch and starch: lignin in a 90:10 ratio. Preparation of the starch and lignin solutions followed that of Vengal & Srikumar [1] in which tensile strength of films was investigated. After testing the chemical composition of these films by FTIR, it was found that the films identified as starch: lignin were chemically similar to those of starch alone. During the manufacture of biopolymeric films, it is likely that compositional changes may occur in one or more components that renders the end product significantly different from the intended composition. As a result of this research, we suggest caution in the preparation of mixed component films.

Introduction

Biodegradable polymeric films are a possible alternative to the synthetic plastics so common in modern life. Most synthetic plastics are known to degrade at incredibly slow rates and are a known contributor to landfill mass. As an alternative to these synthetic plastics, research in the last decade or so has attempted to develop biodegradable polymer films from natural sources, such as starch, pectin, cellulose, and lignin [2,3,4].

In addition to the biodegradable nature of these films, they also offer important benefits to researchers requiring homogenous, smooth biological substrates for study of decomposition patterns in microbes and fungi. These materials represent analogous sub-sets of the more complex chemistry of plant leaves and stems, allowing more detailed investigation of selective enzyme activities on these chosen substrates [5,6]. In our studies, we required such a substrate to investigate the relative enzymatic activities of various fungi on lignin containing substrates. It was important that the substrate was a flat film that could be analyzed using both atomic force microscopy (AFM) and micro-attenuated total reflectance Fourier transform infrared spectroscopy (micro-ATR FTIR).

Fourier transform infrared (FTIR) spectroscopy involves the absorption of infrared radiation by the sample resulting in molecular vibrations (i.e. stretching or bending of infrared active covalent bonds in the mid-IR region of 4000 and 400 cm^{-1}). Each type of molecular vibration absorbs IR radiation at a specific spectral wavelength thereby providing qualitative and quantitative chemical information about the sample. The complex pattern of peaks produced by a sample, its IR spectrum, can then be analyzed to obtain compositional information. Peaks can be correlated with bonds (e.g. C-H stretch vs. O-H stretch), while the fingerprint region (~1500 – 400 cm^{-1}) exhibits a unique signature including many overlapping vibrations from various parts of each distinct molecule in the sample. FTIR-ATR (attenuated total reflectance) microscopy utilizes a microscope in conjunction with a traditional FTIR bench. This enables the infrared spectrum to be obtained from a specific point located under the microscope approximately 10 x 10 microns in size. Spectral information from the surface of the sample is obtained by the ATR sampling method; the sample must be in good contact with the internal reflectance element, generally Ge.

Atomic force microscopy (AFM) is a physical microscopy technique that can be used for measuring surface topography, adhesion, and elasticity. This is accomplished by deflecting a laser off a scanning probe that rapidly taps the surface of the sample and onto a photodiode that detects the surface characteristics [7]. Atomic force microscopy measures these characteristics at the μm and nm scales with limited height variability. It is this limitation in height that requires the use of flat films as the substrate for the fungal decomposition.

Our proposed study was to evaluate the extent of influence of enzymes produced by an individual fungal hypha growing across defined substrates using a combination of ATR-FTIR and AFM at a resolution of μm to nm away from the hyphal surface. However, after reproducing starch: lignin films according to the process of Vengal & Srikumar [1] it was found that lignin was not present in the starch: lignin films. Further research indicates that the process of preparing the lignin as a dissolved solute in sodium hydroxide (NaOH) causes alkaline hydrolysis of the molecule. The resulting film, therefore, had no lignin present, as is supported by our ATR-FTIR spectra.

It is imperative that the films produced via the method of Vengal & Srikumar [1] are composed of the materials published, as other researchers depend upon this accuracy for their continuing studies.

Methods

The methods of Vengal & Srikumar [1] were followed in preparation of starch: lignin and starch-only films, with exception of the lignin source. Vengal & Srikumar extracted their own lignin from wood, whereas we obtained lignin from Sigma Aldrich. Starch: lignin films were 90% starch, 10% lignin, whereas the starch-only films were 100% starch. Tapioca starch was used to produce the starch solution. The starch: lignin polymer films (90:10) were cast from a solution of

4g of tapioca starch with 75 ml of water at 100^{o} C until the starch was dissolved. Glycerol (5 drops) was added to the mixture (as a plasticizer) and 10 ml of lignin solution (3g / 75 ml NaOH). The resulting solution was cast on plastic cover slips and allowed to cure. Starch only films were cast in the same manner excluding the addition of the lignin/NaOH solution.

Following curing, the films were analyzed on an Agilent (formerly Bio-Rad) FTS 6000 infrared spectrophotometer with an attached UMA 500 microscope with a germanium ATR crystal. 256 scans were averaged at a resolution of 4 cm^{-1} ; background was air. As spectra were compared to each other, no ATR correction was applied. All spectra were normalized. Spectra were obtained from 3 replicates of the 90:10, starch: lignin films and 3 replicates of the starch only films. Spectra of pure lignin were also obtained by pressing lignin into a pellet and contacting the pressed lignin pellet against the ATR crystal. The pellet was prepared by grinding lignin in a mortar and pestle then loading a small amount into a KBr pellet press to produce a solid pellet of lignin.

Results

The infrared spectra of the starch: lignin and the starch-only films are nearly identical, see Fig. 1. Both films generated spectra with peaks at 1457, 1151, 1079, 1019, 931, and 852 cm^{1}. Table 1 shows the main spectral peaks in the lignin pellet and both the starch: lignin and starch only films. It can be seen that other than a peak at 1079 cm^{-1}, there are no common peaks between the lignin and starch: lignin film. The starch: lignin film has complete congruence of major peaks with the spectrum of starch alone.

Conclusion

The results outlined above and in figure 1 and table 1 indicate that during the preparation of the starch: lignin films, there appears to be a reaction resulting in the loss of lignin from the system. The strong similarities of the starch and starch: lignin spectra, as well as their overwhelming contrast to the lignin spectra clearly indicate that there is no lignin present in the resulting starch: lignin films. According to Miller et al. [8], when exposed to an alkaline solvent lignin depolymerizes. This coincides with the known process of alkaline degradation of polysaccharides as outlined in Kennedy & White [9]. The only spectral peak that is common between the lignin and starch: lignin film is that at 1079 cm^{-1}. This peak at 1079 cm^{-1} is common in many polysaccharides [10], so it would be expected to still be present in the NaOH degraded lignin.

As a result of this research, we suggest caution in the manufacture of mixed component films. During the manufacture of films it is likely that compositional changes may occur in one or more components that renders the end product significantly different from the intended composition. The original intent of use of films by Vengal & Srikumar [1] was different from ours and may not have been influenced as much by the actual chemical composition of the end product of film casting. However, if one is attempting to produce films of known composition of the identical chemistries of component parts, caution must be taken to ensure that the end product does indeed have the desired components. For example the films created by the Vengal & Srikumar [1] process are inappropriately named as starch: lignin films, when the films are more representative of starch alone.

Tables

Table 1. Comparison of main spectral peaks between lignin, starch, and 90:10 starch: lignin films. X's indicate the presence of a peak within the spectrum and blank boxes indicate the absence of a peak. Starch only and starch: lignin films share the same peaks , but contrast with lignin in all peaks, with exception of 1079.

Wavenumber (cm^{-1})	Lignin	Starch	Starch Lignin
1594	X		
1512	X		
1457		X	X
1453	X		
1368	X		
1266	X		
1214	X		
1151		X	X
1139	X		
1130	X		
1079	X	X	X
1030	X		
1019		X	X
931		X	X
852		X	X

Figures

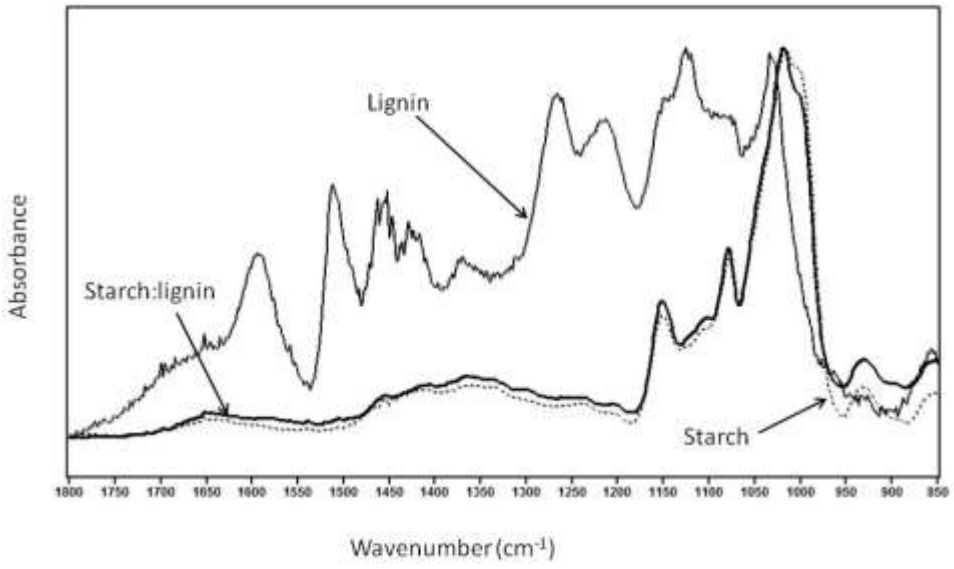

Figure 1. Overlaying spectra from the three films highlights similarities in peak presence between the starch and the starch: lignin films that contrasts from those of lignin.

References

1. J.C. Vengal and M. Srikumar, Processing and Study of Novel Lignin-Starch and Lignin-gelatin Biodegradable Polymeric Films, Trends in Biomaterials and Artificial Organs, 237-241 (2005).
2. L. Mariniello, P. Di Pierro, C. Esposito, A. Sorrentino, P. Masi, and R. Porta, Preparation and Mechanical Properties of Edible Pectin-Soy Flour Films Obtained in the Absence or Presence of Transglutaminase, Journal of Biotechnology, 191-198 (2003).
3. R. Singh, S. Singh, K.D. Trimukhe, K.V. Pandare, K.B. Bastawade, D.V. Gokhale, and A.J. Varma, Lignin-Carbohydrate Complexes from Sugarcane Bagasse: Preparation, Purification, and Characterization, Carbohydrate Polymers, 57-66 (2005).
4. D. Tapia-Blacido, P. J. Sobral, and F.C. Menegalli, Development and Characterization of Biofilms Based on Amaranth Flour (*Amaranthus caudatus*), Journal of Food Engineering, 215-223 (2005).
5. P.M. Latter and D.W.H. Walton, The Cotton Strip Assay for Cellulose Decomposition Studies in Soil: History of the Assay and Development, Cotton Strip Assay: An Index of Decomposition in Soils,7-10 (1988).
6. J.C. Went and F. De Jong, Decomposition of Cellulose in Soils, Antonie van Leeuwenhoek, 39-56 (1966).
7. V.J. Morris, A.R. Kirby, and A.P. Gunning, Atomic Force Microscopy for Biologists, 2nd edition (Imperial College Press, 2010) p 1-33.
8. J. E. Miller, L.R. Evans, J.E. Mudd, and K.A. Brown, “Batch Microreactor Studies of Lignin Depolymerization by Bases”, Sandia National Laboratories, SAND2002-1318, (2002)
9. J.F. Kennedy and C.A. White, Bioactive Carbohydrates (Ellis-Horwood Publishers, 1983) p66-76.

10. H.H. Mantsch and D. Chapman, Infrared Spectroscopy of Biomolecules (John Wiley and Sons, Inc., Publications, 1996) p 207-210.

CHAPTER FIVE

Atomic force microscopy and micro-ATR-FT-IR imaging reveals fungal enzyme activity at the hyphal scale of resolution

Previously published in *Mycology: An International Journal of Fungal Biology,*

DOI:10.1080/21501203.2012.759631

Abstract

We have combined the use of atomic force microscopy (AFM) and micro-attenuated total reflectance Fourier transform infrared (micro-ATR-FT-IR) imaging to show the extent of exoenzyme influence around individual hyphae of three fungal species growing on cellophane. AFM data shows that surface roughness of the cellophane substrate is significantly lower adjacent to hyphae of *Armillaria* and *Aspergillus*, which produce cellulase enzyme, than for *Mucor,* which has lower cellulase activity. Additionally, the adhesive properties of the cellophane surface are significantly altered within the sphere of influence of the hyphae of *Armillaria* and *Aspergillu*s. Micro--ATR-FT-IR imaging indicates that the cellophane substrate changes composition immediately adjacent to the hypha of *Armillaria* and *Aspergillus*, but similar spectral changes do not occur in the presence of *Mucor*. This is consistent with the difference in cellulase enzyme activity in these fungal species. The appearance of new spectral peaks, consistent with those expected in the presence of enzymes and the minor decrease in peaks associated with cellophane adjacent to these hyphae are consistent with the hypothesis that the changes observed by AFM are due to local effects of enzyme action around individual hyphae.

Introduction

Atomic force microscopy (AFM) has been used in biology (excluding molecular and biochemical studies), to measure surface morphology of structures (Morris *et al*. 2010) and surface and elastic properties of hyphal cell walls (Ma *et al.* 2005; Zhao *et al*. 2005a; 2005b; Paul *et al.* 2011) . The application of AFM to mycology has been extensively discussed by Ma *et al.* (2006) and Kaminskyj & Dahms (2008) who show the benefits of this technique by providing not only visualization of the fungal structures, but also information about the physicochemical nature of the fungal structures. We present here preliminary data to show changes in the physical properties of substrates affected by individual fungal hyphae at the micrometer scale of resolution using a combination of AFM and micro-attenuated total reflectance Fourier transform infrared (micro-ATR FT-IR) microspectroscopic imaging. These are initial investigations of a larger study to evaluate the functional relationships between fungal hyphae of contrasting species and the underlying leaf substrates they are decomposing at the hyphal scale.

In mycology, AFM has largely been used for observational studies of fungal structures. Holder & Keyhani (2005) and Holder *et al*. (2007) imaged fungal spores and germinating hyphae. Kim (2006) and Kim *et al*. (2007) imaged spores of the smut *Ustilago* and basidiospores of puffballs, Kaminskyj & Dahms (2008) imaged fungal cell walls and Zhao *et al*. (2005a; 2005b) measured topography and elasticity of *Aspergillus* spores. Dague *et al*. (2008) showed changes in the shape and surface physicochemical structure of germinating spores of *Aspergillus fumigatus*. Holder *et al*. (2007) studied germinating conidiospores of the entomopathogenic fungus *Beauvaria bassiana* and Kaminskyj & Dahms (2008) provided good images of germinating *Aspergillus* conidia. Closely related to our study is the work of Ma *et al*. (2005) who investigated

the adhesion forces along developing fungal hyphae by AFM. One of their conclusions was that the rigidity of the fungal hypha increased proximally from the tip as elasticity decreased.

Examination of the enzymatic effects on substrate surfaces using AFM have often used commercially available fungal-derived enzymes to follow changes in surface characteristics of substrates. However, these studies have not been conducted in association with fungal hyphae. Studies have included the esterase activity on water soluble wheat xylans (Adams *et al*. 2005) and laccase and tyrosinase effects on polymeric phenolics. Desentis-Mendoza *et al*. (2006) show changes in the physical structure of quercetin and kaempferol due to the effects of laccase and tyrosinase enzymes at the 5 µm scale of resolution. Effects of xylanase activity on kraft pulp bleaching (Medeiros *et al*. 2007), *Penicillium* derived depolymerases action on poly[(R)-3-hydrobutyric acid] (Numata *et al*. 2007), *Trichoderma* derived cellulose hydrolysis of cotton fibers (Wang *et al*. 2006), lipase degradation of poly(trimethylene carbonate) (Zhang *et al*. 2005) and adsorption of laccase from *Trametes* and *Melanocarpus* on cellulose and lignin (Saarinen *et al*. 2009) have also been investigated. Yokata *et al*. (2008) also appliedAFM to investigate the cellulose-binding domain/cellulose interface in paper pulp.

Our interest lies in the fungal decomposition of plant remains. There are a limited number of AFM studies of plant material, which include surface morphology of ivy leaves (Canet *et al*. 1996), morphology and chemistry of *Prunus* leaves (Perkins *et al*. 2005) and leaf surface topography for microbial habitats (Mechaber *et al*. 1996) and barley straw (Wiśniewska *et al*. 2003). These studies have highlighted the problems of interference from surface wax layers of leaves, restricting observation of the underlying cellulose cell wall (Koch *et al*. 2003; 2004; 2006).

FT-IR spectroscopy is a well-known analytical method for the analysis of biological materials. The IR spectrum contains both useful group frequency vibrational information that

provides clues to the chemical structure of the substance as well as unique 'fingerprint' peaks whereby an unknown compound can be matched against that of an authentic sample (Socrates 1994). The extremely complex spectra of biological samples which are by their nature a mixture of substances can be probed at the micro-scale using micro-FT-IR spectroscopy. More recently, FT-IR micro imaging has emerged as a tool to analyze heterogeneous materials (Kidder *et al*. 2002). The advancements in multi-pixel IR detectors (focal plane array or FPA detector) provide fast imaging due to the ability to simultaneously record thousands of spectra (Lewis *et a*l. 1995). In addition, the use of Attentuated Total Reflection (ATR) FT-IR spectrochemical imaging in conjunction with an interferometer coupled to the FPA, results in a significantly higher spatial resolution with good signal to noise since the spatial resolution is not achieved by passing the infrared through an aperture that is isolating the area of interest but by making use of the small size of the native detector pixels to achieve the high spatial resolution. In addition in the ATR experiment, there is a magnification effect of the germanium internal reflection element in contact with the sample (Milosevic 2004).

Numerous advances have occurred in FT-IR microspectroscopy over the past two decades. In addition to the ability to examine biological samples at the microscopic scale using transmission techniques (Stewart 1996), micro-ATR (attenuated total reflectance) imaging provides enhanced spatial resolution as a result of the germanium internal reflection element (IRE) (Griffiths 2009). Micro-ATR-FT-IR imaging utilizes a Ge ATR crystal in contact with the sample. Micro-ATR-FT-IR imaging has recently been used as a tool to investigate chemical composition of biological samples (surface of skin, cross-section of blood vessels, hair) with higher resolution than was previously possible using traditional IR methods (Kazarian & Chan 2010).

Using synchrotron FT-IR microspectroscopy (transmission mode) Szeghalmi *et al.* (2007) identified differences in IR spectra between hyphae of *Aspergillus*, *Neurospora* and *Rhizopus* and slight spectral changes in each of these when grown in sub-optimal conditions. Similarly, we have identified significant differences in spectral properties of a number of fungal species, using a Bio-rad FTS 6000 FT-IR with attached UMA 500 ATR microscope (Ge IRE) in single point mode. These differences existed in both transmission and ATR mode in our studies. (Oberle-Kilic *et al.* unpublished).

In this study we have combined the utility of AFM to measure surface physical properties of a substrate with Micro-ATR-FT-IR imaging which analyzes chemical characteristics. Micro-ATR FT-IR imaging illustrates changes at the micro-scale which can be attributed to the influence of contrasting fungal species on the substrate in the immediate vicinity of specific hypha. The degree of substrate surface change correlates with the enzymatic competency of the fungi. In this study, we reduced the complexities of both chemical and physical heterogeneity by observing hyphal growth over cellophane films, which have long been used for studies of the decomposition of cellulose in soil (Went & DeJong 1966; Nilsson 1974; Moore *et al*. 1979). The particular fungi growing on these films were selected for their enzyme production, with *Aspergillus* and *Armillaria* possessing cellulase activity, while *Mucor* has limited enzymatic ability.

Materials and Methods

Three fungal species were selected to represent fungi with contrasting enzymatic capabilities. *Mucor* sp. was selected for its limited enzyme capacity since its ecological niche is mainly in the utilization of readily available carbon sources from simple sugars. *Aspergillus niger* and *Armillaria mellea* were selected as they have known cellulase activity, allowing them to degrade more complex carbohydrates than *Mucor* (Frankland 1966). The *Armillaria* and

Aspergillus cultures were obtained from Carolina Biological Supply Company. The *Mucor* culture was isolated from cranberries in the NJ Pinelands and identified in Dr. Jim White's plant pathology laboratory at Rutgers University. Each culture was grown on cellulose agar to confirm the presence or absence of a clearing zone (Rautela & Cowling 1996). *Aspergillus* and *Armillaria* were confirmed to clear the cellulose agar, and *Mucor* did not clear cellulose (as expected). The three fungal species were grown on optimal media; the *Mucor* and *Aspergillus* were grown on potato dextrose agar and *Armillaria* on bread crumb agar. A square piece of cellophane film (1 cm x 1cm) was mounted to a glass microscope slide as a substrate and a small agar cube of fungal inoculum was placed on the corner of the cellophane square. The entire slide was placed in a sterile damp chamber consisting of a sterile glass Petri plate containing sterilized moist filter paper and sealed with Parafilm. Three replicate cellophane films were prepared for each fungal species; from these, one hyphal tip per replicate was analyzed. After 48 hours, the agar cube and hyphae growing out from it were severed and the agar cube was removed. Hyphal growth was permitted for an additional 24 hours in the damp chamber to allow the fungus to be released from the nutrient and carbon source provided by the agar and to stimulate enzyme activity that might affect the cellophane. At the end of the incubation period the slide and cellophane were air dried at room temperature. Samples were not washed before drying as we wanted to retain any solubilized end products of decomposition and enzymes *in situ*.

Each sample was processed on an Asylum Research MFP-3D Atomic Force Microscope using an Olympus AC240TS silicon tip of spring constant 2 (0.5-4.4) N/m and resonance frequency of 70 (50-90) kHz. A 20x20 micron scan was performed on a randomly selected individual hyphal tip at 0.22 Hz with 1024 scan points and 1024 scan lines in AC (tapping) mode.

Following the scan, a force map was generated using 40 scan points on 40 lines, or 1 force measurement every 0.5 μm^2. All scans and their associated force maps were performed with the same tip within the same image to ensure that different areas of individual force maps could be compared even though the tip was not calibrated against an infinitely hard surface as a reference. Frequency histograms of force measurements adjacent to the fungal hypha and at a distance from the hypha were plotted to determine differences in force characteristics of the cellophane film as influenced by the hyphal presence.

Surface roughness of the cellophane was measured adjacent to the hypha (between 0 to 5 µm of the hyphal cell wall) and at a distance from the hypha (10 – 15 µm away from the cell wall) using the height trace image. The root mean squared (RMS) height was calculated from an area outside the perceived area of influence of the hypha as determined by the AFM image by masking out the hypha and area immediately around it which showed changes in texture. This was compared with the area influenced by the hypha, which was masked out both from the hypha proper and from the outside area.

Roughness was calculated, by the Asylum MFP-3D software, using the root mean squared (RMS) method (Morris *et al*. 2010). This calculation produces a measure of variance between the maximum and minimum heights over the surface area, resulting in a positive correlation; higher RMS values mean higher variation in surface topography (Eaton & West 2010). The differences between the RMS values were compared between locations near and far from each hypha using one way ANOVA. These were then compared to RMS data from unmanipulated cellophane.

Micro-ATR-FT-IR images were collected from each sample of fungus growing on cellophane with a continuous scan spectrometer, Agilent 680 FT-IR interfaced to a 620 infrared

microscope with a 64 x 64 focal plane array (FPA) detector and Ge ATR objective for micro-ATR. Each pixel obtains a full IR spectrum for a total of 4096 spectra. Background spectra were collected from a clean ATR crystal (i.e. without sample). The germanium crystal of the ATR microscope was lowered onto the surface of each sample for a contact area of approximately 100 x 100 µm. Spectra were collected at 8 cm^{-1} resolution. Chemical images shown in Figure 5 were obtained from samples of each fungus. The standard IR imaging technique, in which the spectra are ratioed against an unchanged peak, was applied to the entire image. The fingerprint region is shown from ~1800 cm^{-1}; the FPA cuts off at 950 cm^{-1}.

Using the focal plane array detector, spatial resolution of approximately 2 m (at 1,000 cm^{-1} or 10 microns) can be achieved. The spatial resolution varies with wavelength according to the Rayleigh criterion. The depth of penetration resulting from ATR imaging is also wavelength dependent. The use of the germanium crystal (refractive index = 4) in contact with the surface of the sample increases the resolution approximately four-fold (Griffiths 2009).

Results and Discussion

AFM has been used for observing topographical and other physical surface phenomena at the micro- to atomic scale. Other than its application to molecular and biochemical studies, its use in biology has largely been for the observation of surface structures of organisms. In the field of mycology, a number of topographical observations of fungal hyphae and spores have been made along with some measures of the surface properties of these entities (Ma *et al.* 2005; Zhao *et al.* 2005a; 2005b; Paul *et al.* 2011). In this article we show that this technique can address functional aspects of mycology. Our application is to the fine scale of interaction between fungal hyphae of contrasting species and enzymatic capabilities and the substrate they are colonizing.

AFM height images of each fungal species on cellophane are shown in Figure 1. The cellophane surface immediately surrounding the *Aspergillus* and *Armillaria* hypha (for approximately 5 μm) are visibly different in the height images, suggesting changes proximal to the hypha in both the cellophane surface and accumulation of hyphal exudates not present in *Mucor*.

The area proximal to the hypha of *Aspergillus* and *Armillaria* appears to be much smoother than the general matrix of cellophane distant from the hypha. Indeed, measures of surface roughness (RMS values) of the cellophane indicate that there is a statistically significant difference (Table 1) in surface roughness between the areas near the hypha and those far from the influence of the hypha in both *Aspergillus* and *Armillaria;* this is not observed in *Mucor.* This is supported by the RMS data of unmanipulated cellophane where there is no significant difference in surface roughness between pure cellophane and cellophane located away from the hyphae on our samples. These results support observations in the height images in which the area surrounding both *Aspergillus* and *Armillaria* appear different than the remainder of the image; again, this is not found in the AFM image of *Mucor*. Although they did not report RMS values, Zhang *et al.* (2005) showed increased heterogeneity in height of a poly (trimethylene carbonate) film during decomposition by lipase. Similarly, Wang *et al.* (2006) showed increasing RMS values from 23.7 through 30.9 to 91.5 nm in cotton microfibrils at zero, 6 and 12 d incubation in cellulase from *Trichoderma*. In contrast, a decrease in RMS was detected over time as kraft lignin pulp was degraded by xylanase (XYL III) (Medeiros *et al.* 2007). Examples of transects of height trace across hyphae into the outlying cellophane are given in Fig. 2. For *Aspergillus* and *Armillaria*, these traces show a smooth connection between the hyphae and the substrate. We hypothesize that the fungus secreted enzymes which dissolved cellophane. Preliminary micro-ATR-FT-IR imaging is consistent with this hypothesis and a more detailed IR

analysis is planned. We attribute the changes found via AFM to the solubilizing action of cellulase enzymes secreted by these fungi as no such changes are evident in the *Mucor* image where the cylindrical hypha appears to sit directly on the cellophane with minimal changes to the neighboring cellophane surface. This is somewhat consistent with data from Ma *et al*. (2005) who showed decreasing elasticity of fungal hyphae distally from the tip. Elastic areas are presumed to be sites where enzyme secretions occur, depending on the substrate and enzyme production potential of the fungal species.

Beneath each image (Fig. 1) is its respective force map indicating contrasting areas of adhesion work (see Fig. 4). For example, dark red squares represent surfaces with low adhesion and dark blue squares surfaces with higher adhesive properties. Significant differences in the pattern of forces can be seen adjacent to the hyphae of *Aspergillus* and *Armillaria,* but not so for *Mucor*. Fig. 3 shows examples of frequency distribution histograms of adhesion work from stratified random pixels selected adjacent to and distant from hyphal surfaces. These show that there are differences close to and distant from hyphal surfaces in *Aspergillus* and *Armillaria,* but not for *Mucor*. Again we attribute these differences to the changes in the physical properties of cellophane and the presence of cellulase enzymes secreted by *Aspergillus* and *Armillaria*; similar enzymes are not produced by *Mucor*. Fig. 4 shows examples of force curves for the extreme conditions of dark red and dark blue pixels for *Armillaria*, along with the intermediate force curve colored light yellow. The predominance of blue pixels on the force map occurring distant to the hypha show the greatest adhesion work required to pull the tip from the surface. In contrast, the red pixels predominant around the hyphal surface exhibit very little adhesion work required.

In addition to the AFM results, the IR spectra obtained from the micro-ATR-FT-IR images of *Armillaria* and *Aspergillus* on cellophane indicate spectrochemical differences between areas adjacent to and distant from the hypha (Fig. 5). A representative point adjacent to the hypha (black star) and distant from the hypha (red star) for each fungal species has been selected to show representative spectra at these positions (Fig. 5). Spectra obtained from the *Mucor* sample indicate little difference between locations adjacent to the hypha or at a distance from the hypha. IR peaks of interest are labeled in Figure 5 and summarized in Table 2. These IR bands may be attributable to cellophane (1020, 1155cm^{-1}), cellophane degradative products or conjugated carbonyl structures (1732 cm^{-1}), and enzymes (1252, 1420, 1650 cm^{-1}) (Table 2). These spectra can be compared to the ATR FT-IR spectrum of cellophane alone (Fig. 6). *Aspergillus* and *Armillaria* spectra obtained near the hypha indicate a reduction in intensity of 1020 cm^{-1} (cellophane peak), loss of peak 1155 cm^{-1} (cellophane peak), and the appearance of peak 1732 cm^{-1}consistent with cellophane decomposition. Furthermore, *Armillaria* and *Aspergillus* spectra indicate the presence of enzymes adjacent to the hypha with increased intensity of peaks 1252 cm^{-1} (Amide III, N-H), 1420 cm^{-1} (CH of carboxylic acid or aliphatic aldehyde), and 1650 cm^{-1} (Amide I, C=O). The increase in the band at 1420 may be due to a combination of factors, including protein exudates as well as a number of organic acids that fungi are known to produce as secondary metabolites. In *Mucor*, there was a slight increase at wavenumber 1650 cm^{-1}, that may be attributable to very small amounts of enzyme secretion, but there appears to be no evidence of cellophane degradation (Fig. 5). This may indicate that what little enzyme *Mucor* may have produced was not capable of cellophane degradation.

Recalling that different functional groups may vibrate at similar frequencies, the pattern of peaks produced by many complex organic mixtures may be used to obtain basic compositional information with regards to specific functional groups, but it does not provide

enough information to positively identify specific compounds. It is clear from the spectra taken near the hypha and far from the hypha that changes are occurring in the substrate, however, these changes are difficult to characterize.

We show that we can observe changes in surface roughness and adhesion work in the surface of a model cellophane film as influenced by enzymes secreted by fungal hyphae. These changes have been mapped at the micrometer scale along the length of the advancing hyphae and perpendicular to its direction of growth. Thus we feel we are able to interpret the sphere of influence of an individual hypha on a substrate.

Our results show significant changes in the cellophane surface within 3 – 5 μm of the hyphal surface which we attribute to enzymatic activity. This activity is species specific, being found in *Aspergillus* and *Armillaria,* which are known to possess cellulase enzyme activity, and not in *Mucor*, which has more limited enzymatic competence. Fungal decomposition of resources has been studied by measuring gross chemical changes in resource chemistry over time (Norby *et al*. 2001). Until recently methodology to measure changes in resource chemistry at the scale of resolution of individual fungal hyphae (of the order of 5 – 10 μm) has not been available.

Although we have simplified our experimental conditions to investigate changes in a relatively homogenous resource, there is interest in identifying changes in heterogenous resource quality during fungal decomposition (Rayner 1991; Ritz 1995). It is possible to detect changes in resource carbohydrate chemistry due to a variety of fungal enzyme activities (Mascarenhas *et al*. 2000) using microscopic ATR FT-IR; the complexities of mixed carbohydrate skeletons within the matrix of leaf tissues can be de-convoluted near the scale of resolution of fungal hyphae (approximately 100 x 100 μm) (Dighton *et al*. 2001). The patchiness of diverse

resources in dead leaves results in a micro-scale mosaic which is exploited by individual fungal hyphae capable of secreting appropriate enzymes to utilize the resources and whose chemistry changes over time (Swift *et al*. 1979). Such micro-scale patchiness in enzyme production has been reported by mapping enzymes on 5 mm diameter disks decomposing American Sycamore leaves in aquatic systems (Smart & Jackson 2009). They provided krigged maps of enzyme activity (β-glucosidase, cellobiohydrolase and of the combination of phenol oxidase and peroxidase) across leaf surfaces. This mapping of enzyme activity suggested areas of microbial activity, but were neither related to actual microbial presence, nor to the nature and changes of the leaf chemistry at the locations of high enzyme activity.

In this paper, we are able to make the connection between fungal hyphae, the resource over which they are growing and the influence of their enzymes at the appropriate scale of an individual fungal hypha. Although the chemical complexity of the substrate, fungus, and enzymes makes specific chemical characterization difficult, we absolutely observe changes in both the physical and chemical properties surrounding hyphae of *Armillaria* and *Aspergillus* growing on cellophane, but not *Mucor*. There are still considerable problems in de-convoluting the complexity of a mixed organic system where FT-IR is not specific in its analysis of discrete molecules. The same band can be interpreted as belonging to a variety of compounds and each molecule can have hundreds or more signatures; an average protein molecule can have up to 20,000 vibrational degrees of freedom (Barth & Zscherp 2002). FPA methods and the tight association between spectral acquisition and small spatial scale resolution is the only way in which some degree of understanding of changes in chemical composition can be made. We have made an initial step in this direction by looking at both the physical and chemical changes at the micro-scale of resolution between fungal hyphae and their resources (substrates).

Our next challenge is to measure similar effects of hyphae that are growing over a leaf surface and are producing enzymes that decompose the resources within that leaf. We are in the position now to address questions of the functionality of growth patterns of fungal hyphae (Rayner 1991; Ritz 1995). We predict that hyphal branching patterns and space filling by fungal hyphae colonizing and utilizing resources is energetically efficient with minimal overlap of areas into which enzymes are secreted; i.e. fungal hyphae of the same individual do not compete for resources.

Tables

Table 1. Mean surface roughness (RMS) difference between cellophane surface within 5µm of the hypha and > 10 µm away. Different superscript letters indicate significant differences at α=0.05 between means (Tukey's Honestly Significant Difference Test) with like letters being not significantly different.

Species	Mean RMS (µm) difference (± SE)
Armillaria	0.180 ± 0.025 ^{A}
Aspergillus	0.176 ± 0.027 ^{A}
Mucor	-0.026± 0.018 ^{B}
ANOVA between species	$F = 24.4_{(2,6)}$, P = 0.0013

Table 2. Interpretation of the specific wavenumbers shown to vary significantly due to the influence of fungal hyphae (Fig. 5).

Wavenumber (cm^{-1})	Functional Group	Associated Compound	Reference
1732	C=O	Aliphatic aldehydes, conjugated carbonyl structures	Socrates, 1994; Cohen & Gabriele, 1982
1650	C=O	Amino acid-protein (Amide I)	Mantsch & Chapman, 1996
1420	C-H	Carboxylic acid, aliphatic aldehyde	Socrates, 1994
1252	N-H	Amino acid-proteins (Amide III)	Socrates, 1994
1155	C-O-C	Cellulose (cellophane)	Stewart, 1995
1020	C-OH	Complex sugar ring modes (cellophane)	Mantsch & Chapman, 1996

Figures

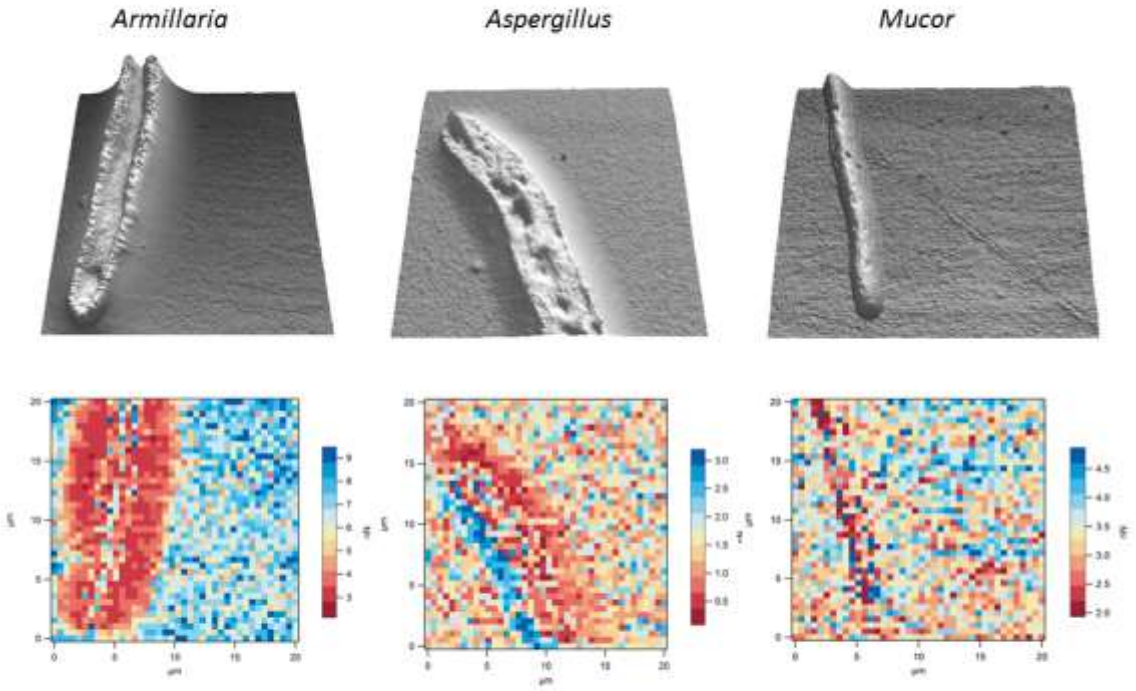

Figure 1. Three-dimensional height images (20 x 20 µm areas) obtained from the AFM scans of cellophane overgrown with *Armillaria*, *Aspergillus* and *Mucor* hyphal tips (upper row) and corresponding force maps (lower row). Colors on force map indicate adhesive force (nN) from low (red) to high (blue) as seen in Figure 4.

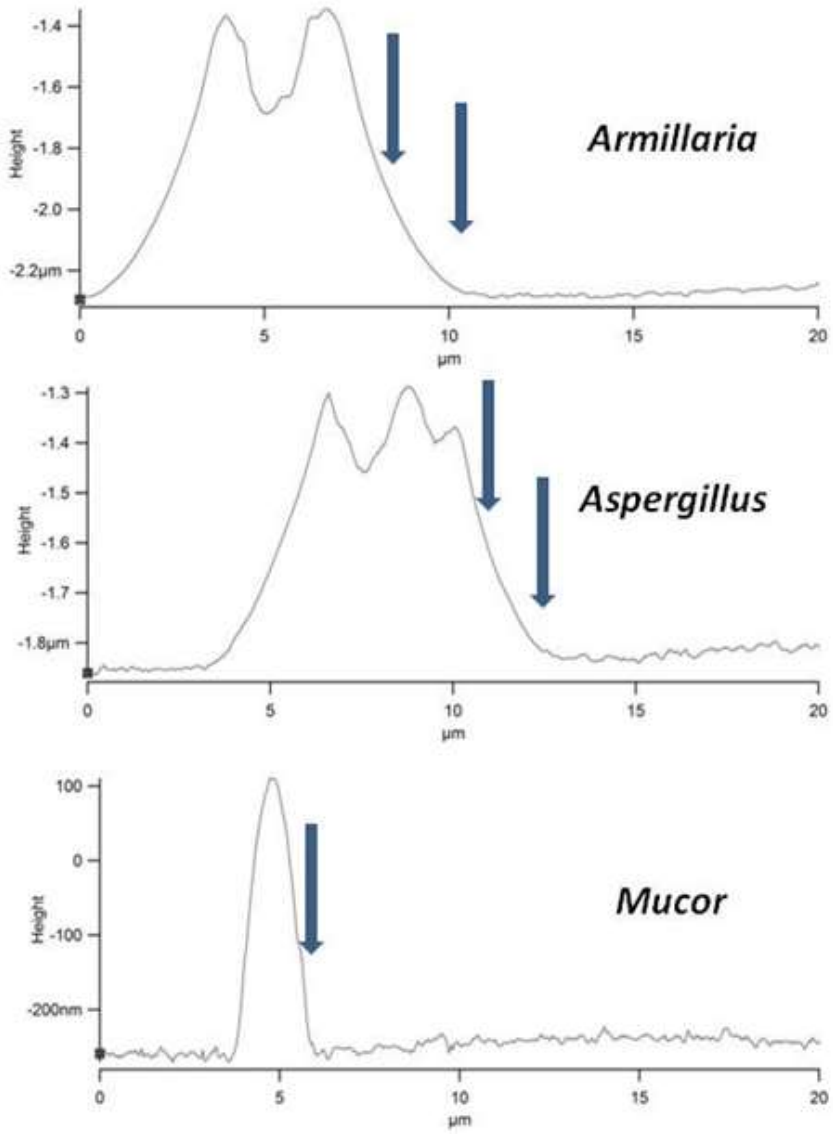

Figure 2. AFM Height traces of transverse sections of *Armillaria*, *Aspergillus* and *Mucor* hyphae growing on cellophane showing defined shoulders on *Armillaria* and *Aspergillus*, which is interpreted as dissolution of the cellophane by fungal enzymes and which is absent in *Mucor*. The region between arrows in *Armillaria* and *Aspergillus* highlights the area of interest where the cellophane has been influenced by the hyphae and is smoother than the rest of the cellophane, but does not exist in *Mucor* (hence a single arrow at the edge of the hypha). The Y-axes of the traces are scaled relative to the maximal height (Z-axis) encountered in the scan.

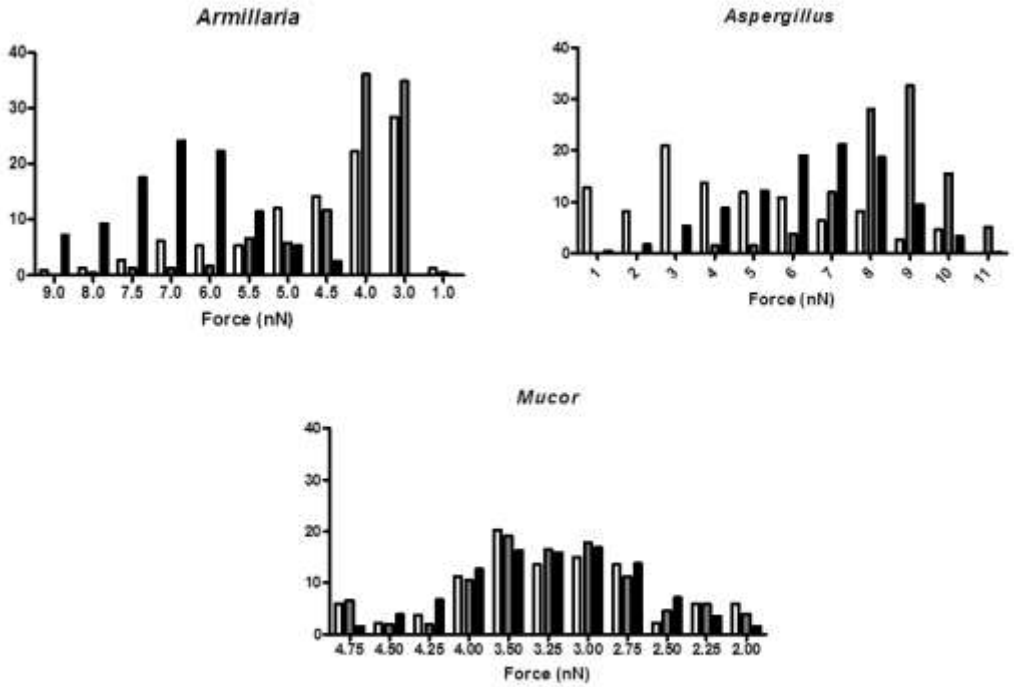

Figure 3. Frequency distributions of adhesive force of cellophane films adjacent to the approach (white), departing (gray) side of hyphae and distant to hyphae (black) for *Armillaria*, *Aspergillus* and *Mucor*.

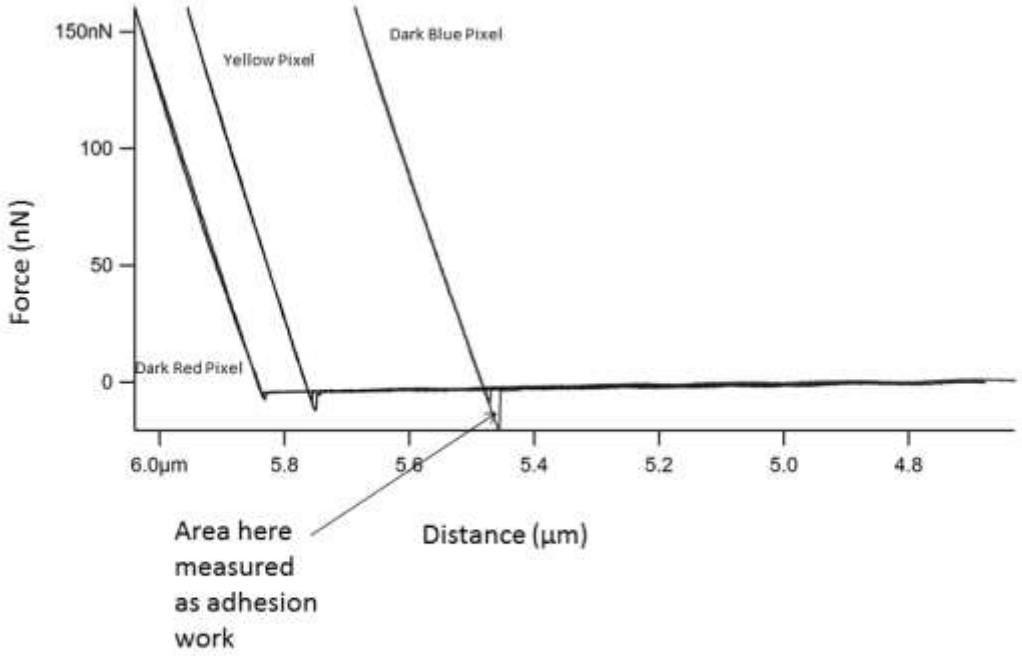

Figure 4. Representative force curves for the areas on *Armillaria* force map with the right curve being for the dark red pixel, middle curve for light yellow and left curve for the dark blue pixels. Measure of adhesive force *sensu* Morris *et al*. (2010).

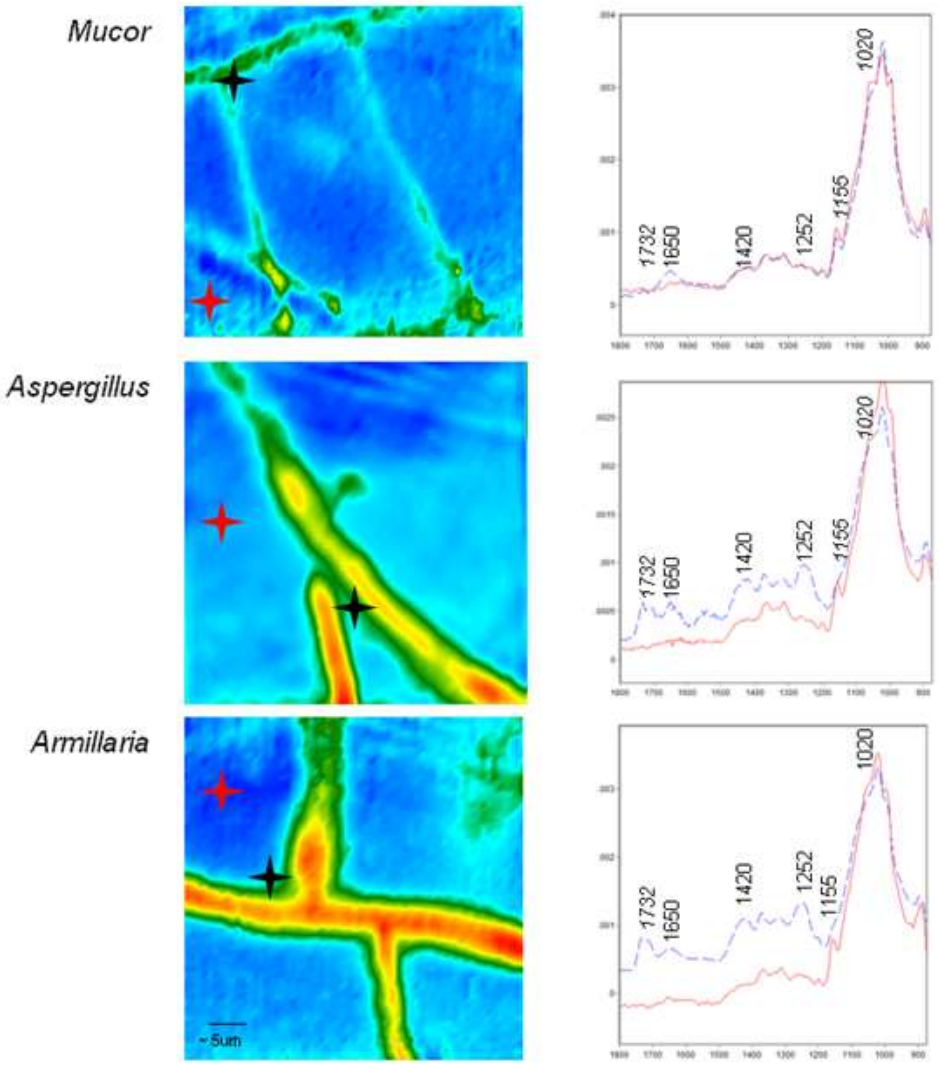

Figure 5. Micro-ATR-FT-IR chemical maps of fungal hyphae grown on cellophane (left column) and associated IR spectra taken at highlighted points (right column). The red star corresponds with the red spectrum on the right, taken at distance from the hypha and the black star corresponds with the hashed blue spectrum on the right, taken adjacent to the hypha. In the images, red indicates higher intensity and blue lower intensity of the map obtained at the specific wavenumber (1650 cm^{-1}). The X-axis of the spectra are wavenumbers within the fingerprint region and the Y-axis the normalized absorbance values. Peaks of interest that changed in intensity, appeared, or diminished are labeled. Italicized labels are associated with changes in carbohydrate chemistry (decomposition of cellophane). Remaining peaks are associated with the appearance of proteins (enzymes) in the sample.

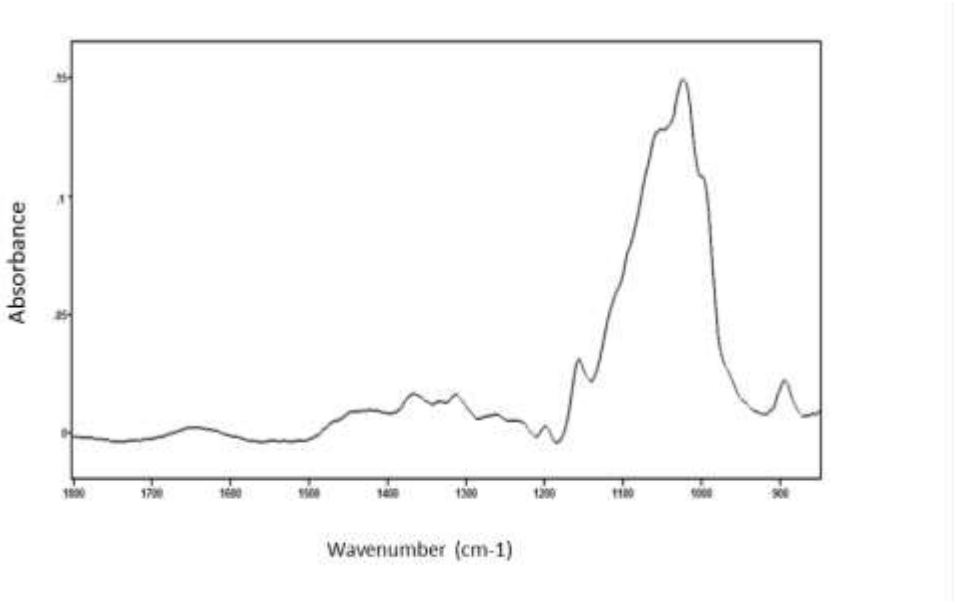

Figure 6. Micro-ATR-FTIR spectrum of normal (unmanipulated) cellophane. Spectral peaks are consistent with those peaks present in cellophane areas far from fungal hyphae (figure 5).

References

Adams EL, Kroon PA, Williamson G, Morris VJ. 2005. AFM studies of water-soluble wheat arabinoxylans – effects of esterase treatment. Carb. Res. 340: 1841-1845.

Barth A, Zscherp C. 2002. What vibrations tell us about proteins. Quart. Rev. Biophys. 35: 369-430.

Canet D, Rohr R, Chamel A, Guillain F. 1996. Atomic force microscopy study of isolated ivy leaf cuticles observed directly and after embedding in Epon. New Phytol. 134: 571-577.

Cohen MS, Gabriele PD. 1982. Degradation of coal by the fungi *Polyporus versicolor* and *Poria monticola*. Environ. Microbiol. 44: 23-27.

Dague E, Alsteens D, Latgé J-P, Dufrêne YF. 2008. High-resolution cell surface dynamics of germinating *Aspergillus fumigatus* conidia. Biophys. J. 94: 656-660.

Desentis-Mendoza M, Hernández-Sánchez H, Moreno A, Rojas del CE, Chel-Guerrero L, Tamariz J, Jaramillo-Flores ME. 2006. Enzymatic polymerization of phenolic compounds using laccase and tyrosinase from *Ustilago maydis.* Biomacromol. 7: 1845-1854.

Dighton J, Mascarenhas M, Arbuckle-Keil G. 2001. Changing resources: assessment of leaf surface carbohydrate resource change at a microbial scale of resolution. Soil Biol. Biochem. 33:1429-1432.

Eaton P, West P. 2010. Atomic Force Microscopy. Oxford University Press, Oxford, pp 116-117.

Frankland JC. 1966. Succession of fungi on decaying petioles of *Pteridium aquilinum*. J. Ecol. 54**:** 41-63.

Griffiths PR. 2009. Infrared and Raman Instrumentation for Mapping and Imaging. In: Salzer R, Siesler HW (Eds). Infrared and Raman Spectroscopic Imaging, Wiley-VCH. pp. 21-24.

Holder DJ, Keyhani NO. 2005. Adhesion of the entomopathogenic fungus *Beauveria* (*Cordiceps*) *bassiana* to substrata. App. Environ. Microbiol. 71: 5260-5266.

Holder DJ, Kirkland BH, Lewis W, Keyhani NO. 2007. Surface characteristics of the entomopathogenic fungus *Beauvaria* (*Cordyceps*) *bassiana*. Microbiol. 153: 3448-3457.

Kaminskyj SGW, Dahms TES. 2008. High spatial resolution surface imaging and analysis of fungal cells using SEM and AFM. Micron, 39: 349-361.

Kazarian S, Chan KLC. 2010. Micro- and macro- attenuated total reflection fourier transform infrared spectroscopic imaging. Appl. Spectrosc. 64: 135A-152A.

Kidder LH, Haka AS, Lewis EN. 2002. Instrumentation for FT-IR Imaging in Handbook of Vibrational Spectrsscopy, Chalmers, Griffiths, (Eds): John Wiley & Sons: p 1386-

Kim KW. 2006. Atomic force microscopy for direct imaging and nanoscale morphometry of rice false smut fungus *Ustilaginoidea virens*. J. Phytopath. 154: 751-754.

Kim M, Kim KW, Jung HS. 2007. Morphological discretion of basidiospores of the puffball mushroom *Calostoma* by electron and atomic force microscopy. J. Microbiol. Biotechnol. 17: 1721-1726.

Koch K, Dommisse A, Neinhuis C, Barthelott W. 2003. Self-assembly of epicuticular waxes on living plant surfaces by atomic force microscopy. In: Koenraad PM, Kemerink M (Eds). Scanning Tunneling Microscopy and Related Techniques. 12th International Conference, American Institute of Physics. pp. 457-460.

Koch K, Neinhuis C, Ensikat H-J, Barthlott W. 2004. Self assembly of epicuticular waxes on living plant surfaces imaged by atomic force microscopy (AFM). J. Exp. Bot. 55: 711-718.

Koch K, Barthlott W, Koch S, Hommes A, Wandelt K, Mamdouth W, De-Feyter S, Broekmann P. 2006. Structural analysis of wheat wax (*Triticum aestivum*, c.v. 'Naturastar' L.): from the molecular level to three dimensional crystals. Planta 223: 258-270.

Lewis EN, Treado PJ, Reeder RC, Story GM, Dowrey AE, Marcott C, Levin IW. 1995. Fourier-transform spectroscopic imaging using an infrared focal-plane array detector. Anal. Chem. 67, 3377-3381.

Ma H, Snook LA, Kaminskyj SGW, Dahms TES. 2005. Surface ultrastructure and elasticity in growing tips and mature regions of *Aspergillus* hyphae describe wall maturation. Microbiol. 151**:** 3679-3688.

Ma H, Snook LA, Tian C, Kaminskyj SGW, Dahms TES. 2006. Fungal surface remodeling visualized by atomic force microscopy. Mycol. Res. 110:879-886.

Mantsch HH, Chapman D. 1996. Infrared Spectroscopy of Biomolecules. Wiley-Liss, New York, NY.

Mascarenhas M, Dighton J, Arbuckle G. 2000. Characterization of plant carbohydrates and changes in leaf carbohydrate chemistry due to chemical and enzymatic degradation measured by microscopic ATR FT-IR spectroscopy. Appl. Spectrosc. 54**:** 681-686.

Mechaber WL, Marshall DB, Mechamber RA, Jobe RT, Chew FS. 1996. Mapping leaf surface landscapes. Proc. Natl. Acad. Sci. 93: 4600-4603.

Medeiros RG, Silva LP, Azevedo RB, Silva FG Jr, Filho EXF. 2007. The use of atomic force microscopy as a tool to study the effect of a xylanase from *Humicola grisea* var. *thermoidea* in kraft pulp bleaching. Enzyme Microb. Technol. 40: 723-731.

Milosevic M. 2004. Internal Reflection and ATR Spectroscopy, Appl. Spect. Rev. 39 :365-384.

Moore RL, Basset BB, Swift MJ. 1979. Development in the remazole brilliant blue dye-assay for studying the ecology of cellulose decomposition. Soil Biol. Biochem. 11 : 311-312.

Morris VJ, Kirby AR, Gunning AP. 2010. Atomic Force Microscopy for Biologists. Imperial College Press, London (2nd Edition), 406 pp.

Nilsson T. 1974. Microscopic studies on the degradation of cellophane and various cellulosic fibres by wood-attacking microfungi. Stud. For. Suec. 117: 1-32.

Norby RJ, Cotrufo MF, Ineson P, O'Neill EG, Canadell JG. 2001. Elevated CO_2, liter chemistry, and decomposition: a synthesis. Oecologia 127**:** 153-165.

Numata K, Yamashita K, Fujita M, Tsuge T, Kasuya K-I, Iwata T, Doi Y, Abe H. 2007. Adsorption and hydrolysis reactions of poly(hydroxybutyric acid) depolymerases secreted from *Ralstonia picketti* T1 and *Penicillium funiculosusm* onto poly[R-3-hydroxybutyric acid]. Biomacromol. 8: 2276-2281.

Paul BC, El-Ganiny AM, Abbas M, Kaminskyj SGW, Dahma TES. 2011. Quantifying the importance of galactofuranose in *Aspergillus nidulans* hyphal wall surface organization by atomic force microscopy. Eukaryotic Cell May 2011: 646-653.

Perkins MC, Roberts CJ, Briggs D, Davies MC, Friedman A, Hart CA, Bell GA. 2005. Surface morphology and chemistry of *Prunus laurocerasus* L. leaves: a study using X-ray photoelectron spectroscopy, time-of-flight secondary-ion mass spectrometry, atomic-force microscopy and scanning electron microscopy. Planta 221: 123-134.

Rautela GS, Cowling EB. 1996. Simple cultural test for relative cellulolytic activity of fungi. Appl. Microbiol. 14: 892-898.

Rayner ADM. 1991. The challenge of the individualistic mycelium. Mycologia. 83: 48-71.

Ritz K. 1995. Growth responses of some fungi to spatially heterogenous nutrients. FEMS Microbiol. Ecol. 16**:** 269-280.

Saarinen T, Orelma H, Grönqvist S, Andberg M, Holappa S, Laine J. 2009. Adsorption of different laccases on cellulose and lignin surfaces. BioResources 4: 94-110.

Smart KA, Jackson CR. 2009. Fine scale patterns in microbial extracellular enzyme activity during leaf litter decomposition in a stream and its floodplain. Microb. Ecol. 58: 591-598.

Socrates G. 1994. Infrared Characteristic Group Frequencies, 2nd ed. John Wiley & Sons, West Sussex, UK.

Stewart D. 1996. Fourier-transform infrared microspectroscopy of plant tissues. Appl. Spectrosc. 50: 357-365.

Swift MJ Heal OW Anderson MJ. 1979. Decomposition in Terrestrial Ecosystems, Oxford, Blackwell Scientific.

Szeghalmi A, Kaminskyj S, Gough KM. 2007. A synchrotron FTIR microspectroscopy investigation of fungal hyphae grown under optimal and stressed conditions. Anal. Bioanal. Chem. 387: 1779-1789.

Wang L, Zhang Y, Gao P, Shi D, Lui H, Gao H. 2006. Changes in the structural properties and rate of hydrolysis of cotton fibers during extended enzymatic hydrolysis. Biotechnol. Bioengineer. 93, 443-456

Went JC, de Jong F. 1966. Decomposition of cellulose in soils. Antonie van Leeuwenhoek 32: 39-56.

Wiśniewska SK, Nalaskowski J, Witka-Jeżewska E, Hupka J, Miller JD. 2003. Surface properties of barley straw. Colloids and Surface Biointerfaces 29: 131-142

Yokata S, Matsuo K, Kitaoka T, Wariishi H. 2008. Specific interaction acting at a cellulose-binding domain/cellulose interface for papermaking application. BioResources 3: 1030-1041.

Zhang Z, Zou S, Vancso GJ, Grijpma DW, Feijen J. 2005, Enzymatic surface erosion of poly(trimethylene carbonate) films studied by atomic force microscopy. Biomacromol. 6: 3404-3409.

Zhao L, Schaefer D, Marten MR. 2005a. Assessment of elasticity and topography of *Aspergillus nidulans* spores via atomic force microscopy. Appl. Environ. Microbiol. 71: 955-960.

Zhao L, Schaefer D, Xu H, Modi SJ, LaCourse WR, Marten MR. 2005b. Elastic properties of the cell wall of *Aspergillus nidulans* studied with atomic force microscopy. Biotechnol. Prog. 21: 292-299.

CHAPTER SIX

Conclusions

The initial aims of this dissertation were to investigate decomposition of leaf material at the hyphal scale of resolution, and investigate the changes occurring both chemically and physically at the fungal/leaf interface. With success in these investigations, the results were to be used to develop methods to further investigate and model fungal decomposition of leaf material in terms of the fungal foraging and community structure development through competitive interactions of fungi at the hyphal level.

With a better understanding of how a fungus "experiences" its environment as that environment changes through resource succession, we could then begin to develop methods to understand fungal foraging at the level of an individual hypha. Questions such as: How much overlap is there in enzyme secretion between neighboring hypha? What is the trade-off involved in the overlap (or lack thereof)? Is hyphal branching correlated with resource quality at the microscale? If so, is there a certain point (chemical or physical state of the litter) during decomposition that the fungus changes its foraging strategy?

Two main analytical tools were used in these studies. Microscopic ATR FTIR to assess the chemistry of leaves and fungal hyphae at the scale of tens of micrometers and atomic force microscopy to measure changes in the physical properties of leaves at the nano- to micro-meter scale.

In order to attempt to separate fungal chemistry from that of the leaf material they were to be grown upon, the analysis (chapter 2) of FTIR and FTIR-ATR spectra of different fungal species yielded interesting results. Although the methods used had their limitations with

regards to detailed chemical interpretation at the molecular level, useful information was obtained. It was unexpected that there would be so few differences between fungal species, particularly living fungi producing enzymes, organic acids, and other secondary metabolites. Metabolically active fungal cells have been shown to produce FTIR spectra rich in lipid, protein, and nucleic acid signatures that differ between species and were dependent on environmental stresses including changes in pH and temperature (Szeghalmi, Kaminskyj, and Gough, 2007; Jilkine *et al.,* 2008)

A second aspect of the dissertation was to investigate the changes occurring in the chemistry of leaves decomposing over time in the field (Chapter 3). The research presented here was successful in investigating the chemical and physical changes occurring on a substrate during decomposition. FTIR and FTIR-ATR enabled an in depth analysis of the chemistry of a decomposing leaf. Unfortunately, much of the data obtained from the use of FTIR and FTIR-ATR is difficult to interpret. Whereas, chemical changes in leaf litter were clearly evidenced through statistical and visual interpretation of the FTIR spectra, those changes were ambiguous in many cases. The assignment of particular functional groups can be redundant (multiple bands for multiple functional groups), and the majority of biological molecules share many functional groups.

Unexpectedly, when oak, pine, and huckleberry leaves were compared through time, they did not separate by species, but by the amount of decomposition time. All of the initial leaf spectra clustered together in PCA analysis, except pine. After 6 and 12 months, all litters were more similar to other litters at the same decomposition time. It was determined that it was not possible to subtract fungal spectra from those of leaves, so an additional complexity of interpreting the FTIR from naturally decomposing leaves is the presence of other organisms

(bacteria, fungi, protozoa, *etc*.) and the fecal material of larger grazers such as collembola and mites.

In chapters 4 and 5, the objective was no longer to investigate only the chemistry of a substrate at the fungal/leaf interface, but to also investigate the physical changes to the substrate occurring around individual hypha using the AFM and FTIR. Initially, leaves were to be scanned on the AFM, fungal hyphae were to be grown across the leaf surface, and AFM images (and background physical data) would be collected. These same leaves would then be analyzed using FTIR-ATR imaging to correlate chemical changes to the observed physical changes obtained from the AFM.

There were a few setbacks to this plan; probably the most substantial was the difficulty in scanning a leaf on the AFM. The AFM requires a flat surface to scan, so leaves were soaked in sterile water and pressed flat before scanning. Although leaves are generally thought of as flat, which they are to an organism almost 2 meters in height, they are not even remotely close to being flat at the micron scale. Many broken tips (AFM probes) later, it was decided that a flat film composed of one or a few leaf components should be developed as a leaf model substrate. This led to the research described in chapter 4; the development of starch:lignin biofilms. It was very exciting to find a paper that successfully created films partially composed of lignin, as lignin is notoriously difficult to get into solution. Biofilms were cast using the methods in the published literature (Vengal & Srikumar, 2005) (starch:lignin, starch:lignin:gelatin, and starch only), and using modifications to add other compounds to the films (cellulose, pectin, and hemicellulose). The modified films were never truly successful, with exception of a few pectin films. The films from the published literature appeared to be a perfect substrate for AFM scanning; they were much flatter than a leaf surface. Before inoculating the biofilms with fungi,

they needed to be chemically and physically characterized. AFM scans and data were collected on starch only and starch:lignin biofilms, followed by the collection of FTIR-ATR spectra. As soon as the spectral data from both films was overlaid on the computer screen, it was clear they were identical. There was no trace of lignin in the starch:lignin films! This was disappointing at best, considering it was the lignin component of the film that was desired. This led to the publication of chapter 4 (Oberle-Kilic *et al*., 2012). Although this chapter did not contribute to the initial aims of this dissertation, it certainly contributed to my education and is counted fairly high on my list of lessons learned.

This led to the idea of using cellophane as a model for cellulose films on the AFM (Chapter 5). Initial scans on the AFM were successful. Preliminary studies degrading cellophane in varying cellulase enzyme concentrations then scanning on the AFM were encouraging. Cellophane films were attached to microscope slide, inoculated with individual fungal species, and incubated in damp chambers. They were dried, and then processed on the AFM. We were successful in not only scanning fungal hypha, but also scanning fungal hypha on a flat carbohydrate substrate, and observing the regions around the hyphal tip that was influencing the substrate. After processing cellophane degraded by three fungal species on the AFM, the samples were analyzed using FTIR-ATR imaging. The results of the FTIR-ATR images provided evidence that there were physical changes occurring adjacent to the hyphae. These measurements allowed us to measure the zone of influence of individual hypahe on their underlying substrate, which could be used in the future to model optimal foraging of fungal hphae and may explain resource specific hyphal growth and branching patterns. This led to the publication of chapter 5 (Oberle-Kilic *et al*. 2013).

Publication of chapter 5 was difficult, and met with much resistance regarding the interpretation of the FTIR portion. At the time, there appeared to be one or two biased reviewers. After completing my own analysis on chapters 2 and 3 of this dissertation, I now have a much better understanding of the reviewers' comments on that paper. I now understand the complexity of assigning IR bands to specific molecules, and the inherent limitations of using FTIR to study complex biological molecules.

Although many of the studies included in this dissertation were based on chemical and physical data collected, the overall theme was to use this data to better understand the ecology of a fungus as it operates at the hyphal level. Unfortunately, we did not accomplish that particular goal on the scale originally intended. Now armed with more information, preliminary data, and experience, we can move forward to develop better techniques that will enable us to reach that goal. With the possibility of obtaining an AFM/Raman IR bench, we could simultaneously scan the same region of the hyphal tip on a leaf collecting both AFM and IR data. Additionally, after over two years of using the AFM and many failed attempts at scanning plant material (blades of grass, onion skin, leaves, and leaves soaked in acetone to remove waxes, etc.), I have finally obtained the skill to scan a leaf on the AFM.

Now, with the capability to scan leaves on the AFM and the potential to have access to a combination AFM Raman IR, we could continue to investigate the physical changes occurring on a leaf during decomposition. The AFM has a moisture chamber, which three years ago I was not able to use due to my own lack of knowledge and skill. Using this moisture chamber now, with more experience, we could image a fungus, in real time, foraging across a leaf surface and track the physical changes occurring in that leaf at the fungus proceeds. This will bring us one step closer to developing better theories on exactly how a fungus interacts with its substrate as it

forages, and how the changing substrate, in turn, impacts the foraging of the fungus, all at the level of the individual fungal hypha.

References

Jilkine K, Gough KM, Julian R, Kaminshyj SGW. 2008. A sensitive method for examining whole-cell biochemical composition in single cells of filamentous fungi using synchrotron FTIR spectromicroscopy. *Journal of Inorg. Biochem.* 102: 540-546.

Oberle-Kilic J, Dighton J, Arbuckle-Keil G. 2012. Chemical characterization of starch and starch:lignin films using micro-attenuated total reflectance Fourier transform infrared spectroscopy (micro-ATR FTIR). *Trends in biomaterials and artificial organs* 26(2):107-109.

Oberle-Kilic J, Dighton J, Arbuckle-Keil G.2013. Atomic force microscopy and micro-ATR-FT-IR imaging reveals fungal enzyme activity at the hyphal scale of Resolution. *Mycology: An International Journal of Fungal Biology,* DOI:10.1080/21501203.2012.759631

Szeghalmi A, Kaminskyj S, Gough KM. 2007. A synchrotron FTIR microspectroscopy investigation of fungal hyphae grown under optimal and stressed conditions. *Anal. Bioanal. Chem*. 387: 1779-1789.

Vengal JC, Srikumar M. 2005. Processing and study of novel lignin-starch and lignin-gelatin biodegradable polymeric films. *Trends in Biomaterials and Artificial Organs* 18(2):237-241

Appendix A

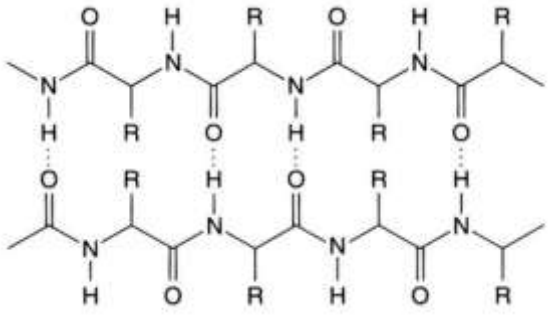

Figure A.1. General structure of a protein molecule highlighting the C=O and N-H of the peptide bond, as well as the presence of hydrogen bonding within a protein molecule between different peptide bonds.

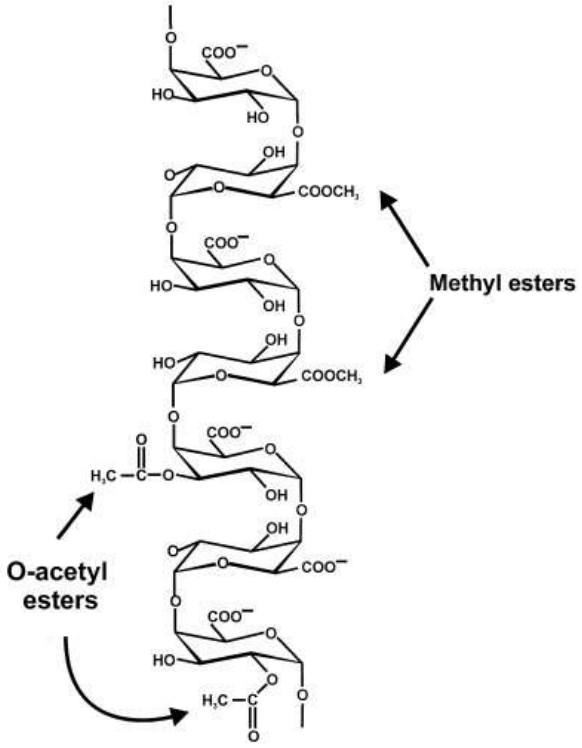

Figure A.2. The chemical structure of homogalacturonan, a common pectin. The presence of methyl esters and O-acetyl esters are noted (from Ridley *et al.,* 2001).

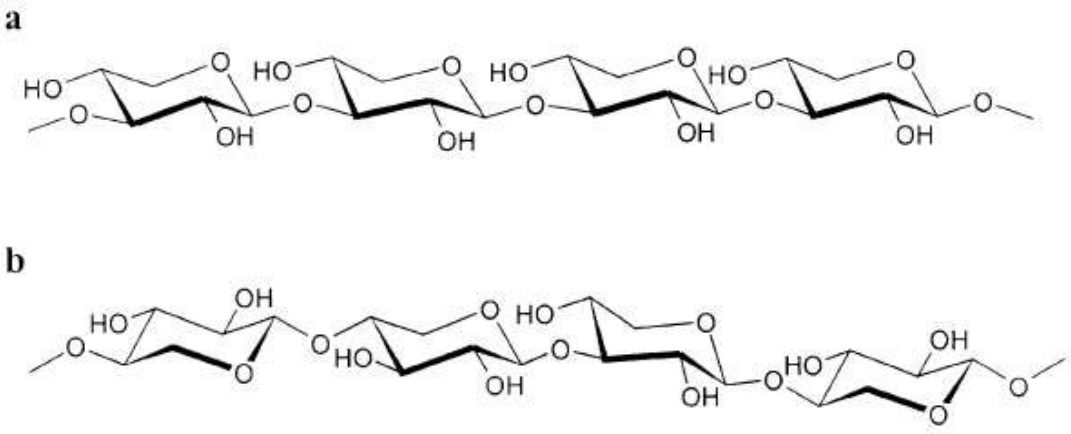

Figure A.3. Chemical structures of two different hemicellulose molecules composed of D-xylans (from Ebringerova *et al.,* 2005).

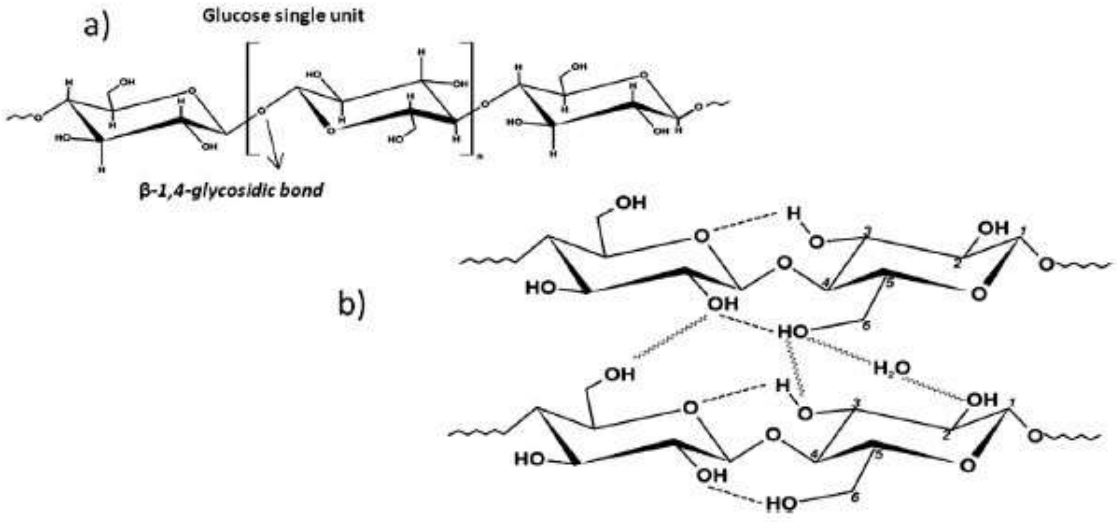

Figure A.4. Chemical structure of a cellulose chain(a) and a cellulose network (b) (from Baccaro *et al.,* 2013).

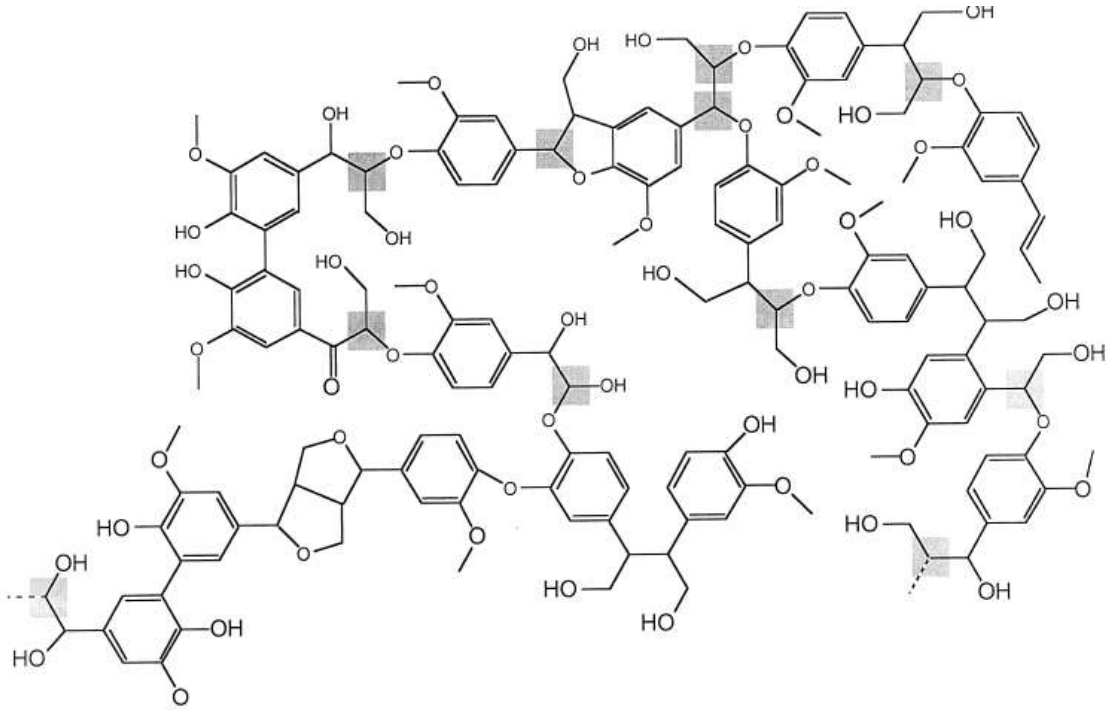

Figure A.5. Proposed chemical structure of a softwood lignin (from Cody and Saghi-Szabo, 1999).

References

Baccaro A, Carewska M, Casieri C, Cemmi A, Lepore A. 2013. Structure modifications and interaction with moisture in γ-irradiated pure cellulose by thermal analysis and infrared spectroscopy. *Polymer Degradation and Stability* 98:2005-2010.

Cody GD and Saghi-Szabo G. 1999. Calculation of the ^{13}C NMR chemical shift of ether linkages in lignin derived geopolymers: constraints on the preservation of lignin primary structure with diagenesis. *Geochimica et Cosmochimica Acta* 63(2):193-205.

Ebringerova A, Hromadkova Z, Heinze T. 2005. Hemicellulose. *Advanced Polymer Science* 186: 1-67.

Ridley BL, O'Neill MA, Mohnen D. 2001. Pectins: structure, biosynthesis, and oligogalacturonide-related signaling. *Phytochemistry* 57:929-967.

Appendix B

Figure B.1. Images of leaves at 0, 6, and 12 months (left to right) of natural decomposition. Top: huckleberry sample #7; middle: oak sample # 7; bottom: pine sample #9.